Departamento de Química

Synthesis, photophysical characterization and biological evaluation of promising theranostic agents for cancer

Márcia Alexandra de Campos Aguiar

Dissertação no âmbito do Mestrado em Química Medicinal, orientada pela Doutora Mafalda Sofia Laranjo Cândido, co-orientada pela Professora Doutora Teresa Margarida Vasconcelos Dias de Pinho e Melo e apresentada no Departamento de Química da Universidade de Coimbra.

setembro de 2018

UNIVERSIDADE Ð
COIMBRA

Acknowledgments

To all my family, especially my mother for all the values, unconditional support, love and affection. Sorry for the constant absences.

And last, but not least, to my Star who was struck down by cancer. You saw me begin this stage, but not to conclude it, however, wherever you are, you are certainly proud. You will always be one of my references, it is in you that I seek the courage to fight the greatest battle, the battle of Life. I hope one day to be for my grandchildren half of what you have been to me. Love you ever and forever.

Table of Contents

Abbreviations

AnV	annexin V
Ar	aryl group
aq.	aqueous
a.u.	arbitrary units
BODIPY	boron-dipyrromethene
cmc	critical micellar concentration
d	doublet
DC	dendritic cells
DCF	2',7'-dichlorofluorescein
DCFH	2',7'-dichlorodihydrofluorescein
DCFH$_2$DA	2',7'-dichlorodihydrofluorescein diacetate
dd	double doublet
DHE	dihydroethidium
DMEM	Dulbecco's Modified Eagle's Medium
DMSO	dimethyl sulfoxide
DMSO-d$_6$	deuterated dimethyl sulfoxide
DNA	deoxyribonucleic acid
EDTA	ethylenediaminetetraacetic acid
e.g.	for example
equiv.	equivalents
ESI	electrospray ionization
Et	ethyl
FDA	Food and Drug Administration
FITC	fluorescein isothiocyanate
GSH	reduced glutathione
HOMO	Highest Occupied Molecular Orbital
Hp	hematoporphyrin
HpD	hematoporphyrin derivative
HRMS	high-resolution mass spectroscopy
IC	internal conversion
IC$_{50}$	concentration that inhibits cell proliferation in 50 %
IL-1	interleukin-1
IL-6	interleukin-6
IR	infrared
ISC	intersystem crossing

J	coupling constant
JC-1	5,5',6,6'-tetrachloro-1,1',3,3'-tetraethylbenzimidazolcarbocyanine iodide
LUMO	Lowest Unoccupied Molecular Orbital
m	multiplet
M	Molar
M^+	molecular ion
M/A	monomers/aggregates ratio
mCPBA	m-chloroperoxybenzoic acid
Me	methyl
MTT	3-(4,5-dimpethylthiazol-2-yl)-2,5-diphenyltetrazolium bromide
MW	microwave
NIR	near infrared
NMR	nuclear magnetic resonance
PBS	Phosphate Buffer Saline
PDT	Photodynamic Therapy
Ph	phenyl group
PI	propidium iodide
PS	photosensitizer
s	singlet
ROS	reactive oxygen species
RPMI	Roswell Park Memorial Institute
RT	room temperature
SRB	sulforhodamine B
S_0	ground state
S_1	singlet excited state 1
S_n	singlet excited state n
T	temperature
t	triplet
T_1	triplet excited state
Tris	tris(hydroxymethyl)aminomethane
1,2,4-TCB	1,2,4-trichlorobenzene
THF	tetrahydrofuran
TLC	thin layer chromatography
TMS	tetramethylsilane
TNF-α	tumour necrosis factor α
UV-Vis	ultraviolet-visible
ε	molar absorptivity coefficient

$\Delta\Psi m$	mitochondrial membrane potential
Φ	quantum yield
λ	wavelength

x

Resumo

Este projeto centrou-se no desenvolvimento de novos fotossensibilizadores (PS) para serem aplicados em terapia fotodinâmica (PDT) do cancro e, simultaneamente, serem usados no diagnóstico através da obtenção de imagem biológica (agentes de teranóstico).

O grupo de investigação em Química Orgânica havia anteriormente relatado a síntese de um novo tipo de clorinas de platina(II), obtidas através de uma reação de cicloadição [8π+2π] do anião metil diazafulvénio com porfirinas de platina(II). Estas clorinas revelaram interessantes propriedades luminescentes na região espetral do vermelho e infravermelho próximo (NIR) e intensas bandas de absorção dentro da janela espectral terapêutica (~590 nm). Estas características fotofísicas e fotoquímicas favoráveis, combinadas com a elevada estabilidade térmica, tornam estes compostos excelentes matéria-prima para serem estudados como agentes de teranóstico.

Neste contexto, na **Parte I** desta dissertação é descrita a síntese de um conjunto de clorinas de platina com diferentes grupos substituintes no seu macrociclo tetrapirrólico (Ar = Ph, 4-ClC$_6$H$_4$ e 4-MeOC$_6$H$_4$) e com diferentes polaridades (ésteres, ácidos e álcoois). Estes PS foram caracterizados por RMN ^{1}H, RMN ^{13}C, espectrometria de massa e espectroscopia de absorção UV-visível.

Atendendo a que se tem comprovado que a agregação dos PS usados em PDT tem um papel decisivo na sua atividade fotodinâmica, pela dificuldade de incorporação pelas células e pela diminuição da geração de oxigénio singleto (considerada por vários autores como a principal espécie citotóxica produzida na terapia fotodinâmica), estes complexos de platina também foram estudados quanto à sua agregação num meio aquoso (PBS). Tendo-se verificado que agregavam procedeu-se a um estudo de desagregação usando diferentes surfactantes neutros. Os surfactantes estudados foram o Glicerol, Pluronic F127, Pluronic P123 e Tween 20.

Na **Parte II** deste trabalho experimental, procedeu-se à verificação da citotoxicidade no escuro dos dois surfactantes que demonstraram espetroscopicamente desagregar as metaloclorinas de platina. Estes surfactantes foram o Pluronic P123 e o Tween 20. A linha celular tumoral usada foi de melanoma melanocítico (A375). Com este estudo comprovou-se que a citotoxidade destes desagregantes era significativamente superior à do veículo previamente usado (dimetilsulfóxido), razão pela qual os ensaios biológico prosseguiram com os compostos na forma agregada.

Posteriormente, ainda na **Parte II**, pretendeu-se verificar o efeito fotodinâmico destas clorinas em três linhas celulares tumorais humanas, esclarecendo deste modo as suas vias moleculares de atuação. As linhas celulares tumorais usadas foram de carcinoma da bexiga (HT1376), carcinoma do esófago (OE19) e melanoma melanocítico (A375). O ensaio de MTT permitiu verificar que o valor de concentração para a inibição de 50 % da atividade metabólica (IC$_{50}$) de alguns destes PS nas três linhas celulares tumorais foi na ordem de nanomolar, o que aponta para um efeito terapêutico promissor. Entre os complexos de platina estudados, verificou-se que as metaloclorinas com caraterísticas mais hidrofílicas (ácidos e álcoois) tinham um maior efeito na inibição da atividade metabólica, e que os complexos com Ar = Ph eram mais potentes, do que os correspondentes

complexos com Ar = 4-ClC$_6$H$_4$ e Ar = 4-MeOC$_6$H$_4$. A linha tumoral do melamoma melanocítico foi a que demonstrou ser a mais sensível ao efeito destes derivados.

Sabendo que determinados fotossensibilizadores exibem uma elevada seletividade para as células tumorais, estudou-se também o efeito dos fotossensiblizadores mais promissores numa linha não tumoral, a linha humana de fibroblastos HFF1, não se verificando diferenças estatisticamente significativas. Foi demonstrado que o decréscimo da atividade metabólica, nas células submetidas à PDT estava relacionado com os mecanismos de morte celular, a disfunção mitocondrial e a produção intracelular de espécies reativas de oxigénio (ROS). O tipo de morte celular ativado, apoptose ou necrose, é influenciado pela concentração dos fotossensibilizadores. Várias ROS estão implicadas no efeito fotodinâmico dos fotossensibilizadores mais potentes e os mecanismos citoprotetores não parecem ser suficientes para inibir os danos celulares.

Com este trabalho, foi possível concretizar o objetivo de desenvolver um agente de teranóstico e, caracterizar as suas vias subcelulares de atuação, ainda que estes fotossensibilizadores se encontrem na sua forma agregada. Todos os resultados biológicos obtidos neste estudo poderão estar sujeitos a melhoria utilizando surfactantes não citotóxico *per si*.

Abstract

This project focused on the development of new photosensitizers (PS) to be applied in cancer photodynamic therapy (PDT) and, simultaneously, to be used in the diagnosis by obtaining a biological image (theranostic agents).

The Organic Chemistry research group had previously reported the synthesis of a new type of platinum(II) chlorins obtained through an $[8\pi+2\pi]$ cycloaddition reaction of the diazafulvenium methides with platinum(II) porphyrins. These chlorins revealed interesting luminescent properties in the red and near infrared (NIR) regions and intense absorption bands within the spectral therapeutic window (~590 nm). These favourable photophysical and photochemical characteristics, combined with the high thermal stability, make these compounds excellent materials to be studied as theranostic agents.

In this context, in **Part I** of this dissertation, it is described the synthesis of a set of platinum chlorins with different substituent groups in their tetrapyrrolic macrocycle (Ar = Ph, 4-ClC$_6$H$_4$ and 4-MeOC$_6$H$_4$) and with different polarities (esters, acids and alcohols). These PS were characterized by ^{1}H NMR, ^{13}C NMR, mass spectrometry and UV-visible absorption spectroscopy.

Considering that it has been proven that the aggregation of PS used in PDT plays a decisive role in its photodynamic activity, due to the difficulty of incorporation by the cells and the decrease in the generation of singlet oxygen, these platinum complexes were also studied for their aggregation in an aqueous medium (PBS). Having been found that they aggregate, a disaggregation study using different neutral surfactants was carried out. The surfactants studied were Glycerol, Pluronic F127, Pluronic P123 and Tween 20.

In **Part II** of this experimental work, the dark cytotoxicity of the two surfactants which demonstrated spectroscopically the disaggregation of the metallochlorins, was performed. These surfactants were Pluronic P123 and Tween 20. The tumour cell line used was melanocytic melanoma (A375). With this study it was found that the cytotoxicity of these surfactants was significantly higher than the vehicle previously used (dimethylsulfoxide), whereby the biological assays proceeded with the compounds in the aggregate form.

Subsequently, it was intended to verify the photodynamic effect of these chlorins in three human tumour cell lines, clarifying their molecular pathways of action. The tumour cell lines used were bladder carcinoma (HT1376), esophageal carcinoma (OE19), and melanocytic melanoma (A375). The MTT assay showed that the concentration value for the 50% inhibition of the metabolic activity (IC$_{50}$) of some of these PS in the three tumour cell lines was in the nanomolar range, which points to a promising therapeutic effect. Among the platinum complexes studied, it was found that metallochlorins with more hydrophilic characteristics (acids and alcohols) had a greater effect on the inhibition of metabolic activity, and that the complexes with Ar = Ph were more potent than the complexes with Ar = 4-ClC$_6$H$_4$ and Ar = 4-MeOC$_6$H$_4$. The melanocytic melanoma tumour line was shown to be the most sensitive to the effect of these derivatives.

Knowing that certain photosensitizers exhibit high selectivity for tumour cells, the effect of more promising photosensitizers in a non-tumour line, the human HFF1 fibroblast line, was also studied, and no statistically significant differences were observed. The decrease in metabolic activity in cells submitted to PDT was shown to be related to the mechanisms of cell death, mitochondrial dysfunction and intracellular production of reactive oxygen species (ROS). The type of activated cell death, apoptosis or necrosis, is influenced by the concentration of the photosensitizers. Several ROS are involved in the photodynamic effect of more potent photosensitizers and cytoprotective mechanisms do not appear to be sufficient to inhibit cell damage.

With this work, it was possible to achieve the goal of developing a theranostic agent and to characterize its subcellular pathways, even though these photosensitizers are in their aggregate form. All biological results obtained in this study may be subject to improvement using non-cytotoxic surfactants.

Chapter 1: Introduction

Recently, novel photosensitizers for photodynamic therapy (PDT) of cancer were developed by the Organic Chemistry research group. These are photo and chemically stable platinum(II) chlorins, which are remarkable photosensitizers to be used in PDT due to their therapeutic capacity. Simultaneously, due to its highly luminescence proprieties, in the biological relevant 700-850 nm red and NIR spectral region, they may be used for biological imaging. As such, in this chapter it is intended to present introductory concepts about this class of promising theranostic agents for cancer.

Theranostic agents (diagnosis + therapy)

In the last years, the scientific community has invested in the development of theranostic agents, that is, compounds that, simultaneously, allow the diagnosis through image and the treatment due to their therapeutic properties (Ethirajan et al. 2011; Kelkar and Reineke 2011; M Laranjo 2014).

One of the classes of structures that have been well studied and developed in this field are tetrapyrrole macrocycles. Of these compounds, porphyrins and their derivatives are among the most important (Che et al. 2011; Ethirajan et al. 2011; Lindoy, Park, and Lee 2013; Pereira et al. 2017; Saito and Osuka 2011).

1.1. Tetrapyrrole macrocycles as theranostic agents

Porphyrinic macrocycles are composed of four pyrrole rings linked together by four methine bridges, presenting a highly conjugated system. Of the 22 π-electrons in the porphyrin base structure, 18 of them form an aromatic conjugate system following the Huckel rule (4n+2). As a result of this extensive conjugation, porphyrins are coloured compounds that exhibit strong absorption in the region of the visible at around 400 nm, the band called Soret, and other bands of lesser intensity between 450-700 nm, called Q bands (Eastwood et al. 1966; Giovannetti 2012; Gouterman 1961). In **Figure 1.1** other reduced forms of porphyrins **1** are shown, such as chlorins (dihydroporphyrins) **2**, bacteriochlorins **3** and isobacterioclorins (tetrahydroporphyrins) **4**. These pyrrole macrocycles can complex with metals (e.g **5**).

Chlorins have, like porphyrins, 18 π-electrons in the aromatic conjugate system, exhibiting less 2 π-electrons than the porphyrins, resulting from the saturation of a double bond in one pyrrole unit. In the case of bacteriochlorins the conjugation is achieved with the same 18 π-electrons, which, in this case, correspond to their total number of π-electrons. Bacteriochlorins have double bond saturation in two opposite pyrrole units, whereas the isobacterioclorins, isomeric forms of bacteriochlorins, have two adjacent pyrrole units reduced. As a consequence, isobacterioclorins are not aromatic macrocycles. The structural variances between these porphyrinic compounds make them to differ in certain photophysical properties. Hydroporphyrins exhibit higher absorption in the red and near infrared regions (NIR) compared to porphyrins. Chlorins have typical absorption bands around 650 nm and bacteriochlorins around 730-750 nm (Sternberg, Dolphin, and Brückner 1998).

In general, chlorins and bacteriochlorins have good spectral and photophysical characteristics for use as near infrared luminescent compounds. However, chlorins and bacteriochlorins prepared by the classical route of porphyrin reduction are very unstable under ambient conditions, and tend to be rapidly oxidized back to the porphyrin precursor or to degrade by oxygen to other kind of macrocycles. Chlorins and bacteriochlorins with particular structures that avoid the oxidation back to porphyrin, among other transformations, are required in order to produce efficient near infrared luminescent compounds with high enough stability to be used in imaging and theranostics or other applications, which require prolonged contact with air.
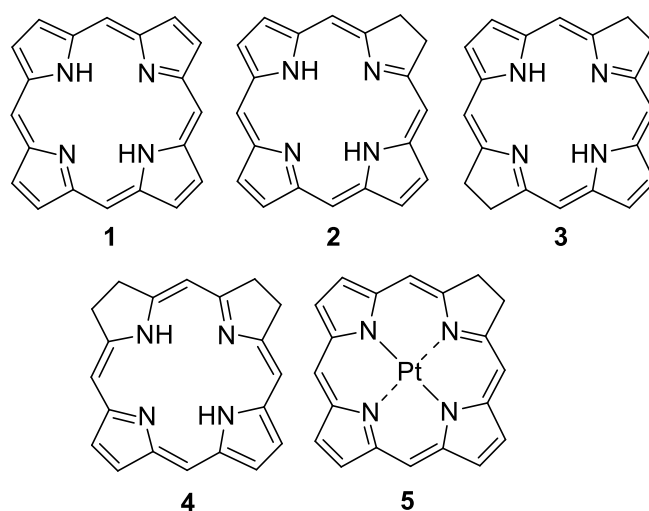
Figure 1.1. Structure of porphyrin **1**, chlorin **2**, bacteriochlorin **3**, isobacterioclorin **4** and platinum(II) metallochlorin **5**.

1.2. Diagnosis - biological imaging

Molecular imaging is becoming increasingly important in clinical diagnosis and biomedical research for the study of processes at the cellular and subcellular levels, with much effort being placed on targeting and reporting disease and metabolism *in vivo* (Massoud and Gambhir 2003).

Imaging techniques are typically considered in terms of the region of the electromagnetic spectrum involved, with the most important methods corresponding to radiation in the radiofrequency (magnetic resonance imaging), visible/near infrared (optical imaging) and high energy X-rays and γ-rays (X-ray computed tomography, positron emission tomography, and single-photon emission computed tomography) regions (Pansare et al. 2012).

Optical imaging using luminescent materials is of particular relevance for biological applications since it is relatively low cost, non-invasive, requires low cost equipment and has reasonable sensitivity and good temporal resolution (Massoud and Gambhir 2003). NIR emitters are particularly important for these applications since their light output is in a region where organisms are highly transparent (the optical or therapeutic window). At these wavelengths there is little light absorption by cell constituents, such as proteins, hemoglobin, melanin and water, and light scattering is reduced. Particularly important applications include NIR luminescence imaging of cells for diagnostic studies of cancer and other conditions (Frangioni 2003; Hötzer, Medintz, and Hildebrandt 2012; Luo et al. 2011; Sevick-Muraca, Houston, and Gurfinkel 2002).

The optimal requirements for an imaging agent for biological systems are high molar absorption coefficient, good luminescence quantum yield, large Stokes shift between absorption and emission maxima, good chemical and photochemical stability, low toxicity, and the possibility of dissolution in aqueous media.

4

The most important classes of NIR emitters are inorganic fluorophores, such as quantum dots, or upconverting fluorophores containing lanthanide ions, and organic dyes, such as cyanines, squaraines, phthalocyanines, porphyrins, chlorins, boron dipyrromethanes (BODIPYs), perylene dyes and carbon nanotubes (Luo et al. 2011; Pansare et al. 2012). However, until now the only long wavelength emission compound approved by the US Food and Drug Administration (FDA) for direct usage in medical diagnostics is the cyanine dye indocyanine green (Pansare et al. 2012). There is, therefore, the urgent need to develop new materials with these properties.

Very recently, chlorins that coordinate with platinum(II) (**Figure 1.2**) have been reported as potential theranostic agents (Pereira et al. 2017). These compounds show good light emission (fluorescence and phosphorescence), in solution at room temperature, in the biologically important 700-850 nm near-infrared (NIR) spectral region. They have a high thermal and photochemical stability, which makes them excellent materials for use in biological imaging. In addition, due to quenching of excited states of compounds by molecular oxygen can lead to reactive oxygen species, such as singlet oxygen or superoxide radical anion, which can kill malignant cells through a treatment called photodynamic therapy (PDT).
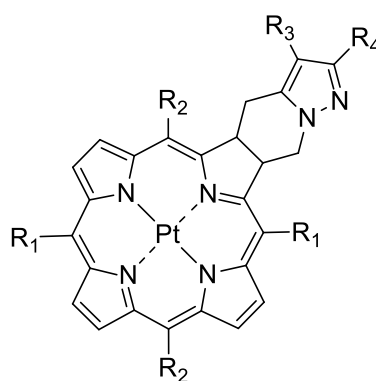
Figure 1.2. General structure of platinum(II) chlorins synthesized by Pereira et *al.* 2017.

1.3. Therapy - photodynamic therapy (PDT)

In clinical practice, photodynamic therapy (PDT) is an innovative therapy approved for use in certain neoplastic and non-neoplastic diseases. In the case of cancer, this technique has generated great interest in the scientific community because it offers some advantages relatively to conventional treatments, namely, chemotherapy and radiotherapy (Agostinis et al. 2011; M Laranjo 2014; Sousa Brites 2016).

1.3.1. PDT - historical facts

PDT origin dates to ancient Egypt, Greece and India, being that these people used sunlight in combination with a photosensitizing plant to treat various skin diseases, including vitiligo and psoriasis (Josefsen and Boyle 2008). However, it was only in the beginning of the 20th century, that PDT, as a therapeutic modality, began to develop. This is largely due to the work done by German

medical student Oscar Raab, which working with Professor Herman von Tappeiner in Munich, discovered the photodynamic effect of acridine orange on protozoa and parasites in the presence of sunlight (Kübler 2005). Three years later, the same group published the first treatment in patients (Allison and Sibata 2010; Kübler 2005).

In the following years, the phototoxicity and fluorescence of hematoporphyrin was investigated (Kübler, 2005). In the 1960s, Lipson and Buckets synthesized a hematoporphyrin derivative (HpD) compound to increase tumour accumulation of the dye, and subsequently this compound was used as a fluorescent marker for diagnosis of cancer. But in 1972, Diamond *et al.* showed that HpD, besides being a diagnostic tool, could also have therapeutic applications, evidencing its efficacy in rat gliomas (Nyman and Hynninen 2004). Subsequently, in 1975, Dougherty *et al.* demonstrated complete eradication of breast tumours in animal models after treatment with HpD (Dougherty et al. 1975). In 1976, Kelly and Snell conducted the first clinical study of HpD in bladder cancer treatment. Even in this same decade, in 1978, Dougherty *et al.* have shown several successful case results obtained in patients undergoing PDT.

After these outcomes, PDT studies were intensified, and several clinical cases were published, showing PDT potentialities in the treatment of various kinds of tumours, such as bladder, brain, intraocular, pancreatic, and liver, among others (Hamblin and Mroz 2008; Nyman and Hynninen 2004). Despite the promising results of PDT in cancer treatment, it was only in 1993 that the first photosensitizer was approved in Canada, an HpD designated Photofrin®, for the treatment of bladder cancer (Grossweiner et al. 2005; Triesscheijn et al. 2006). This was, in 1995, approved by the FDA for the treatment of oesophageal cancer, and later in several countries in Europe.

1.3.2. PDT - fundamentals

Photodynamic therapy consists of a therapeutic approach that requires the combination of three factors: a light source with adequate wavelength, the presence of molecular oxygen and an intermediary agent, called photosensitizer (PS), capable of absorbing and transferring energy from the light source to the oxygen, leading to the formation of reactive oxygen species (ROS), which are cytotoxic, causing damage and, consequently, cell death (Agostinis et al. 2011; Josefsen and Boyle 2008; Nyman and Hynninen 2004).

In the clinical practice, the procedure consists in the administration of the photosensitizer, which should be preferentially accumulated in the tumour cells, later the excitation and activation of the photosensitizer is carried out, at the wavelength corresponding to an absorption band of PS, leading to the generation of cytotoxic species and tumour destruction (Agostinis et al. 2011; Josefsen and Boyle 2008; Nyman and Hynninen 2004).

1.3.3. PDT - advantages and disadvantages

PDT has a local action, which at the same time may have advantages and disadvantages. The high selectivity of this therapy is due to the ability of many PS to accumulate preferentially in tumour cells, and because the cytotoxic action occurs only in the time interval and in the place where light interacts with the PS (Brown, Brown, and Walker 2004). Selective PS accumulation in the tumour is facilitated if the application is topical, since the PS is applied locally only on the lesion to be treated. In cases where administration is intravenous, it is necessary that the PS be kept in circulation for long enough to reach and accumulate in the tumour, taking advantage of the specific microenvironment of most solid tumours. These have fenestrated blood capillaries, reduced lymphatic drainage and low pH, which favours the passage and accumulation of the PS into the desired site (Ana P. Castano, Demidova, and Hamblin 2005).

Despite the reduced systemic effects, temporary cutaneous photosensitivity reactions have been identified as the most significant adverse effect of this therapy. This is a problem that occurs due to accumulation of PS in the skin of patients. PS molecules accumulated in the skin can initiate the photodynamic reaction, by the action of sunlight or strong artificial light, causing skin lesions or photosensitivity. The same can occur at the ocular level. To avoid this problem, patients should stay at home a few weeks after treatment, until PS levels in the skin decrease to safe values. As such, it is essential that PS have fast kinetics of elimination of the organism (Mazor et al. 2005).

The main disadvantage of the localized character of PDT is that it does not allow the treatment of metastatic tumours (Brown, Brown, and Walker 2004; Triesscheijn et al. 2006). As such, many research groups have attempted to understand and modulate the response of the immune system, favouring a specific antitumor immune response (Ana P. Castano, Mroz, and Hamblin 2006; St. Denis et al. 2011).

1.3.4. PDT - Light - matter interaction

As result of the interaction of light with matter, light energy can be transformed into other forms of energy (absorption, light emission, heat release and photochemical reactions). The search for an understanding of this interaction led to a series of studies in different areas of knowledge.

Photophysics and photochemistry are respectively concerned with describing the physical and chemical processes induced by the absorption of light, involving energetic, structural and dynamic studies. A molecule by absorbing light and being excited can lose its energy through physical processes or participate in chemical reactions. To quantify each of these processes, quantum yield (Φ) measurements are used, where Φ is the ratio of the number of photons involved in a specific process by the number of photons absorbed or number of molecules of product formed per unit of time.

1.3.5. PDT - photochemistry and photophysics

The incidence of light on a photosensitive compound can provide sufficient energy to trigger photochemical processes. When a PS, in the ground state (S_0), absorbs light, one electron is excited to a higher orbital level. This electron maintains its spin according to the spin selection rule. The excitation to a higher singlet state can be from highest occupied molecular orbital (HOMO) to lowest unoccupied molecular orbital (LUMO) or to a higher orbital, being that singlet excitation states (S_n) can have different energies (**Figure 1.3**). $S_n > S_1$ have a short lifetime (nanoseconds), so the photosensitizer rapidly loses energy to the first singlet excited state (S_1) by internal conversion (IC). From this state, the photosensitizer can experience two types of processes, one radiative and one non-radiative (Benov 2015).
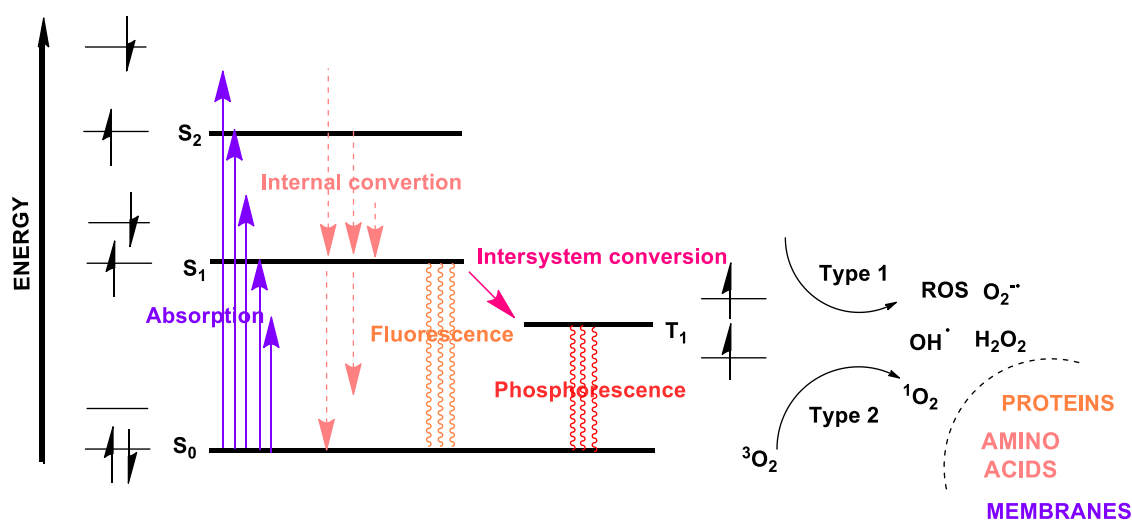
Figure 1.3. Perrin-Jablonski energy diagram for a photosensitizer.

In the radiative process, the photosensitizer returns to the S_0, by emission of fluorescence (**Figure 1.3**). Fluorescence emission is only possible in the transition from the S_1 state to the S_0 state, whereby, normally, the fluorescence wavelength is less than the excitation wavelength. The difference between the maximum excitation wavelength and the maximum emission wavelength is referred as the Stokes shift (Ana P Castano, Demidova, and Hamblin 2004; Celli et al. 2010; M Laranjo 2014). In this case the photodynamic reaction doesn't occur with therapeutic effect, however this property can potentially be used for diagnosis by obtaining fluorescence images (Celli et al. 2010; M Laranjo 2014).

In the non-radiative process, the electrons undergo a spin inversion, called intersystem crossing (ISC), passing to a triplet excited state (T_1) (Benov 2015; Martinez De Pinillos Bayona et al. 2017), **Figure 1.3**. The production of this state by the photosensitizer determines its phototherapeutic effects and the probability of triplet state formation. A high triplet state formation is required for a high efficacy of the photosensitizer in PDT. In this state (T_1), the photosensitizer may dissipate energy and return to the S_0 through a radiative emission process, referred to as phosphorescence, **Figure 1.3**, or may undergo quenching (nonradiative de-excitation process). The quenching mechanisms of

the triplet excited state occur according to two types of photodynamic reactions, Type I and Type II, **Figure 1.3**.

In the Type I reaction, the photosensitizer in the T_1 state reacts directly with the substrate(s), such as cell membranes or molecules, with the transfer of an electron or a proton between them, giving rise to an anion radical or a radical cation, respectively (Ana P Castano, Demidova, and Hamblin 2004; Martinez De Pinillos Bayona et al. 2017; Obata et al. 2009). In the presence of oxygen, and because these free radicals are highly unstable species, most react instantly to produce the superoxide anion ($O_2-\bullet$). In biological systems, this radical reacts with water to produce hydrogen peroxide (H_2O_2). Hydrogen peroxide can cross cell membranes and cause damage directly on cell compartments. At higher concentrations, the superoxide anion can form highly reactive hydroxyl radicals ($OH\bullet$), which attack and oxidize biological molecules (Agostinis et al. 2011; Benov 2015; Ana P Castano, Demidova, and Hamblin 2004; M Laranjo 2014; Martinez De Pinillos Bayona et al. 2017).

On the other hand, in the Type II reaction, the photosensitizer in the T_1 state can transfer its energy directly to the molecular oxygen, whose ground state alone is also a triplet state, producing the excited state of oxygen, the singlet oxygen ($^1O_2$). Singlet oxygen is a highly reactive species with a very short lifetime that reacts directly with biological molecules near its site of formation. Theoretically, singlet oxygen can only interact with nearby molecules and structures within its range of action.

Reactive oxygen species (ROS) formed by the photodynamic reaction are known to trigger various reactions with biomolecules including: amino acid residues in proteins, unsaturated lipids, such as cholesterol, and bases of nucleic acids. These interactions cause damage, potential destruction of cell membranes and deactivation of enzymes, inducing cell death. The singlet oxygen is considered the main cytotoxic species formed during the photodynamic process (Josefsen and Boyle 2008; Yano et al. 2011). Both reactions (Type I and II) occur simultaneously, and the ratio between them depends on the type of photosensitizer used, the substrate and oxygen concentration and the amount of available oxygen. The efficiency of the Type II reaction depends on the duration (lifetime) of the triplet state and the triplet quantum yield of the photosensitizer. Both reaction types have been implicated in the efficacy of the photosensitizer and are also involved in the distinction between the two types of photodynamic reactions (Type I and II).

1.3.6. PDT - characteristics of an ideal photosensitizer

An ideal photosensitizer for PDT must have the following characteristics: high purity and chemical stability; easy synthesis; low dark toxicity of photosensitizer and their metabolites; strong absorption in the infrared region, of the electromagnetic spectrum (600-850 nm, the so-called "therapeutic window"); have suitable photophysical characteristics such as low quantum fluorescence yield, high quantum singlet oxygen yield and a triplet state with a high half-life, as well as a partition coefficient suitable for the intended route of administration and allowing dissolution in biocompatible formulations, if necessary (Moghissi 2004; Ormond and Freeman 2013).

1.3.7. PDT - mechanisms of tumour cytotoxicity

Tumour destruction may occur due to direct tumour cell death, or indirectly due to injury to the tumour vasculature or induction of inflammatory reaction with subsequent immune system activation (Plaetzer et al. 2009).

Several clinical studies have shown that PDT may be curative, particularly in the case of non-advanced tumours. On the other hand, it is known that it can prolong survival in the case of inoperable tumours and improve the patients' quality of life (Agostinis et al. 2011; M Laranjo 2014).

Cytotoxic effects caused by PDT *in vivo* are multifactorial and depend on the type of tumour and its level of oxygenation, the characteristics of the photosensitizer, its concentration, location at the moment of irradiation, the time between its administration and irradiation, light sources' power and total light energy received (Agostinis et al. 2011; Allison 2014; M Laranjo 2014; Sousa Brites 2016). The balance of these parameters influences the extent of the various mechanisms of tumour destruction: direct destruction of tumour cells (apoptosis, autophagy or necrosis), destruction of tumour vascularization and activation of an immune response.

1.3.7.1. Direct cytotoxicity of PDT

The direct action of PDT on tumour cells is the most studied effect when this therapeutic strategy is applied to cancer. The three main mechanisms of cell death, necrosis, apoptosis and cell death associated with autophagy can be activated in response to ROS produced in the photodynamic reaction.

Oxidative damage irreversibly destroys biomolecules and key cellular structures leading to cell death. The mechanism of cell death may be influenced by the cellular organelles where the PS molecules were located at the time of irradiation (Buytaert, Dewaele, and Agostinis 2007).

Typically, photosensitizers located in the mitochondria or endoplasmic reticulum induce cell death by apoptosis, whereas PS located on the plasma membrane or lysosomes may induce cell death by necrosis. There is also evidence that autophagy can be induced by PDT. Autophagy is activated in an attempt by the cell to repair and survive damage to certain key organelles. If this response fails, it is transformed into a cell death signal (Buytaert, Dewaele, and Agostinis 2007).

The known results suggest that in more aggressive PDT protocols (high doses of PS, high light doses, or both, and short times between PS administration and irradiation) tend to cause extensive necrotic cell death, unlike less intense protocols, which seem to favour cell death by apoptosis (M Laranjo 2014; Mroz et al. 2011; Sousa Brites 2016).

Apoptosis

Apoptosis is described as a programmed cell death mechanism that is genetically encoded and ATP-dependent. In morphological terms, is characterized by chromatin condensation, chromosomal DNA cleavage, cell contraction, membrane shrinkage with formation of apoptotic bodies, and phosphatidylserine exposure in the outer leaflet of the cell membrane (Garg et al. 2010; Mroz et al. 2011). The process of apoptosis leads to the secretion of signalling molecules into the extracellular medium that attract phagocytic cells responsible for the elimination of the apoptotic bodies formed, avoiding the inflammatory process and the consequent activation of the immune system (A.P. Castano, Demidova, and Hamblin 2005). The fact that less aggressive PDT protocols favour cell death by apoptosis might be explained by the need for all the complex cellular machinery required to be functional, which may not happen after more aggressive PDT protocols (Mroz et al. 2011).

Autophagy

Autophagy is a highly controlled process in which cellular organelles are captured by membrane vesicles, fused with lysosomes and degraded allowing the reuse of cellular components (Buytaert, Dewaele, and Agostinis 2007; Klionsky 2005).

The functional contribution of this process to PDT cell death is still unclear, however, available data seem to indicate that when apoptosis is the major cell death pathway, autophagy functions as a mechanism of cell repair, protecting the cells affected by the destruction oxidative and counteracting the effect of the treatment. In other situations, when the mechanism of apoptosis in cells affected by PDT is damaged, there is a brutal increase in autophagic activity that promotes cell death, favouring the destruction of the tumour. However, the mechanism responsible for the alternation between the protective effect and the destructive effect of the autophagic pathway is still unknown (Agostinis et al. 2011; Garg et al. 2010).

Necrosis

Necrosis is morphologically characterized by increased cell volume and rupture of the plasma membrane, resulting in an inflammatory reaction due to the release of cellular content and proinflammatory molecules (Buytaert, Dewaele, and Agostinis 2007). It is suggested that the necrosis process results from a decrease in ATP levels, in a manner incompatible with cell survival (Buytaert, Dewaele, and Agostinis 2007).

Necrosis is the main type of death induced when photosensitizers are located on the plasma membrane, probably due to the loss of its integrity. Studies with Photofrin® and zinc (II) phthalocyanine showed an inability to maintain ion flow through the plasma membrane and a sudden reduction of ATP (Buytaert, Dewaele, and Agostinis 2007).

The major difference between necrosis versus apoptosis is the existence of an inflammatory response caused by necrosis which, however, may generate an antitumor immune response.

1.3.7.2. Effect of PDT in blood vessels

PDT may not only have tumour cells as the targets of action. Since the early 1980s, an additional indirect mechanism coexists with the cytotoxic effect of PDT, which is the effect of vascular obstruction, which causes death by induction of ischaemia and therefore provides another pathway for the treatment of solid cancers. As such, there has been a great deal of research into the development of photosensitizing molecules both with high selectivity for tumour cells and for tumour vasculature itself (M Laranjo 2014; Mafalda Laranjo et al. 2013; Sousa Brites 2016).

The vascular damage of PDT is because the photosensitizers are irradiated, confined in the bloodstream or accumulated in the endothelial cells or still attached to vessel walls, inducing loss of the tight junctions in the endothelial cells. These primary damages within the vessel lumen lead to thrombus formation and induce a cascade of reactions, namely, platelet aggregation, release of vasoconstricting molecules, lymphocyte adhesion, and increased vascular permeabilization. This collapse of the microvasculature associated with microhaemorrhage can cause severe hypoxia and, as such, tissue death (A.P. Castano, Demidova, and Hamblin 2005; Huang et al. 2008).

1.3.7.3. Immunity response to PDT

Several studies suggest that PDT induces an immune response in the host, and the innate immune system can be activated as the adaptive (M Laranjo 2014; Mroz et al. 2011; Sousa Brites 2016).

Direct destruction of tumour cells, vessel occlusion, and ischemia caused often result in an acute local inflammatory reaction initiated by the secretion of proinflammatory mediators (innate immunity), such as tumour necrosis factor α (TNF-α), interleukin-1 (IL-1) or interleukin-6 (IL-6), thereby activating adaptive immunity components, such as neutrophils, mast cells, macrophages and dendritic cells, which will restore homeostasis to the region affected by the treatment (local inflammation) (Mroz et al. 2011; Sousa Brites 2016).

Crosstalk between innate immunity and adaptive immunity is established through dendritic cells (DC). DCs, when activated by inflammatory mediators, pick up the tumour antigens, and go to the nearest lymph nodes. There, they expose the antigens to CD4+ T lymphocytes, making them active. In turn, these cells activate CD8+ T lymphocytes, which recognize and destroy tumour cells (Agostinis et al. 2011; Ana P. Castano, Demidova, and Hamblin 2005; Ana P. Castano, Mroz, and Hamblin 2006).

As such, in response to the photodynamic action of PDT, a local inflammatory response, as well as a systemic inflammatory response, may occur in the long term, thus allowing the eradication of metastases that are far from the irradiated site. In 2015, Rocha *et al.* have developed a photosensitizer

that can eliminate the primary tumour, eliciting a systemic immune response capable of controlling the metastasis (Rocha et al. 2015).

However, numerous clinical studies have demonstrated that PDT can not only trigger a stimulatory response on the immune system, as well as an immunosuppressive response (Agostinis et al. 2011; Mroz et al. 2011). The precise mechanisms that lead to each of these responses are not yet fully described, however, they are known to be related to the immune system, the treated area and the type of photosensitizer (M Laranjo 2014; Sousa Brites 2016). Immunosuppressive effects have only been associated with local reactions in skin lesion treatments with high irradiation areas (Ana P. Castano, Mroz, and Hamblin 2006; Mroz et al. 2011).

To improve the efficacy of clinical treatment by PDT, a greater understanding of the mechanisms associated with the immune response is needed (M Laranjo 2014; Sousa Brites 2016).

Chapter 2 : Results and Discussion

This chapter is divided into two parts. In **Part I** it is intended to present and discuss the results on the synthesis of platinum(II) chlorin complexes with different polarity degrees (esters, acids and alcohols) and with different substituents in the aryl groups (Ar = Ph, 4-ClC$_6$H$_4$, 4-MeOC$_6$H$_4$). The ester chlorins result from an [8π+2π] cycloaddition reaction of metalloporphyrins with diazafulvenium methide. The ester chlorins were hydrolysed or reduced to give the diacid or dialcohol chlorins, respectively. Furthermore, the photophysical characterization of the synthesized Pt(II) chlorins, as well as the evaluation of their aggregation in aqueous medium, were carried out. The disaggregation study was done using different surfactants.

In **Part II** it is intended to present and discuss the cytotoxicity of two surfactants (Pluronic P123 and Tween 20) used in Part I for the disaggregation of the Pt(II) chlorins; present and discuss the metabolic activity of all Pt(II) chlorins synthesized in **Part I**. This study was performed in three human tumour cell lines (A375, OE19 and HT1376). The results of the *in vitro* studies performed for the two chlorins (**11a** and **12a**) with more promising metabolic activity are also presented and discussed. These assays were performed for a tumour cell line (A375) and a normal cell line (HFF1).

2.1. Results and Discussion - Part I

The work was started with the synthesis of the diazafulvenium methide, in order to prepare platinum(II) chlorins through an [8π+2π] cycloaddition reaction with metalloporphyrins. From the cycloaddition reaction resulted diester chlorins, which were subsequently hydrolysed to their diacid or reduced to dialcohol chlorins, thereby varying the polarity of the synthesized dihydroporphyrins. The synthesis of the metalloporphyrins resulted from a previous insertion of a high molecular weight ion, platinum, into the free base 5,10,15,20-tetraarylporphyrins. The synthesized compounds had three distinct aromatic groups, a phenyl group, a phenyl group with a chlorine in the *para* position (electron attractor group for inductive effect, but electron donor for conjugation) and a phenyl group with a methoxy group in the *para* position (electron donating group). The general scheme of the synthesis of Pt(II) chlorins presented in this chapter is shown in **Scheme 2**.
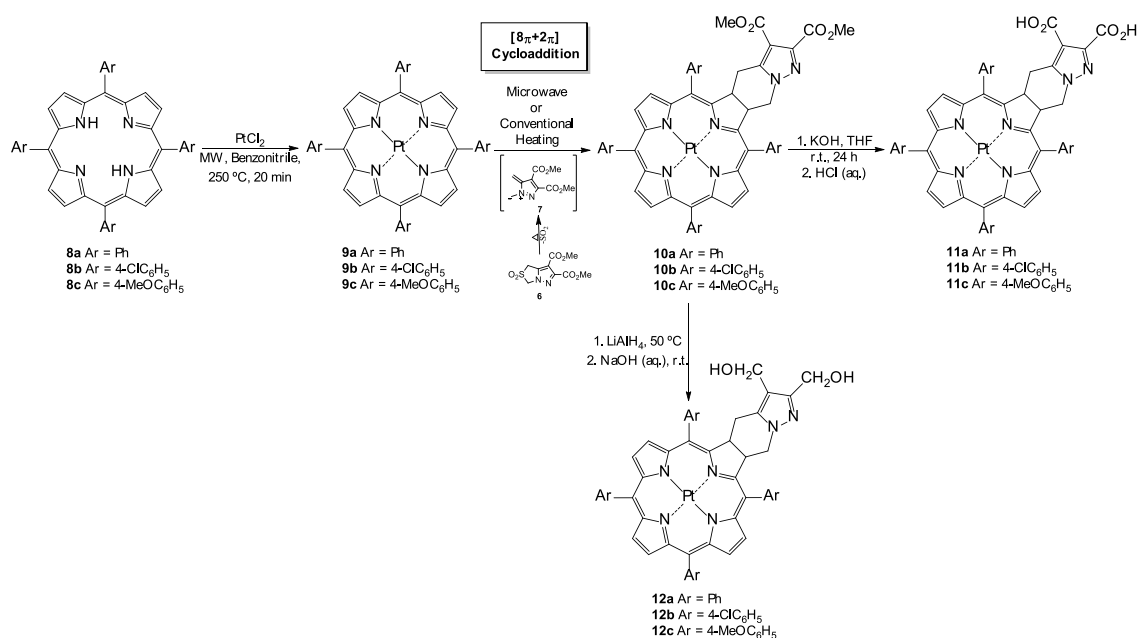
Scheme 2. Synthetic approach to the target Pt(II) chlorins.

2.1.1. Synthesis of precursors

2.1.1.1. Diazafulvenium methide

The synthetic strategy leading to diazafulvenium methide **7** precursors is shown in **Scheme 2.1** (Sutcliffe et al. 2000, 2001). First, thiazolidine **1** was prepared by the reaction between *L*-cysteine and formaldehyde. N-nitrosothiazolidine-4-carboxylic acid (**2**) was prepared by nitrosation of **1** with sodium nitrite in the presence of HCl, which reacted with trifluoroacetic anhydride to generate the mesoionic species **3**. This species can act as 1,3-dipole in cycloaddition reactions. Thus, by reacting dimethyl acetylenedicarboxylate dipolarophile with dipole **3**, cycloadduct **4** was formed. After *in situ* extrusion of carbon dioxide, species **4** gave dimethyl 1*H*,3*H*-pyrazolo[1,5-*c*]thiazole-6,7-dicarboxylate

(**5**) in 62 % yield. Oxidation of **5** with *meta*-chloroperoxybenzoic acid (mCPBA) led to the formation of dimethyl 2,2-dioxo-1*H*,3*H*-pyrazolo[1,5-*c*]thiazole-6,7-dicarboxylate (**6**) in 58 % yield. Diazafulvenium methide **7** is generated *in situ* from the thermal extrusion of sulfur dioxide from sulfone **6**.
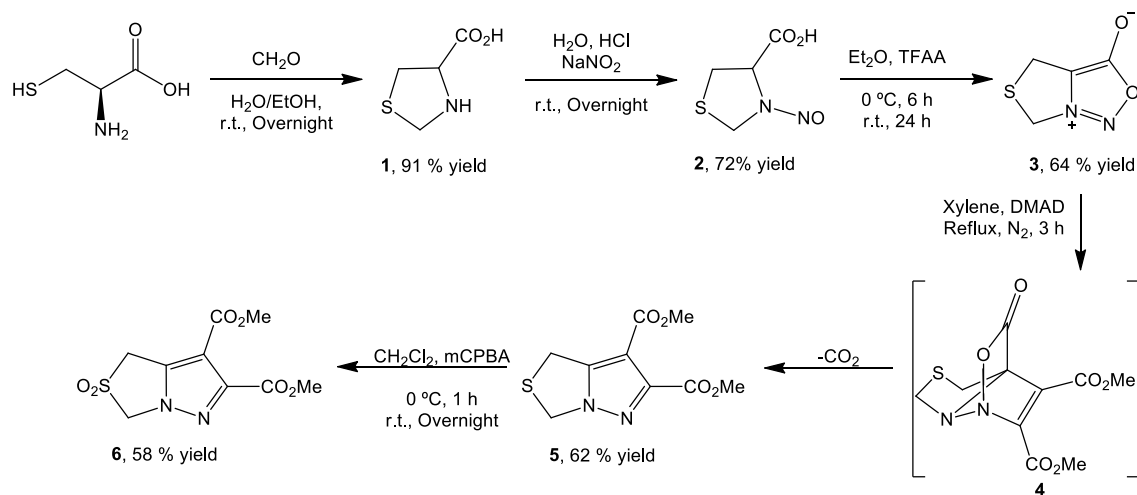
Scheme 2.1. Synthetic strategy for the preparation of the precursor of diazafulvenium methide **7**.

2.1.1.2. Porphyrins

Free base 5,10,15,20-tetraarylporphyrins were synthesized (**Scheme 2.2**), using a method developed by Rocha Gonsalves (Gonsalves, Varejão, and Pereira 1991). By reacting pyrrole with the desired aldehyde in equivalent amounts in a mixture of nitrobenzene and acetic acid (1:2) at 120 °C, the respective porphyrins were obtained. Porphyrins precipitated upon cooling of the mixture and after addition of methanol. Porphyrins **8a**, **8b** and **8c** were obtained in 20 %, 33 % and 31 % yield, respectively. These values are close to those described in the literature (Gonsalves, Varejão, and Pereira 1991; Pineiro et al. 1998).

8a Ar = Ph   20 %
8b Ar = 4-ClC$_6$H$_5$ 33 %
8c Ar = 4-MeOC$_6$H$_5$ 31 %
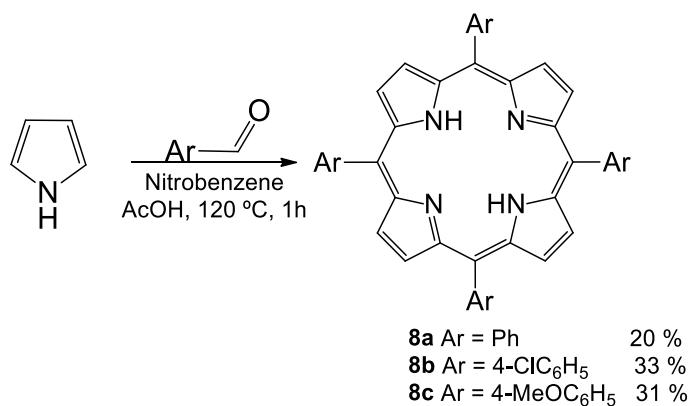
Scheme 2.2. Strategy for the synthesis of free base porphyrins **8**.

2.1.1.3. Metalloporphyrins

The next step was the synthesis of metallated platinum(II) porphyrins. Platinum complexes were prepared following a known general procedure (Naik, Joshi, Kaiwar, & Deshpande, 2003). Porphyrins **8** reacted with $PtCl_2$ in benzonitrile under microwave irradiation at 250 °C for 20 minutes, but varying certain reactional conditions (**Table 2.1**).

Table 2.1. Different synthetic strategies tested for the synthesis of metalloporphyrins **9**.

8a Ar = Ph
8b Ar = 4-ClC$_6$H$_5$
8c Ar = 4-MeOC$_6$H$_5$

9a Ar = Ph   90%
9b Ar = 4-ClC$_6$H$_5$ 58 %
9c Ar = 4-MeOC$_6$H$_5$ 77 %
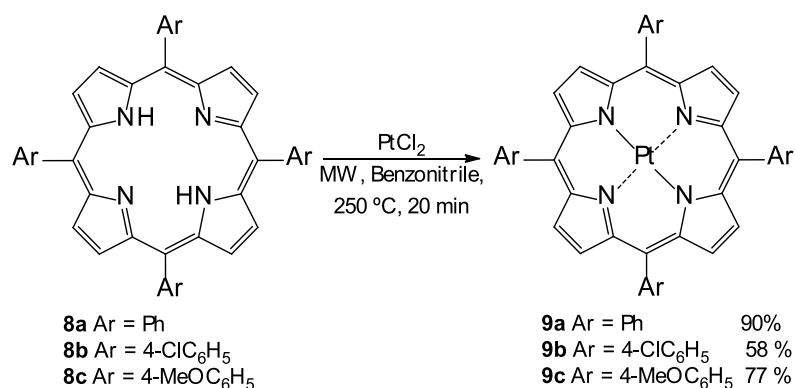
Entry	PtCl$_2$ (equiv.)	Anhydrous sodium acetate (equiv.)	Reaction conditions	Chlorin, % yield
1	3	5	Microwave 250 °C, 20 min	**9a**, 90
2	1.5	5	Microwave 250 °C, 20 min	**9b**, --*
3	3	0	Microwave 250 °C, 20 min	**9b**, 26
4	3	5	Microwave 250 °C, 20 min	**9b**, 58
5	3	5	Microwave 250 °C, 20 min	**9c**, 77

*The yield was undetermined, since by UV-Vis spectroscopy it was verified that, under these conditions, the reaction was not complete. As such, further heating by MW (250 °C, 20 min) was conducted, obtaining chlorin **9b** with 58% yield (Entry 4).

One of the reaction conditions studied for the synthesis of porphyrin **9b** was using of 1.5 equivalents of $PtCl_2$ (Entry 2). However, after microwave irradiation for 20 minutes a UV-Vis absorption spectrum was made, which indicated that only approximately 50 % of the corresponding matalloporphyrin had formed. Whereby, the amount of platinum chloride was doubled (Entry 4, 3 equivalents of $PtCl_2$). The reaction was again MW irradiated at 250 °C for another 20 minutes. At the end of this time, it was confirmed by UV-Vis that the reaction was complete. A further reaction

change consisted in carrying out the reaction in the absence of anhydrous sodium acetate (Entry 3). However, the porphyrin **9b** was obtained in significantly lower yield. On the other hand, carrying out the reaction with 5 equivalents of this salt **9b** could be obtained in 58 % yield which demonstrated that the presence of the anhydrous sodium sulfate is essential (Entry 4). The best yields for the platinum complexes **9a**, **9b** and **9c** were 90 %, 58 % and 77 %, respectively. Despite attempts to optimize the synthetic process of these Pt(II) complexes, the best results were obtained with the procedure described in the literature (Naik, Joshi, Kaiwar, & Deshpande, 2003), using 3 equivalents of platinum chloride and 5 equivalents of anhydrous sodium sulfate.

2.1.2. Synthesis and characterization of platinum(II) chlorins

2.1.2.1. Cycloaddition reaction for the synthesis of diester platinum(II) chlorins

Pinho e Melo et al. demonstrated that 1*H*,3*H*-pyrazolo[1,5-*c*]thiazole **6** reacts with different types of dipolarophiles, rich and electron-deficient. Therefore, the reactivity of metalloporphyrins **9** with diazafulvenium methide **7**, generated *in situ* by thermal extrusion of dimethyl 2,2-dioxo-1*H*,3*H*-pyrazolo[1,5-*c*]thiazole-6,7-dicarboxylate (**6**), was studied under different reaction conditions (**Table 2.2**). In a first approach, 1*H*,3*H*-pyrazolo[1,5-*c*]thiazole **6** was reacted with porphyrins **9** (2 equiv) in 1,2,4-trichlorobenzene under reflux to give chlorins **10a** , **10b** and **10c**, in yields of 8 %, 10 % and 2 %, respectively. In a second approach, 1*H*,3*H*-pyrazolo[1,5-*c*]thiazole **6** was reacted with porphyrins **9** (2 equiv) in 1,2,4-trichlorobenzene under MW irradiation at 250 °C for 20 minutes. Diester chlorins **10a**, **10b** and **10c** were obtained in yields of 20 %, 12 % and 22 %, respectively. Thus, it was possible to conclude that for the three metallochlorins (Ar = Ph, 4-ClC$_6$H$_4$ and 4-MeOC$_6$H$_4$), the best results were obtained under microwave irradiation at 250 °C, 20 min (Entry 2, 4 and 6), although no significant difference was obtained between the two methods in the synthesis of chlorin **10b**. Analysing these results we can conclude that the nature of the substituents in the aryl groups does not significantly affect the reactivity. The difference between conventional heating and microwave irradiation could be overcome by increasing the reaction temperature and/or time, however, such changes could lead to an increase of the chlorins' degradation, as well as an increase of secondary products. On the other hand, the use of an excess of porphyrin (2 equiv.) prevents the formation of *bis*-adducts, bacteriochlorins and isobacteriochlorins, giving selectively chlorins **10**. This represents an advantage over some cycloaddition methods involving porphyrins which, in some cases, give rise to mixtures of isomers and/or *bis*-adducts, always difficult to separate (Lemos and Lourenço 2010; Littler et al. 1999; Sobral et al. 2003).

The reaction control was carried out by UV-Vis absorption spectroscopy and the structural elucidation of the chlorins was achieved by nuclear magnetic resonance (NMR) spectroscopy.

Table 2.2. Synthesys optimization of diester chlorins **10** via [8π+2π] cycloaddition reaction of diazafulvenium methide **7** with metalloporphyrins **9**.
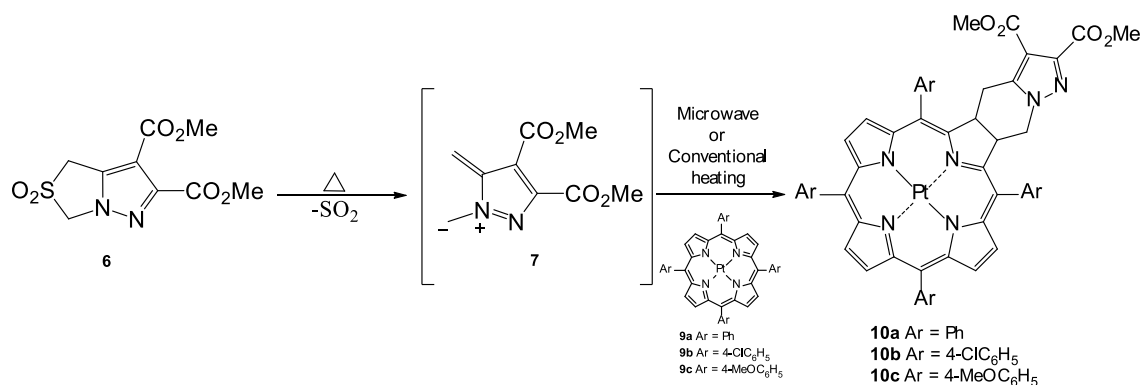
Entry	Reaction conditions	Chlorin, % yield
1	1,2,4-TCB, Conventional heating, 250 ºC, 3.5 h	**10a**, 8
2	1,2,4-TCB, Microwave, 250 ºC, 20 min	**10a**, 20
3	1,2,4-TCB, Conventional heating, 250 ºC, 3.5 h	**10b**, 10
4	1,2,4-TCB, Microwave, 250 ºC, 20 min	**10b**, 12
5	1,2,4-TCB, Conventional heating, 250 ºC, 3.5 h	**10c**, 2
6	1,2,4-TCB, Microwave, 250 ºC, 20 min	**10c**, 22

2.1.2.2. Derivatization of diester platinum(II) chlorins

The following step consisted on the derivatization of diester chlorins **10**, via the transformation of ester groups, in order to improve the hydrophilicity of the Pt(II) complexes for application in biological systems. On the one hand, it is known that a good photosensitizer to be used in PDT requires some amphiphilicity to accumulate in the cells (Boyle and Dolphin 1996; Wiehe et al. 2001), whereby macrocycles **10** were transformed into more hydrophilic compounds (diacids and dialcohols). On the other hand, it is known that the presence of carboxylic groups (diacids) and hydroxymethyl (dialcohols) substituents will allow further functionalization to make conjugates with specific biologically relevant molecules for targeted imaging applications. As such, the synthesis of these derivatives was carried out.

Diacid platinum(II) chlorins

In order to increase the hydrophilic character of the chlorin derivatives, chlorins bearing two carboxylic acid groups were prepared in the presence of KOH (saturated aqueous solution) in THF (**Scheme 2.3**).

Hydrolysis reactions are usually quantitative reactions. However, that was not the case for the studied chlorins as indicated by TLC, using an appropriate eluent [CH$_2$Cl$_2$/methanol (90:10) v/v].

Hence, a chromatographic column was carried out using the same eluent used for TLC control, giving the dicarboxylic acid derivatives **11a-11c** in 61 %, 88 % and 76 % yield, respectively.
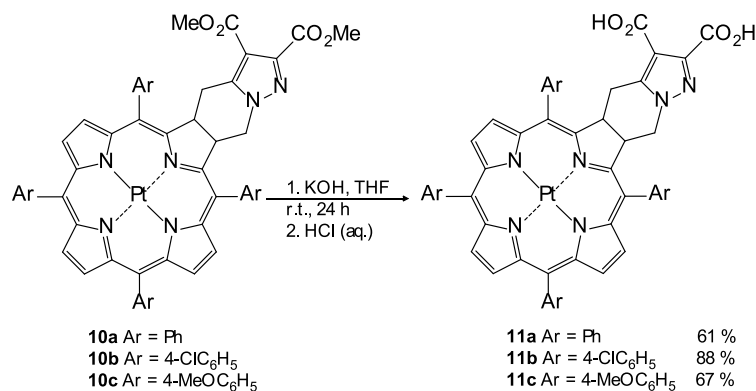
Scheme 2.3. Synthetic approach to diacid platinum(II) chlorins **11**.

Dialcohol platinum(II) chlorins

The derivatization study of Pt(II) diester chlorins **10** proceeded with the reduction of the ester groups to give the corresponding dihydroxymethyl derivatives **12** by using an excess of lithium aluminum hydride (LiAlH$_4$) (**Scheme 2.4**). Reduced chlorins **12a**, **12b** and **12c** were obtained in 81 %, 73 % and 20 % yield, respectively. The required reaction times were very different when varying the aromatic groups of the tetrapyrrolic macrocycles. For the synthesis of chlorins **12a** and **12b**, only 5 hours were required, whereas the synthesis of chlorin **12c** required 32 hours.
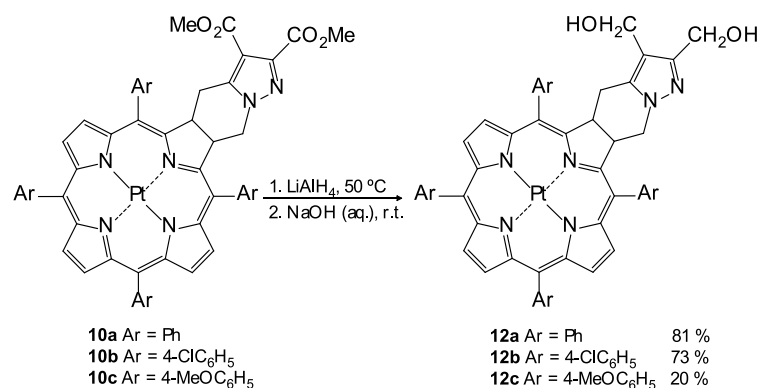
Scheme 2.4. Synthesis of dialcohol platinum(II) chlorins **12**.

2.1.3. Photophysical characterization of porphyrins and chlorins

The compounds presented in this dissertation were also characterized by molecular absorption spectroscopy. This technique provides important information for the possible application of the compounds as therapeutics agents, since the molecules must have some specific characteristics.

One of the characteristics that distinguishes porphyrins from other aromatic compounds is their strong absorption in the visible and NIR spectral regions. This characteristic is due to the different electronic transitions resulting from the high conjugation of the porphyrinic ring, which can occur when these molecules are subjected to irradiation with visible light.

On an absorption spectrum, free base porphyrins have a band with a high absorption coefficient in the near ultraviolet (around 400 nm), called Soret or B band, and a series of four bands of lower absorption coefficient (Q bands), which are located in the visible region (between 500 and 700 nm). However, metalloporphyrins have only three absorption bands, a Soret band, with high molar absorptivity, but with limited applicability as theranostic agent, due to the small degree of penetration of this radiation in the biological tissues and, two Q bands, on visible region (therapeutic window), but with a small molar absorptivity.

Absorption spectra of chlorins show changes in relation to porphyrins, namely an increase in absorption intensity and a bathochromic shift of the bands (to longer wavelengths). The latter feature represents an advantage of chlorins over porphyrins regarding their application as theranostic agents, since light may penetrate deeper into biological tissues by the use of longer wavelengths.

2.1.3.1. The absorption spectra of porphyrins and chlorins

The absorption spectra of porphyrins and chlorins were interpreted by several authors (Ghosh 2000; Longuet-Higgins, Rector, and Platt 1950; Platt 1950; Stillman, Mack, and Kobayashi 2002), but the theoretical model proposed by Gouterman ("four orbital model") (Gouterman 1959, 1961) has prevailed until today, since it explains and interprets, in a simple way, the changes observed in the spectra of the tetrapyrrolic macrocycles, by small structural variations. According to this, the absorption spectrum of this class of compounds can be interpreted on the basis of the electronic transitions between the two occupied high energy orbitals HOMO (highest occupied molecular orbital) designated by b_1 and b_2 and the two low energy unoccupied orbitals, LUMO (lowest unoccupied molecular orbital) designated by c_1 and c_2.

According to Gouterman (Gouterman 1959, 1961) a system of x and y cartesian axes can be arbitrated in the macrocycle structure, being that B_x, B_y, Q_x and Q_y transitions can occur (**Figure 2.1**). Q_y band originates from the transition between the $b_1 \rightarrow c_1$ orbitals and Q_x band at the transition between $b_1 \rightarrow c_2$. On the other hand, the bands B_x and B_y correspond to the transitions $b_2 \rightarrow c_1$ and $b_2 \rightarrow c_2$, respectively. In addition, it is also important to consider the base structure of the porphyrins, which may have D_{4h} symmetry if they are metallated or D_{2h} symmetry if they are in the free base form (**Figure 2.1**). In the case of porphyrins with D_{4h} symmetry, the two HOMO orbitals (b_1 and b_2) and the two LUMO (c_1 and c_2) orbitals are practically degenerate, resulting in a pair of lower energy transitions, Q_x and Q_y, and a pair of energy transitions of higher energy, B_x and B_y. However, in porphyrins with D_{2h} symmetry, degeneracy is lost and the orbitals energy changes, resulting in a division of the transitions Q_x and Q_y (lower energy) and the transitions B_x and B_y (higher energy).

Bands B_x, B_y, Q_x and Q_y can be represented by B_x(0-0), B_y(0-0), Q_x(0-0) and Q_y(0-0), in case of transitions between the zero vibrational level from the ground state to the zero vibrational level of the excited state. And, associated with the transitions Q_x(0-0) and Q_y(0-0), there are still Q_x(1-0) and Q_y(1-0) transitions that are attributed to an electronic movement to a higher vibrational level in relation to the previous ones. However, B_x(0-0) and B_y(0-0) transitions have a minimal energy difference, appearing as a single large band around 400 nm (Minaev et al. 2006).
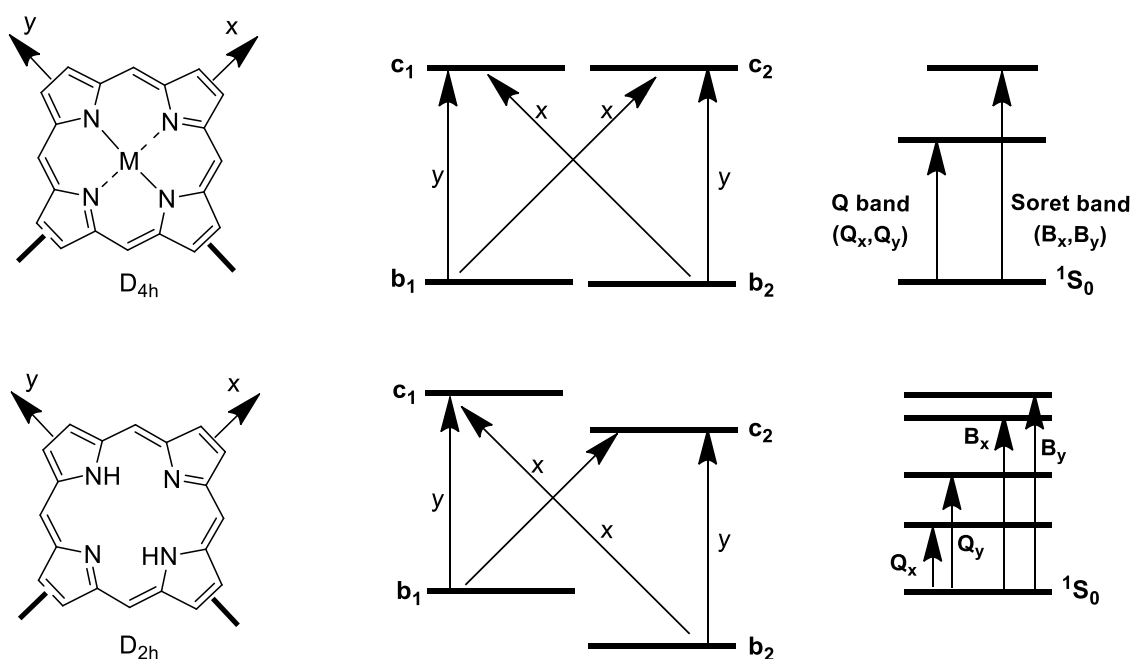
Figure 2.1. Representation of electron transitions of porphyrins with symmetry D_{4h} (ex. metalloporphyrins) and D_{2h} (free base porphyrins) according to the "four orbital model" of Gouterman (adapted from Nemykin and Hadt 2010).

As an example, free base porphyrin **8a** presents four Q bands, with wavelengths at 650, 592, 548 and 515 nm and a Soret band at 412 nm (Pineiro et al. 1998). The respective metalloporphyrin **9a** has two Q bands at 540 and 510 nm and a Soret band at 402 nm (Chizhova, Kulikova, and Mamardashvili 2013). These values are from spectra recorded in dichloromethane.

Influence of substituents on the absorption spectra of porphyrins and chlorins

Intensity of the four Q bands is variable and is entirely related to the substituent groups present in the macrocycle, since they can stabilize or destabilize HOMO and LUMO orbits of the porphyrinic ring (Nemykin and Hadt 2010).

Figure 2.2 shows the absorption spectra of metalloporphyrins **9a**, **9b** and **9c** (Spectrum A) as well as diester chlorins **10a**, **10b** and **10c** (Spectrum B). All spectra were acquired using acetone as

solvent, because the influence of solvent on molar absorption coefficients and on absorption wavelengths has been described in the literature (Academy and Interdisciplinar 2008). By analysing the spectra, it can be observed that the relative intensity of the Q bands is not altered by the substituent, either in porphyrins or in chlorins. This was predictable, since substitution occurs on the phenyl ring and not on the tetrapyrrole macrocycle.
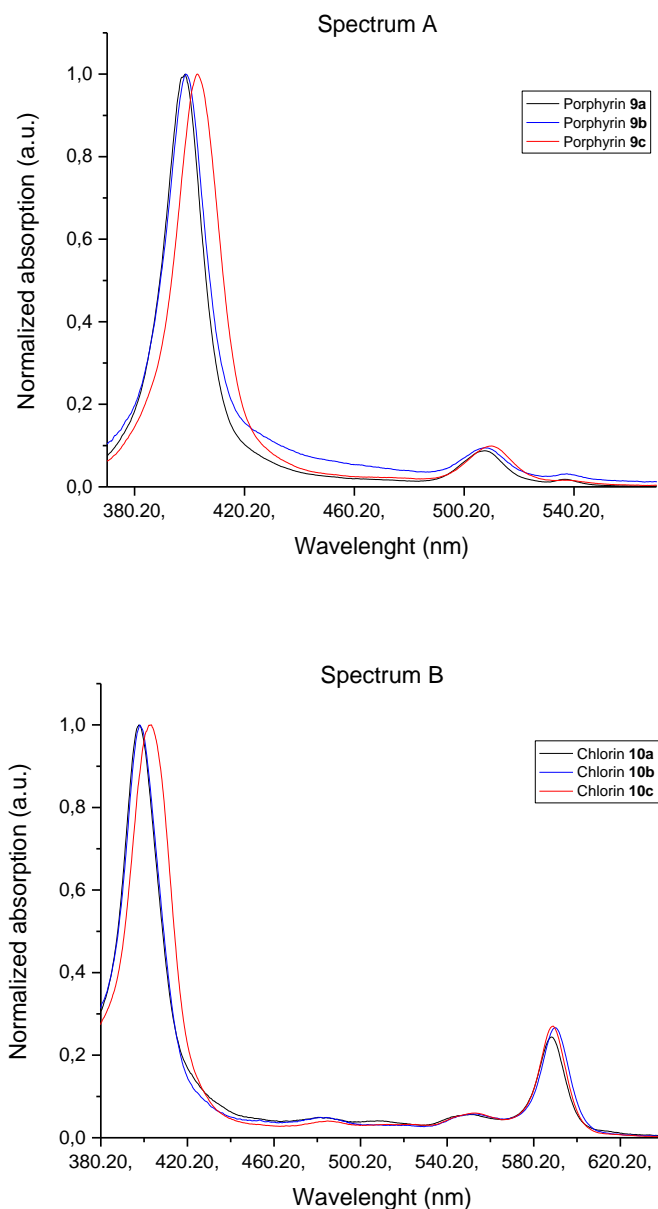
Figure 2.2. Absorption spectra of metalloporphyrins **9** (Spectrum A) and metallochlorins **10** (Spectrum B).

According to Gouterman, substitution of a group in the *meso* positions, namely the reduction of the porphyrins to chlorins, leads to a change in the energy and symmetry of the fundamental state b_1, without affecting b_2, as predicted by the molecular orbitals calculated by Longuett-Higgins (Mesquita

et al. 2014). As state b_1 is directly related to the intensity of Q bands, a perturbation of the molecular orbitals of this electronic state will contribute to a significant change in the relative intensity of these bands. Additionally, in chlorins a bathochromic shift of the UV-Vis spectrum of Q bands is observed in relation to the porphyrins, since the energy required to excite the electron from a state of lower energy to one of higher energy increases with the number of electrons in the porphyrinic ring. Thus, chlorins with 20 π-electrons absorb less energy (longer wavelengths), than porphyrins with 22 π-electrons (MacDonald and Dougherty 2001).

The platinum(II) metallochlorins studied in this Master's dissertation present one Q band of higher intensity around 590 nm, a region located in the therapeutic window. This makes these compounds good for use as theranostic agents. The maximum absorption wavelengths for all synthesized Pt(II) chlorins (chlorins **10**, **11** and **12**) are shown in **Table 2.3**.

Table 2.3. Wavelength of maximum absorption of chlorins **10**, **11** and **12** in acetone.

Entry	Chlorin	Absoption λ_{max} (nm)				
		$Q_{x\,(0\text{-}0)}$	$Q_{x\,(1\text{-}0)}$	$Q_{y\,(0\text{-}0)}$	$Q_{y\,(1\text{-}0)}$	$B_{\,(0\text{-}0)}$
1	**10a**	588	550	509	482	398
2	**10b**	590	550	510	482	399
3	**10c**	589	550	510	482	403
4	**11a**	590	551	509	482	398
5	**11b**	582	561	546	517	409
6	**11c**	591	551	516	482	404
7	**12a**	590	551	513	484	398
8	**12b**	590	551	513	484	398
9	**12c**	590	551	513	484	403

2.1.3.2. Determination of molar absorption coefficients

The molar absorptivity value for each band of the absorption spectra of the synthesized compounds was calculated. Solutions of these compounds were prepared in toluene with concentrations between 10^{-5} and 10^{-6} M. Using the Beer-Lambert law (A=εbc, where A is the absorbance, ε is the molar absorptivity coefficient, b is the optical path travelled by light and c is the concentration of solution), absorption as a function of concentration is plotted on a graph (**Figure 2.3**). The slope of the adjusted line determines the molar absorptivity coefficient (ε) for Q and Soret bands. Correlation coefficients obtained for the straight lines were high and, in the range of the concentrations used, we did not find any deviation to Beer-Lambert law ($r^2>0.99$), which indicates the absence of aggregation of the compounds in the range of concentration and with the solvent studied (Longuet-Higgins, Rector, and Platt 1950).

In **Figure 2.3** we present a selected example of the graph plot used in the determination of ε for the B band of chlorin **11a**. All other ε values were determined in the same way and are presented in **Table 2.4**.
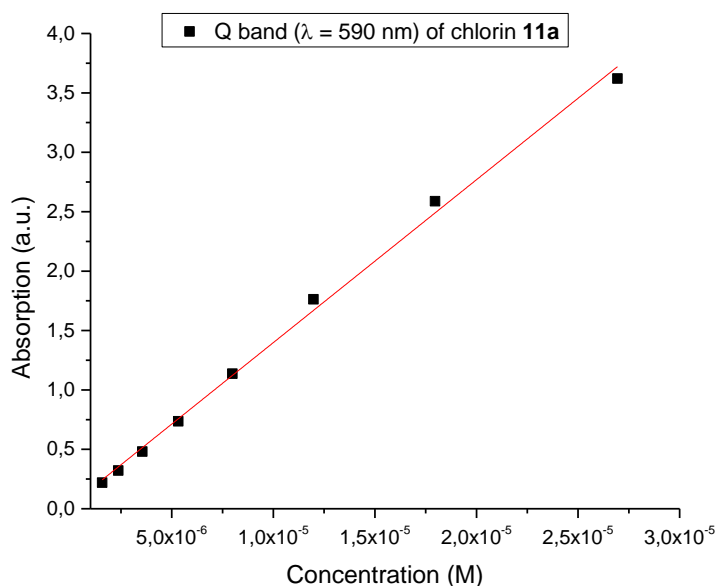
Figure 2.3. Absorbance plot as a function of concentration for $Q_{x(0-0)}$ band (λ = 590 nm) of chlorin **11a**.

In **Figure 2.3** we present a selected example of the graph plot used in the determination of ε for the B band of chlorin **11a**. All other ε values were determined in the same way and are presented in **Table 2.4**.

The resulting metallochlorin **11a** showed an intense $Q_{x\,(0-0)}$ band, with ε_{max} values of more than 1 x 10^4 $M^{-1} \cdot cm^{-1}$ at 590 nm. The λ_{max} and ε_{max} values of **11a** are comparable to those of 5,10,15,20-tetrakis(3-hydroxyphenyl)chlorin (Foscan®) (Obata et al. 2009). Foscan® is a photosensitizer used in photodynamic therapy for the treatment of squamous cell carcinoma of the head and neck. The λ_{max} and ε_{max} values of **11a** are also comparable to those of 5,10,15,20-tetrakis(pentafluorophenyl)chlorins (Obata et al. 2009).

Table 2.4. Wavelength of maximum absorption and molar absorptivity coefficients of chlorin **11a** in toluene.

Entry	Wavelenght (nm)	ε ($M^{-1}cm^{-1}$)
1	402	1.4×10^5
2	511	1.1×10^4
3	540	6.3×10^3
4	590	1.4×10^4

Previously in the research group it was observed that chlorins **10a** and **12a,** in solution at room temperature, show fluorescence and phosphorescence emission (Pereira et al. 2017). This provides the possibilities for using this kind of PS for NIR imaging. On the other hand, the phosphorescence was highly sensitive to oxygen and increased when the concentration of O_2 in solution was reduced. This allowed determination of the fluorescence quantum yields using oxygen saturated solutions, where the phosphorescence was effectively quenched, while the fluorescence was little affected (Pereira et al. 2017). This phototophysical characteristic indicates that these Pt(II) complexes may be used as ratiometric oxygen sensors, and this is important because oxygen concentration can provide information on the cell state.

It was verified that the synthesized platinum(II) chlorins present excellent requirements for use as theranostic agents. They have high thermal stability, absorption bands around 600 nm (biological-applicable absorption), increased absorption coefficients and favourable photochemical properties for molecular imaging.

Another requirement that a theranostic agent must present is the possibility of dissolution in aqueous medium. As such, an aggregation study was performed for chlorins **10**, **11** and **12**.

2.1.4. Aggregation studies of platinum(II) chlorins

It has been shown that the aggregation of PS used in PDT plays a decisive role in the photodynamic activity of these compounds, since this depends on the physicochemical properties and the photophysical behaviour of PS. Aggregation dramatically reduces singlet oxygen generation capacity. This is because the aggregates cause a decrease in the lifetime of singlet and triplet states of the photosensitizer, resulting in a decrease in the quantum yield of singlet oxygen, which decreases the photodynamic efficiency of the PS. Accordingly, it is necessary that the PS is solubilized and in the monomeric form (Crouch and Langford 1990; Daziano et al. 1996). Knowledge of the relationship between aggregation and photodynamic activity may facilitate drug development and may contribute significantly to increasing of PDT efficacy.

It has been described that derivatives of hematoporphyrin present Soret band with maximum absorption at around 370 nm (attributed to aggregates) and/or at 395 nm (attributed to monomeric species) (Rotomskis, Bagdonas, and Streckyte 1996). According to Rotomskis *et al.* the formation of large aggregates is associated to the high concentrations of PS that create anaerobic conditions, making it difficult to penetrate the oxygen that plays an important role in the processes of degradation and formation of photoproducts (Rotomskis, Bagdonas, and Streckyte 1996). Hematoporphyrin derivatives present two types of aggregates formed in aqueous solution, being "J" aggregates (linear type) and "H" aggregates (sandwich type). In the absorption spectrum, "H-type" aggregates (face-to-face arrangement) cause a hypsochromic shift (a blue shift) of both Soret and Q bands, whereas "J-type" aggregates (side-by-side arrangements) promotes a slight shift of the Soret band to the blue and

a bathochromic shift (a red shift) of the Q bands (Rotomskis, Bagdonas, and Streckyte 1996; Streckyt and Rotomskis 1993).

In order to study the occurrence of aggregation at high concentrations, absorption spectra were obtained in the region of 350 to 700 nm. Spectral differences of dissolved Pt(II) complexes in a solution of 10 µM of PS in DMSO and in an equimolar solution of PS in PBS (pH 7.4) were observed. **Figure 2.4** refers to the study for chlorin **10a**.
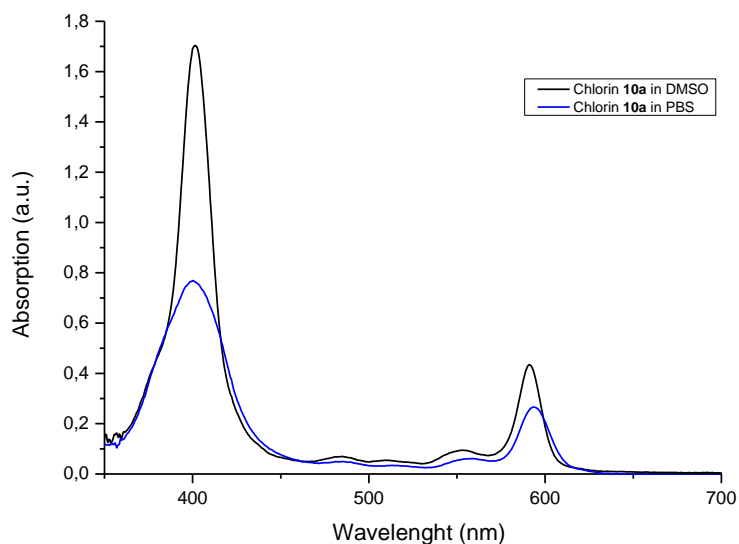
Figure 2.4. Spectral differences of chlorin **10a** dissolved in a solution of 10 µM in DMSO and in an equimolar solution of the same PS in PBS (pH 7.4).

A decrease in Soret and Q bands absorption and a blue shit of the last Q band, which is attributed to the appearance of aggregates, was observed. Thus, it was concluded that with a concentration of 10 µM, the previously synthesized platinum chlorins were aggregated (**Figure 2.4**). Therefore, knowing that the PS in its aggregate form are not very active due to the low generation of singlet oxygen and that the state of aggregation can generate problems of administration and incorporation of the drugs by the cells, disaggregation studies were performed using nonionic surfactants (Ivanov 2000; Menezes et al. 2004; Moan and Kessel 1988).

2.1.5. Effect of non-ionic surfactants on the disaggregation of platinum(II) chlorins

It is known that the incorporation of porphyrins into micelles changes their state of aggregation (Woodburn et al. 1994). Micelles are defined as thermodynamically stable colloidal aggregates, and spontaneously form when a certain concentration of surfactant in solution (critical micellar concentration - cmc) is reached. Surfactants are also known as amphiphilic species. When surfactants are added in solution, they migrate to the interface, reducing the surface tension of solvent, due to its

self-aggregation (Streckyt and Rotomskis 1993). Surfactants are chemical compounds with long carbon chains and a hydrophilic group at one end. This allows the formation of micelles in biological medium, which can carry the PS thereby increasing solubility. In so doing, they have been widely used for enhancing solubilisation of drugs which are poorly soluble in biological médium (Hamzeloo-Moghadam and Taiebi 2014; Patel and Datta 2009). Therefore, we set out to develop a surfactant-based novel formulation.

In this work, experiments were performed in the presence of neutral surfactants in order to investigate how aggregation of Pt(II) complexes is affected by the presence of a micellar medium. Surfactants studied were glycerol (1 and 10 % v/v), Pluronic F127 (1 % v/v), Pluronic P123 (0.2 and 1 % v/v) and Tween 20 (0.003 to 1 % v/v).

In **Figure 2.5** the study with said surfactants for chlorin **10a** is shown. Spectrum A refers to the disaggregation study using 1 and 10 % v/v of glycerol. Spectrum B relates to the use of Pluronics F127 and P123 (1 % v/v) and Spectrum C is related to the use of Tween 20 (1 % v/v).
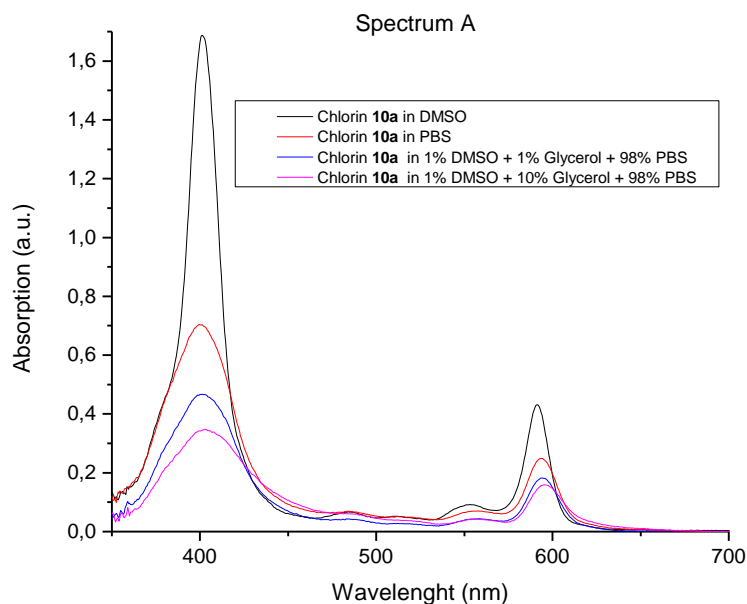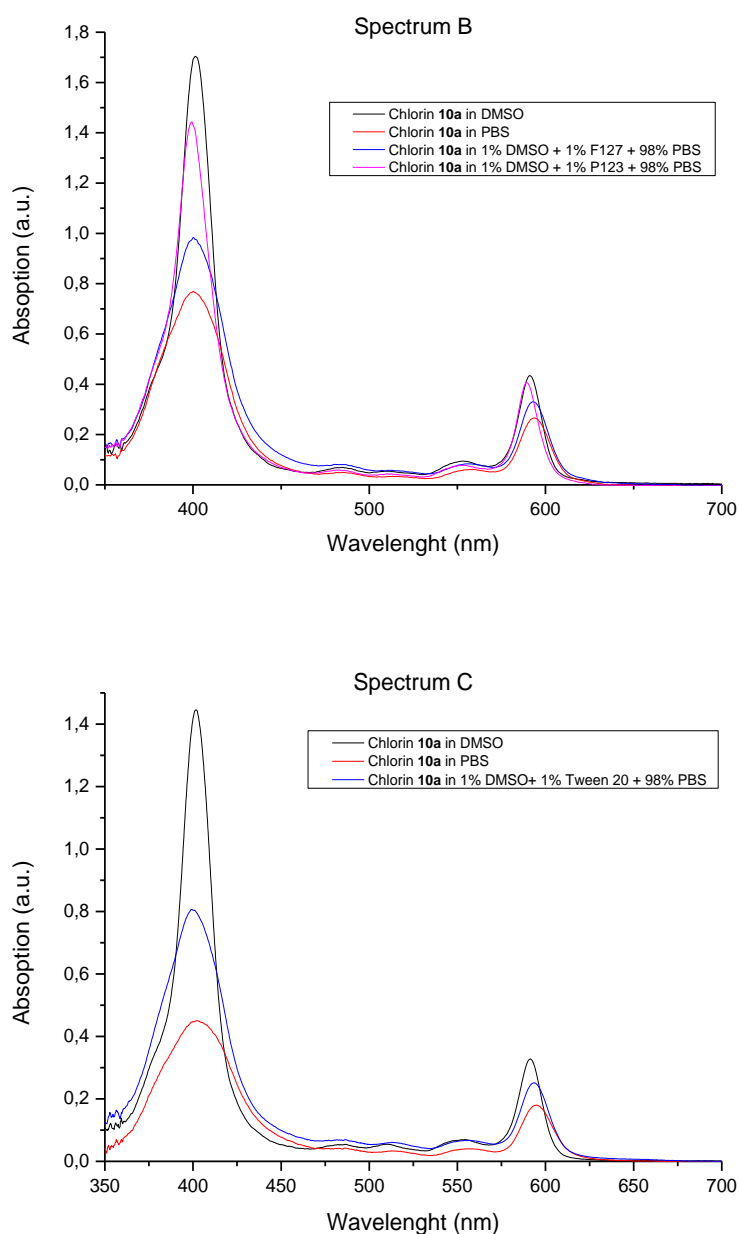
Figure 2.5. Disaggregation studies using Glycerol (Spectrum A), Pluronics P123 and F127 (Spectrum B) and Tween 20 (Spectrum C) as surfactants.

Analysing these spectra, it is possible to conclude that glycerol does not lead to the disaggregation of chlorin **10a**, however, Tween 20 (1 % v/v) and Pluronics (1 % v/v) lead to disaggregation. Pluronic P123 is more effective than F127, since cmc in water at T = 20 °C for F127 is 3.8 % v/v, and for P123 it is about 0.18 % v/v (Alexandridis, Holzwarth, and Hatton 1994). As such, disaggregation of P123 at a concentration of 0.2 % v/v was evaluated. The disaggregation absorption spectrum for chlorin **10a** is shown in **Figure 2.6**.
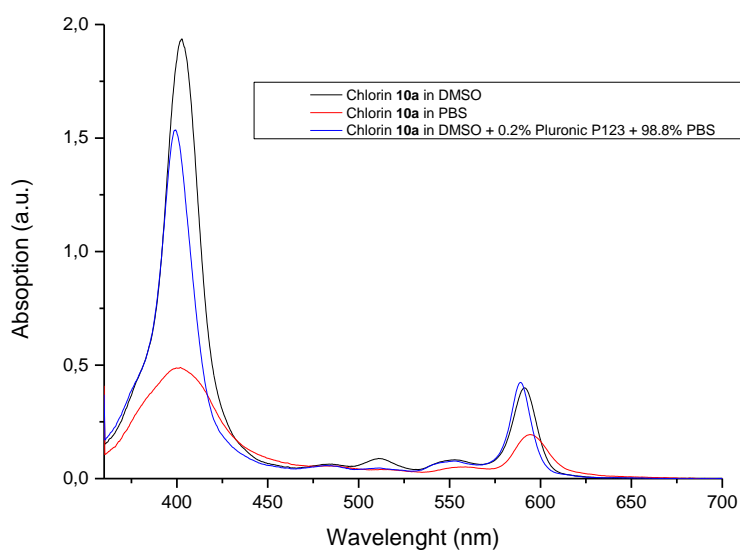
Figure 2.6. Disaggregation with 0.2 % v/v Pluronic P123.

From **Figure 2.6** it can be concluded that there is disaggregation of chlorin **10a** with the concentration of Pluronic used.

As no cmc values for Tween 20 were found in the literature, a screening of concentrations was performed between 0.003 and 0.03 % v/v to determine whether disaggregation using this surfactant was maintained (**Figure 2.7**). With this study it was rea lized that the bands maintained the same maximum absorption wavelengths, which is indicative that the decrease of intensity of the bands is not due to the fact that there is aggregation but only due to the change in concentration.
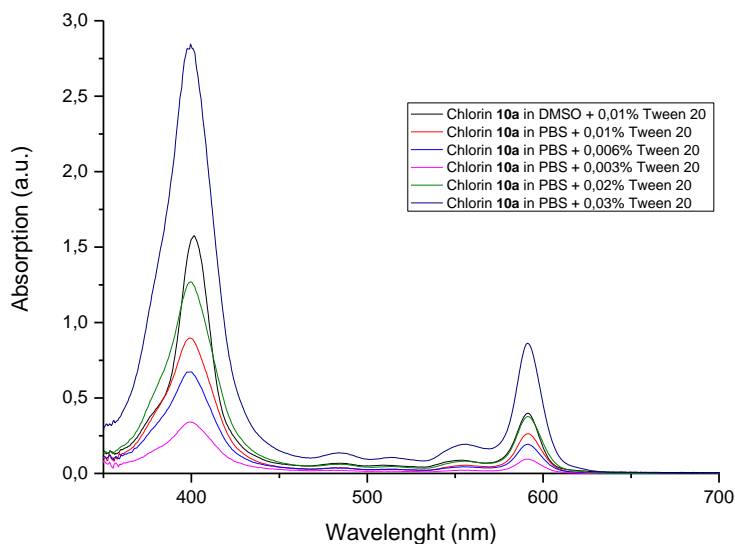
Figure 2.7. Disaggregation with Tween 20 at different concentrations.

33

One of the initial goals of this Master's project was the biological evaluation of platinum(II) chlorins. However, when it was found that they would aggregate in biological medium (aqueous medium, previously mimicked by PBS), cell viability study using Tween 20 and Pluronic P123 was also carried out. Among the studied surfactants, these two were the most promising in the disaggregation of the chlorins under studjmoky. **Part II** will present their cell toxicity results.

2.2. Results and Discussion - Part II

2.2.1. Photocytotoxicity and dark cytotoxicity

Having found in **Part I** of this chapter that the platinum complexes in study aggregated into PBS, and would certainly aggregate in biological medium, they were disaggregated using surfactants. It is known that the aggregation dramatically reduces ROS generation capacity, thereby reducing the photodynamic efficiency of the photosensitizers. As such, the photoactive principle is solubilized and in monomeric form (Crouch and Langford 1990; Daziano et al. 1996). Therefore, after synthesis and chemical analysis, cytotoxicity studies of Pluronic P123 and Tween 20 surfactants were performed against melanocytic melanoma (A375) cell line.

The evaluation of cytotoxicity by the MTT assay is very useful for rapid screening of various compounds since it provides an indication of the metabolic state, with the main contribution of mitochondrial enzymes (Mosmann 1983). The reduction of MTT is influenced not only by viability, but also by several factors intrinsic to the metabolism itself that is not dependent on mitochondria alone (Vistica et al. 1991).

For Pluronic P123 the concentrations studied were 1 %, 0.5 %, 0.25 % and 0.20 % v/v (**Figure 2.8**) and for Tween 20 the concentrations tested were 1 %, 0.5 %, 0.2 %, 0.1 %, 0.05 %, 0.01 %, 0.005 % and 0.001 % v/v (**Figure 2.9**). The results of metabolic activity obtained for each concentration were compared with the values obtained for DMSO (1 % v/v), vehicle previously used in the Group, whose cytotoxicity is well defined.
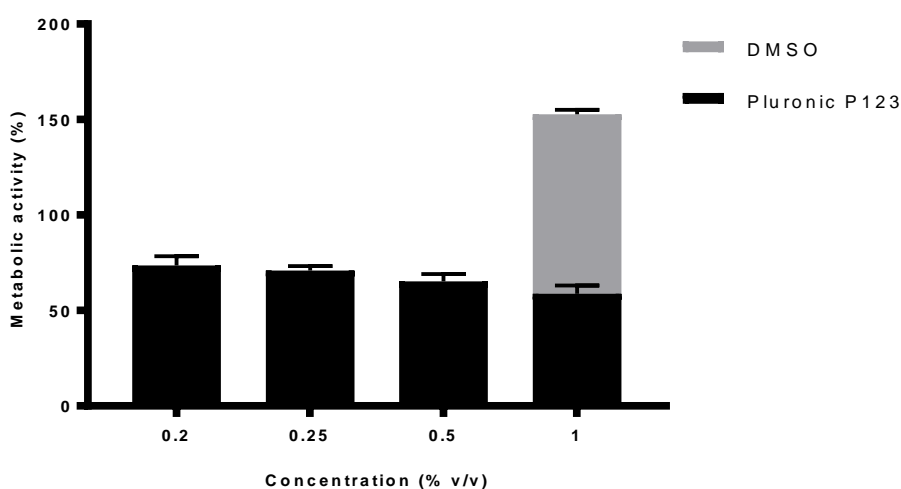
Figure 2.8. Metabolic activity of melanocytic melanoma cells exposed to DMSO 1 % v/v and Pluronic P123 (using different concentrations). Results are presented as mean $\pm$ SE (n = 6).
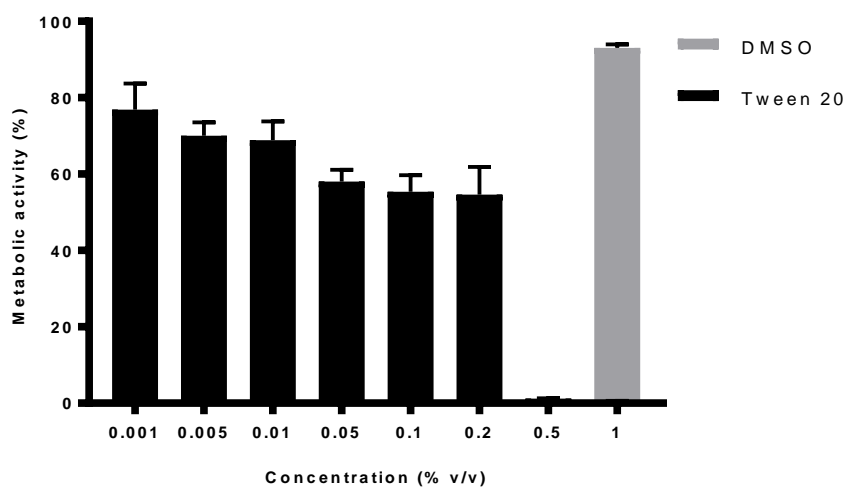

Figure 2.9. Metabolic activity of melanocytic melanoma cells exposed to DMSO 1 % v/v and Pluronic P123 (using different concentrations). Results are presented as mean $\pm$ SE (n = 6).

Analysing the results represented in **Figures 2.8** and **2.9** it was verified that metabolic activity was dependent of surfactants concentration used.

For Pluronic P123 all concentrations tested in biological medium had higher cytotoxicity than DMSO 1 % v/v. The metabolic activity of DMSO 1 % v/v was 94.69 $\pm$ 5.70 % and that of 0.2 % v/v of Pluronic P123 (lowest tested concentration) was significantly lower (73.57 $\pm$ 11.73 %). As such, this surfactant cannot be used for the disaggregation of the platinum chlorins under study.

Likewise, it was verified that Tween 20 also cannot be used for disaggregation of said complexes, since the cellular toxicity obtained at the lowest concentration (0.001 % v/v) was meaningfully higher than that for DMSO 1% v/v. It was verified that the metabolic activity of DMSO 1 % v/v was 93.02 $\pm$ 2.27 % and that at 0.2 % v/v concentration of Tween 20 was 73.57 $\pm$ 11.73 %.

Since it was not possible to completely disaggregate platinum(II) complexes using solvents compatible with the studies in cells, cytotoxic studies of diester (**10a, 10b** and **10c**), diacid (**11a, 11b** and **11c**) and dialcohol (**12a, 12b** and **12c**) chlorins were performed in their aggregate form, using the standard procedure with solubilization in 1 % DMSO (Mafalda Laranjo et al. 2013; Pereira et al. 2015, 2017, 2018). The evaluation of PDT on metabolic activity was performed against three human cancer cell lines, the HT1376 line of bladder carcinoma, the OE19 line of oesophageal carcinoma and the A375 line of melanocytic melanoma.

Experimental results obtained by MTT assay after 24 hours of photodynamic treatment for chlorins **11** and **12** were adjusted to s sigmoid dose-response model as depicted in **Figures 2.10** and **2.11**. From the equation of each curve the mean point corresponding to the IC_{50} value was calculated. IC_{50} values for chlorins **10** were not calculated as being greater than 10 μM (highest concentration tested).
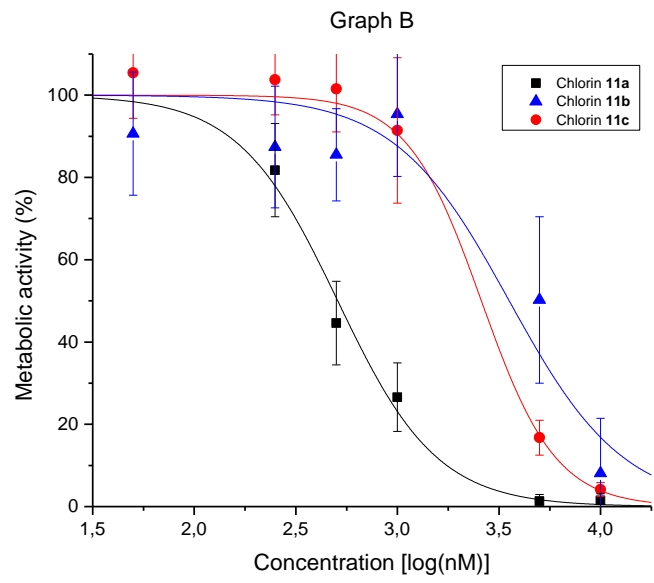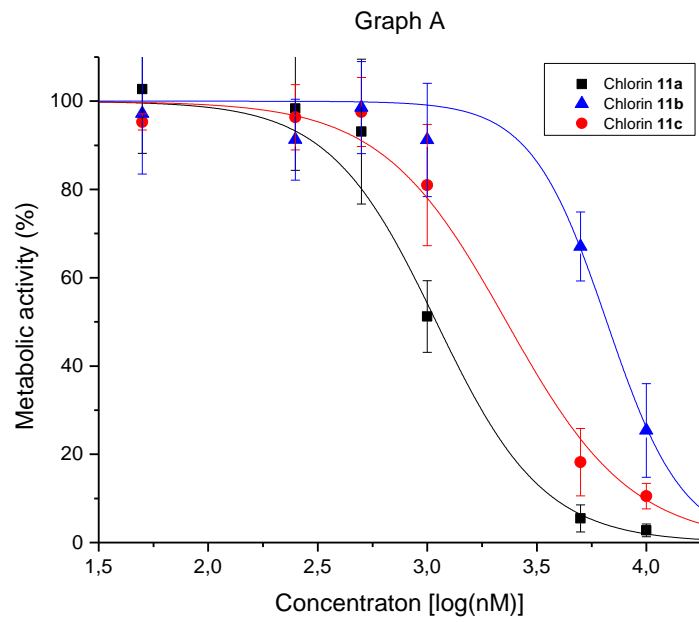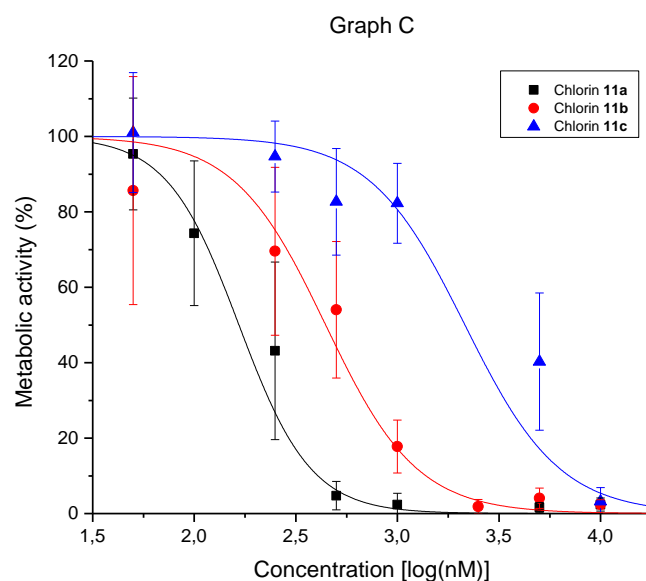
Graph A

Graph B

Figure 2.10. Dose-response curves for chlorins **11** in human bladder carcinoma (Graph A), oesophageal carcinoma (Graph B) and melanoma (Graph C) cell lines after 24 hours of photodynamic treatment. Results are presented as mean ± SD (at least n = 9).

From **Figure 2.10** it can be concluded that for the three tumour cell lines, the diacid chlorin with a lower IC_{50} value was chlorin **11a**. In the bladder carcinoma cell line it had an IC_{50} of 1098 nM, in the oesophageal carcinoma cell line it had an IC_{50} of 499 nM and the melanoma cell line had an IC_{50} of 166 nM. IC_{50} values and respective 95 % confidence intervals are shown in **Table 2.5** (Entry 1, 2 and 3).
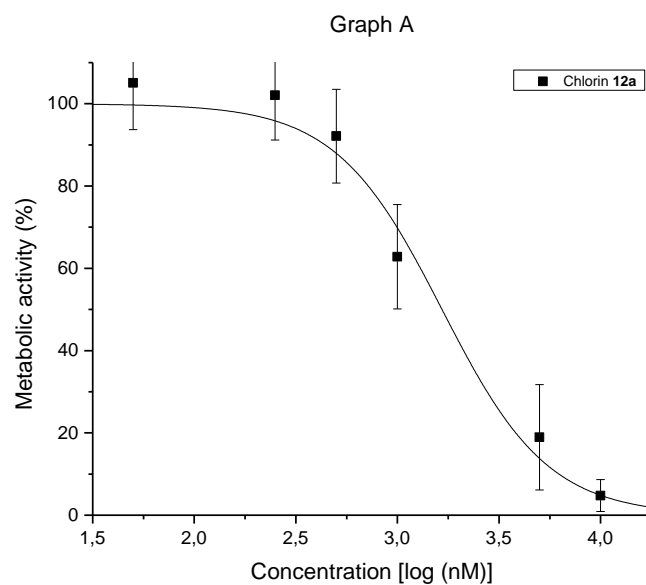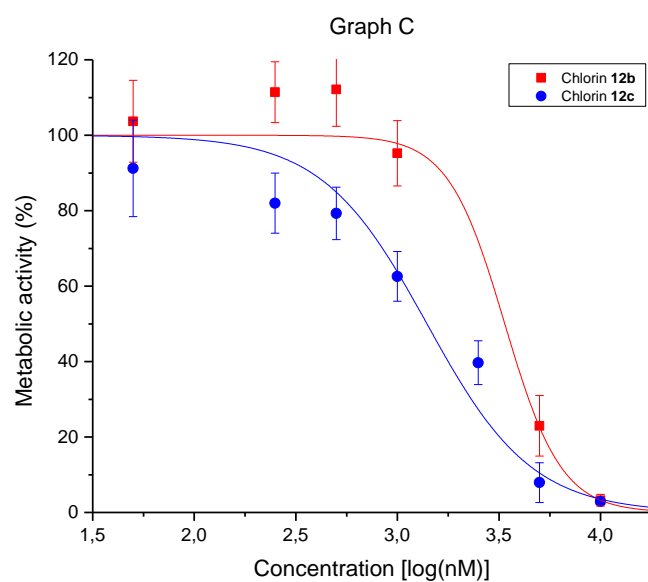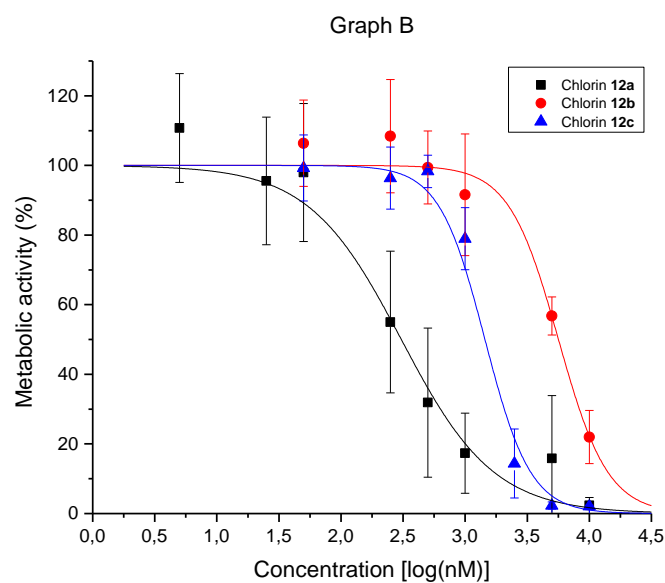
Figure 2.11. Dose-response curves for chlorins **12** in human bladder carcinoma (Graph A), oesophageal carcinoma (Graph B) and melanoma (Graph C) cell lines after 24 hours of photodynamic treatment. Results are presented as mean ± SD (at least n = 9).

From **Figure 2.11** it can be concluded that dialcohol chlorin with a lower IC_{50} value was the chlorin **12a**. In the bladder carcinoma cell line it had an IC_{50} of 1657 nM and in the oesophageal carcinoma cell line it had an IC_{50} of 306 nM. In the melanoma cell line IC50 is 144 nM, and this value had previously been described in the literature (Pereira et al. 2017). IC_{50} values and respective 95 % confidence intervals are shown in **Table 2.5** (Entry 4, 5 and 6).

In Graph A (**Figure 2.11**) the sigmoid curves for chlorins **12b** and **12c** are not represented because they have IC_{50} values greater than 10 μM and it is not possible to adjust the values obtained for this model.

Table 2.5. IC_{50} levels of chlorin **11** e **12** in human bladder carcinoma cell lines (HT1376), oesophageal carcinoma (OE19) and melanoma (A375), 24 hours after photodynamic treatment.

Entry	Chlorin	IC50 ± CI$_{95\%}$ (nM) against HT136 cell line	IC50 ± CI$_{95\%}$ (nM) against OE19 cell line	IC50 ± CI$_{95\%}$ against (nM) A375 cell line
1	**11a**	1098 [797; 1513]	508 [322; 802]	166 [77; 357]
2	**11b**	6595 [5455; 8436]	3551 [1180; 10 683]	2149 [1041; 4437]
3	**11c**	2300 [889; 5950]	2599 [1854; 3616]	433 [182; 1083]
4	**12a**	1657 [1147; 2396]	306 [167; 560]	**144 [122; 171]****
5	**12b**	> 10 000	5644 [5089; 6259]	3376 [1568; 7271]
6	**12c**	> 10 000	1443 [744; 2799]	1397 [892; 2188]

** value described in the literature (Pereira et al. 2017)

Taking into account the results in their entirety it is verified that the melanoma cell line apparently presents a greater sensitivity to the studied platinum complexes. More polar compounds (acids and alcohols) are more potent. The most promising results were obtained for chlorins **11a** and **12a**, whose the aromatic group of tetrapyrrolic macrocycle is a phenyl group (Ar = Ph). The least promising results were obtained for diester chlorins, more hydrophobic compounds.

Although the IC_{50} values obtained with the photosensitizers **11a** and **12a** are very promising (in the order of nanomolar), they should be considered in comparison with IC_{50} values of other photosensitizers which have been evaluated by the same methodology.

Zhang et *al.* developed in 2014 a tetraallyl free base chlorin substituted by methoxyphenyl groups, which they described as effective and of high potential. The concentrations corresponding to the IC_{50} of this compound in human oesophageal carcinoma and nasopharyngeal carcinoma cells submitted to treatment with 12 J/cm^2 were 1.73 μM and 2.87 μM, respectively (Zhang et al, 201). In OE21 cells of oesophageal carcinoma, Foscan® has an IC_{50} greater than 0.5 μM (Paszko et al, 2013).

In a study of colorectal carcinoma (HT29) and retinoblastoma (Y79) cells, several hydroxyphenylporphyrins and chlorins, as well as their glycoconjugate derivatives, including Foscan®, were studied. In such study, in which the cells were irradiated with 1.8 J/cm^2 and the evaluation performed 72 hours after irradiation, mean inhibitory concentrations were obtained in the micromolar order. The inhibitory concentrations of Foscan® against the HT29 cells it was 8 μM, while against the Y79 cells it was 6 μM (Maillard et al, 2007). In another study with several colon carcinoma cell lines, hypericin with an irradiation of 3.15 J/cm^2, was studied. IC_{50} between 40 and 60nM was obtained (Mikešová et al, 2013).

In the present year, diarylchlorins have reported to be extremely active against the A375 melanoma cell line showing IC_{50} values below 20 nM. Cells were irradiated with 12 J/cm² and the evaluation performed 24 hours after irradiation (Pereira et al. 2018). Also Nishie et *al.* already in 2018 developed a novel glucose-conjugated chlorin e6 (G-chlorin e6) and evaluated its antitumor effects against OE21, KYSE30 (oesophageal acncer cell lines), MKN45 (gastric cancer cell line), and HT29 (colon cancer cell line), obtaining IC_{50} of 0.33 nM, 0.34 nM, 0.8 nM and 1.35 nM, respectively. In such study, the cells were irradiated with 16 J/cm² of 660-nm LED light and the evaluation was performed 24 hours after irradiation (Nishie et al. 2018).

In previous studies, by our group, with the free base chlorins corresponding to platinum chlorins **10a** and **12a**, it was verified that the IC_{50} in A375 cells are 1.85 μM and 31 nM, respectively. And the IC_{50} in C32 cells are 0.78 μM and 231 nM, respectively (Pereira et al. 2015). Such results are indicative that the presence of the platinum ion induces a greater cytotoxicity. However, it is to be noted that the incorporation of this high atomic number metal ion can lead to room temperature phosphorescence within the biological spectral window. This and other suitable spectral properties in the NIR region are what allows these photosensitizers to be used not only in the treatment of cancer but also in diagnosis (theranostic agents). This is the biggest innovation of this project.

Chlorins **11a** and **12a**, in addition to the suitable photophysical and photochemical properties and their high activity, also did not show significant cytotoxicity *per se*, i.e. in the absence of light activation. This and the other biological assays that will be presented from this point of the dissertation were performed for these two chlorins, since they were the ones that presented values of more promising metabolic activity.

If we consider a potential clinical use of these platinum complexes, these would be administered systemically. Therefore, cytotoxicity, in the absence of light of chlorins **11a** and **12a** was evaluated against non-tumour human HFF1 cell line (**Table 2.7**). Dose-response curve was not shown since it was not possible to calculate the IC_{50} because it was higher than the highest concentration tested (10 μM). This value is about 100 times higher than the values obtained for photodynamic treatment in tumour cells, which is in agreement with other studies in human fibroblast cell lines to evaluate the cytotoxicity of other photosensitizers (Perry et al., 1990; Pittet et al., 2007; Bergmann et al., 2008).

2.2.2. Cell viability

In a complementary manner, cell viability with photosensitizers **11a** and **12a**, was studied in the melanoma human tumour cell line 24 hours after photodynamic treatment. The SBR assay, which is an indication of the change in total protein content and therefore correlates with cell biomass (Laranjo et al. 2014), was used.

The analysis of **Figure 2.12** shows that the viability of the cell cultures was not significantly reduced after the photodynamic treatment with the photosensitizer **11a**. For photosensitizer **12a**, a statistically significant reduction in viability at concentrations of 250 nM (92.08 ± 6.14 %, p=0.024)

was observed, but biologically does not have great significance. For other hand, a statistically significant reduction in viability at concentrations of 500 nM (56.82 ± 13.49 %, p<0.001) was observed and have biological significance (**Figure 2.12**).

Figura 2.12. Cell viability of the human melanoma 24 hours after the photodynamic treatment (light dose of 10 J) based on the chlorins **11a** and **12a**. Results are presented as mean ± SD (n = 9). Statistical significance: * p<0.05; ** p<0.01, *** p<0.001.

Surprisingly, the results of viability obtained with the SRB assay do not corroborate the results obtained by the MTT assay. This may be explained by the use of TCA during the methodology. Typically, this reagent is used for the fixation of cells in suspension and, as such, the culture medium is not removed after 24 hours of the photodynamic treatment, which leads to dead and living cells being fixed. However, SRB is a technique that indicates the protein content of the fixed cells, regardless of whether they are alive or dead. Given this possibility, a more detailed analysis of the viability and types of death by flow cytometry was performed.

2.2.3. Cell death

In order to characterize the PDT-induced cell death pathways based on the photosensitizers **11a** and **12a**, in human melanoma cell line, several studies were carried out, namely to evaluate the phosphatidylserine membrane exposure, cytoplasmic membrane integrity and mitochondrial membrane potential.

2.2.3.1. Types of cell death

The photocytotoxic effect of photosensitizers **11a** and **12a** was determined by the evaluation of mechanisms of death by apoptosis and necrosis. The number of cells in death by apoptosis, late apoptosis and necrosis are influenced by the photodynamic treatment with the photosensitizers **11a**

and **12a** in a significant way and dependent on the concentration of the PS, as can be observed in **Figure 2.13**.
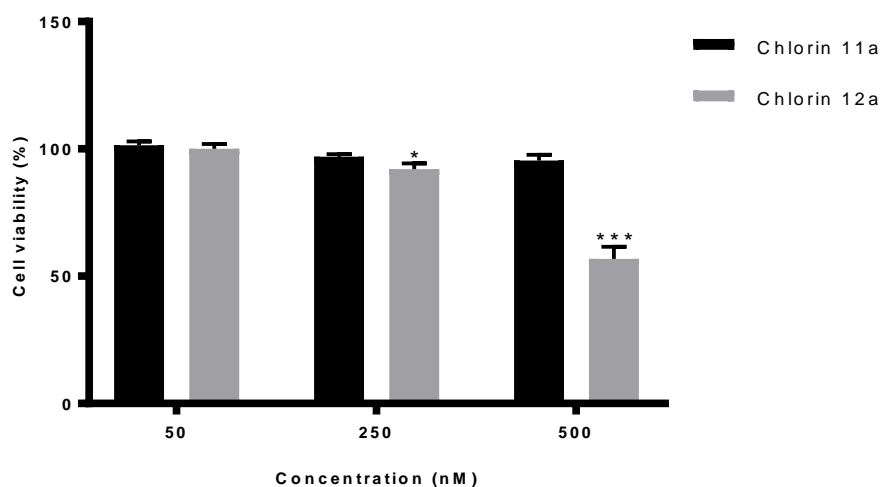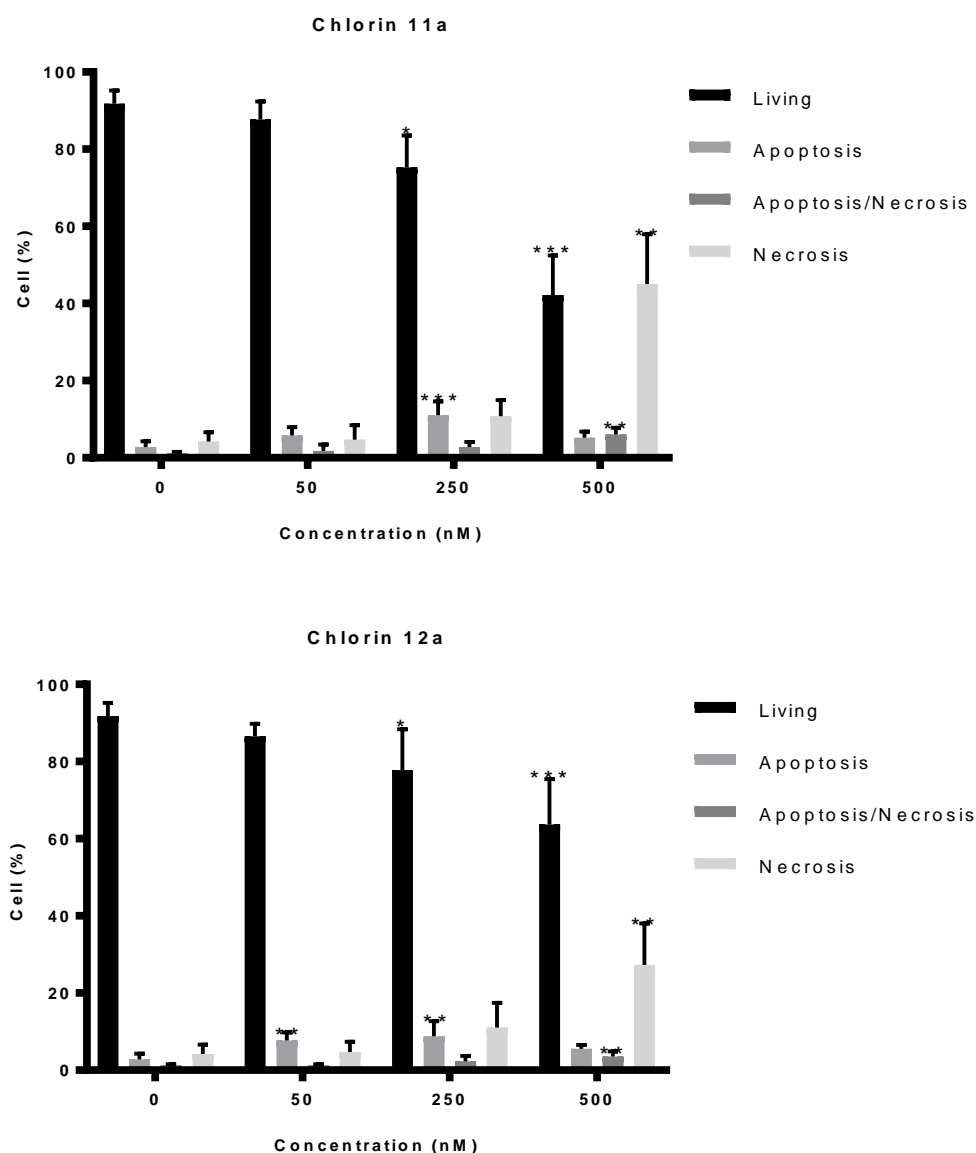

Figure 2.13. Cell death mechanisms induced of the human melanoma 24 hours after the photodynamic treatment (light dose of 10 J) based on the chlorins **11a** and **12a**. The analysis was carried out 24 h after PDT. Results are presented as mean ± SD (n = 6). Statistical significance: * $p<0.05$; ** $p<0.01$, *** $p<0.001$.

After 24 hours of photodynamic treatment with chlorin **11a**, a reduction of live cell population was observed for treatments with concentrations of 250 nM to 75.33 ± 8.21 % (p = 0.036) and 500 nM to 42.17 ± 10.28 % (p<0.001). Concomitantly, with chlorin **12a**, a reduction of live cell population was observed for treatments with concentrations of 250 nM to 77.83 ± 10.57 % (p=0.048) and 500 nM to 63.67 ± 11.81 % (p<0.001).

As regards to the death populations, for PS **11a** there was a significant increase in apoptosis cells to 11.00 ± 3.63 % (p<0.001) at the concentration of 250 nM and, in the treatment with the

concentration of 500 nM there was a significant increase of death by late apoptosis (6.00 ± 1.79 %, p=0.001) and by necrosis (45.00 ± 12.92 %, p=0.001). For PS **12a** a significant increase of apoptosis cells was observed at the concentrations of 50 nM (7.667 ± 2.16 %, p=0.003) and 250 nM (8.83 ± 3.87 %, p=0.003). In the treatment with the concentration of 500 nM there was a significant increase in death by late apoptosis (3.50 ± 1.38 %, p=0.006) and necrosis (27.33 ± 10.75 %, p=0.002).

Both apoptosis and necrosis were response to photodynamic treatment with photosensitizers **11a** and **12a**, however, apoptosis was associated primarily with lower concentrations and necrosis at higher concentrations of photosensitizers.

Several studies have shown that the balance between cell death by apoptosis and necrosis depends to the intensity of the photodynamic reaction (Acedo et al. 2014; Buytaert, Dewaele, and Agostinis 2007; Piette et al. 2003). For example, in the case of hypericin photosensitizer, one study showed that increasing the photosensitizer concentration from 1.25 to 2.5 μM altered the cellular response of apoptosis to necrosis. In the same study, the authors verified that the same concentration associated with a higher fluence also produced the same effect (Kamuhabwa et al. 2001). Apoptosis was observed as the predominant modality of cell death when P388 cells were treated with chloroaluminophthalocyanine (photosensitizer commonly called ALPC) using low doses of light, while necrosis was observed at higher light doses (Kessel, Vicente, and Reiners 2006).

The alteration of one type of cell death to another with increased intensity of damage has also been reported for other types of apoptotic stimuli (Mesquita et al. 2014) and in the case of PDT, the high production of ROS, increased calcium concentration or severe ATP depletion (Yoo and Ha 2012). It is accepted that PDT is an effective inducer of apoptosis, however, at higher concentrations it may cause necrosis, which indicates that the factor determining the type of death is the extent of damage (M Laranjo 2014). Several authors also report that another mechanism that may affect the activation of cell death pathways is the subcellular location of the photosensitizer (M Laranjo 2014).

2.2.3.2. Mitochondrial membrane potential

The mitochondrial membrane potential reflects the activity of the electron transport chain and the mitochondrial function itself (Shao et al. 2012). Disruption of the mitochondrial membrane potential leads to the release of pro-apoptotic molecules, such as cytochrome C, Smac or AIF. These are the typical hallmarks of apoptosis (Mikešová et al. 2013). In this work, the mitochondrial JC-1 membrane potential and flow cytometry analysis were used to evaluate the cells submitted to the treatment. **Figure 2.14** shows that the mitochondrial membrane potential was disturbed only by the use of higher concentrations of photosensitizer **12a**, namely with the concentration of 500 nM (13.66 ± 0.50, p = 0.042). For PS **11a** no significant differences were found.
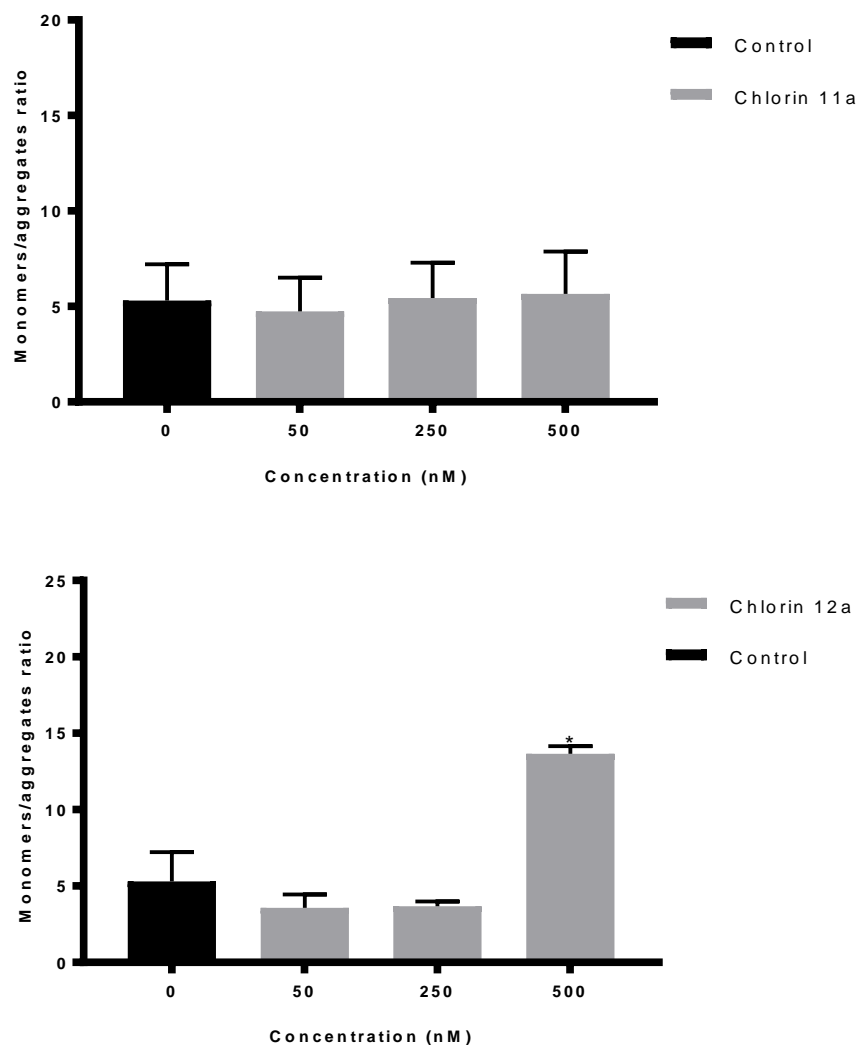
Figure 2.14. Mitochondrial membrane potential, expressed as the monomers/aggregates ratio, after PDT with chlorins **10a** and **12a** in the human melanomacells (light dose of 10 J). The analysis was carried out 24 h after PDT. Results are presented as mean ± SD. Statistical significance: * $p < 0.05$; ** $p < 0.01$, *** $p < 0.001$.

In general, mitochondrial membrane potential disturbance is associated with treatments where phosphatidylserine exposure (death by apoptosis) was observed. For chlorin **12a**, in the treatment with the highest concentration (500 nM), there was a membrane potential disturbance, with a significant increase in populations in late apoptosis and necrosis.

When photosensitizers are located in other organelles, mitochondrial damage can also be effectors in the cell death process since they can be propagated to mitochondria (Sasnauskiene et al. 2009). This is because cells in which photooxidative damage is sufficient for disruption of mitochondrial membrane potential are compromised with a pathway of death, but not necessarily apoptosis (Kessel and Luo 1999). Foscan® is a photosensitizer that is mainly located in the endoplasmic reticulum and in the Golgi complex. After treatment of colorectal carcinoma cells with this photosensitizer it was found that death by apoptosis and necrosis are involved and, as a mitochondrial membrane potential

disturbance was also found, this organelle is also implicated in the response. Sophie Marchal and collaborators proposed that photosensitization of the endoplasmic reticulum can trigger signals that converge in the mitochondria, triggering the death process in a different way from the photosensitizers that accumulate in this organelle (Marchal et al. 2005). As such, membrane potential disruption indicates that mitochondria are implicated in the response to photosensitization with chlorin **12a** and that the apoptosis pathway of death and the necrotic death pathway may be activated. It is the future perspective of this work to evaluate the main hallmarks involved in necrosis.

On the other hand, it should be noted that apoptosis can be triggered by two major pathways. One pathway is mediated by mitochondria and another by death receptors (Almeida et al. 2004; Granville et al. 1998; Scaffidi et al. 1997). The latter pathway may be the explanation for the apoptosis death observed for the lowest concentrations (50 and 250 nM) of chlorin **12a** and for all studied concentrations of chlorin **11a**, without significant changes in membrane potential mitochondrial.

2.2.4. Cell cycle

The cellular nucleus is a fundamental organelle, which as a consequence of the stress induced by the PDT can undergo changes. Thus, in this work, the DNA content of the cells was studied. The evaluation of the DNA content in an individual cell by the progressive alteration of 2n chromosomes to n chromosomes it is a way of evaluating the phase of the cell cycle, namely in G1, S phase and G2 or in division. By the analysis of **Figure 2.15** it is possible to verify that the cell cycle is little influenced by the photodynamic therapy based on the sensitizers **11a** and **12a**.
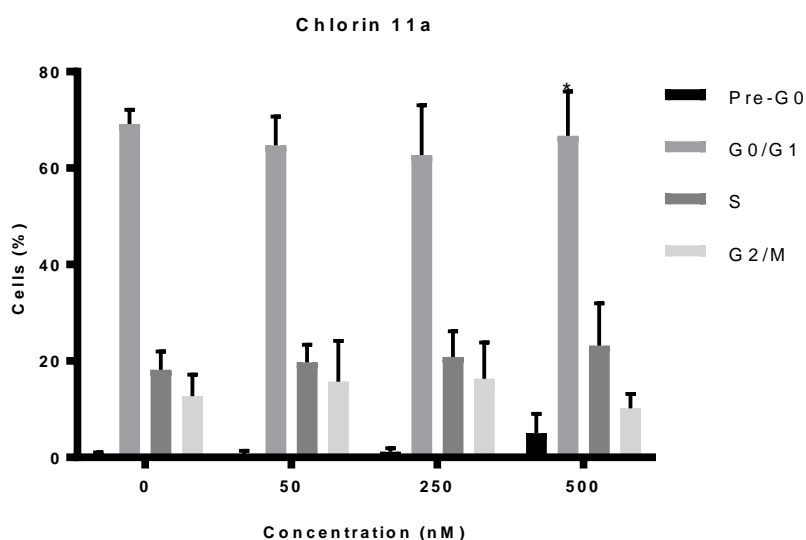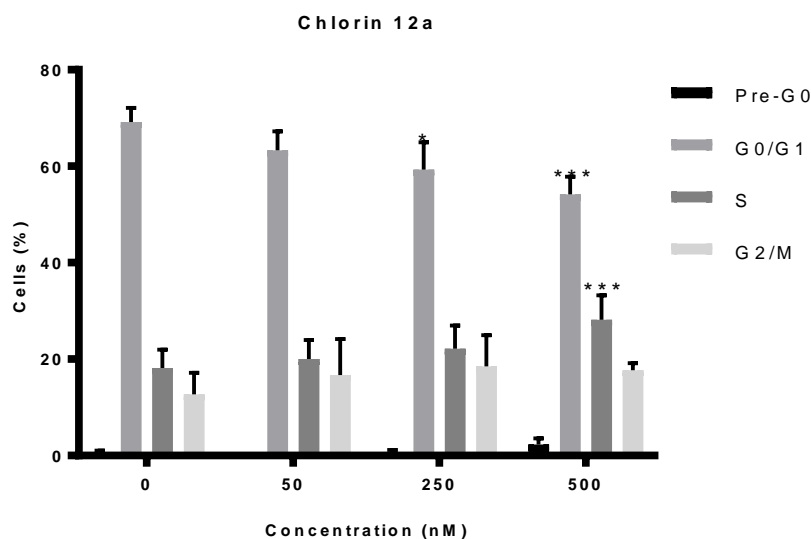
Figure 2.15. Cell cycle analysis of human melanoma cells after PDT based on the chlorins **11a** and **12a** (light dose of 10 J). The analysis was carried out 24 h after PDT. Results are presented as mean ± SD (n = 6). Statistical significance: * $p<0.05$; ** $p<0.01$, *** $p<0.001$.

For PS **11a**, 24 hours after the treatment with the concentration of 500 nM there was a decrease of the cell population in G0/G1 from 69.17 ± 2.93 % to 66.67 ± 9.201 % (p=0.033). For PS **12a** with the concentration of 500 nM, a decrease of the cellular population in G0/G1 from 69.17 ± 2.93 % to 54.17 ± 3.66 % (p<0.001) and increase of the S-phase cellular population from 18.17 ± 3.76 % to 17.67 ± 1.51 % (p=0.045).

Photodynamic treatment with the photosensitizers **11a** and **12a** did not greatly influence the cell cycle progression, with only changes in the distribution of cell populations being observed with the highest concentration treatment (500 nM) for chlorin **12a**.

In some studies with other photosensitizers and other types of tumour cells, the effect of photodynamic therapy in cell cycle progression was studied (Piette et al. 2003). HT29, colorectal carcinoma cells, were retained in the G0/G1 phase after photosensitization, with increased expression of a number of typical cell cycle proteins, namely cyclin A, cyclin E, cdk-2 and pRB (Kleban et al. 2008). However, another work with the same cell line showed G2/M phase blockade (Mikeš et al. 2007). In the case of PDT with hypericin, Kleban et *al.* found after literature review that inhibition or blockade of progression may occur at various control points, depending on the cell type and treatment conditions, namely the concentration of the photosensitizer and the light fluence (Kleban et al. 2008). In HT29, these investigators found G2/M cell cycle blockade, while in leukemia cells they found S phase block in a concentration and time-dependent manner (Kleban et al. 2008). On the other hand, in a study with 5,15-diarylporphyrins (Gariboldi et al. 2009) and 5,15-diarylchlorines (Pereira et al. 2018), the authors also verified that the photodynamic treatment did not introduce significant modifications in the cell cycle.

2.2.5. Oxidative Stress

2.2.5.1. Singlet oxygen and hydroxyl radical

In the photodynamic reaction, a photosensitizer, after absorption of light, can pass to the excited triplet state. The triplet state of the photosensitizer can react with a cellular substrate that subsequently leads to ROS production, being that ROS formation is the event responsible for death-induction in PDT. This reaction is usually called a type I reaction. In the type II reaction, the photosensitizer interacts directly with triplet oxygen, with energy transfer, to form singlet oxygen, considered the most important ROS in PDT (Triesscheijn et al. 2006). In the inability to evaluate the intracellular concentration of this ROS directly, studies were carried out in the presence of sodium azide, a quencher of this species (Maisch et al. 2007; Verna et al. 1998). The results, shown in **Figure 2.15**, for photosensitizer **11a** show that the reduction of metabolic activity inhibition is significant in the case of 250 nM treatment in which the metabolic activity increases from 43.14 ± 23.54 % to 81.29 ± 18.63 % (p=0.002) and with the treatment with 500 nM, in which the metabolic activity increases from 4.75 ± 3.79 % to 32.13 ± 13.61 % (p<0.001). **Figure 2.16** for photosensitizer **12a** shows that the reduction of metabolic activity inhibition is significant in the case of the 250 nM treatment in which metabolic activity increases from 3.01 ± 2.39 % to 55.41 ± 15.23 % (p<0.001) and with treatment with 500 nM in which the metabolic activity increases from 1.56 ± 1.10 % to 25.18 ± 9.68 % (p=0.004).

D-mannitol is a hydroxyl radical scavenger (Obata et al. 2009; Shen, Jensen, and Bohnert 1997). Studies in the presence of this compound are also shown in **Figure 2.16**. For the photosensitizer **12a**, in melanoma cells, it was verified that the metabolic activity in the presence of D-mannitol was significantly higher with the concentrations treatment of 250 nM (41.99 ± 3.98, p=0.032) and 500 nM (6.38 ± 1.69, p=0.016).
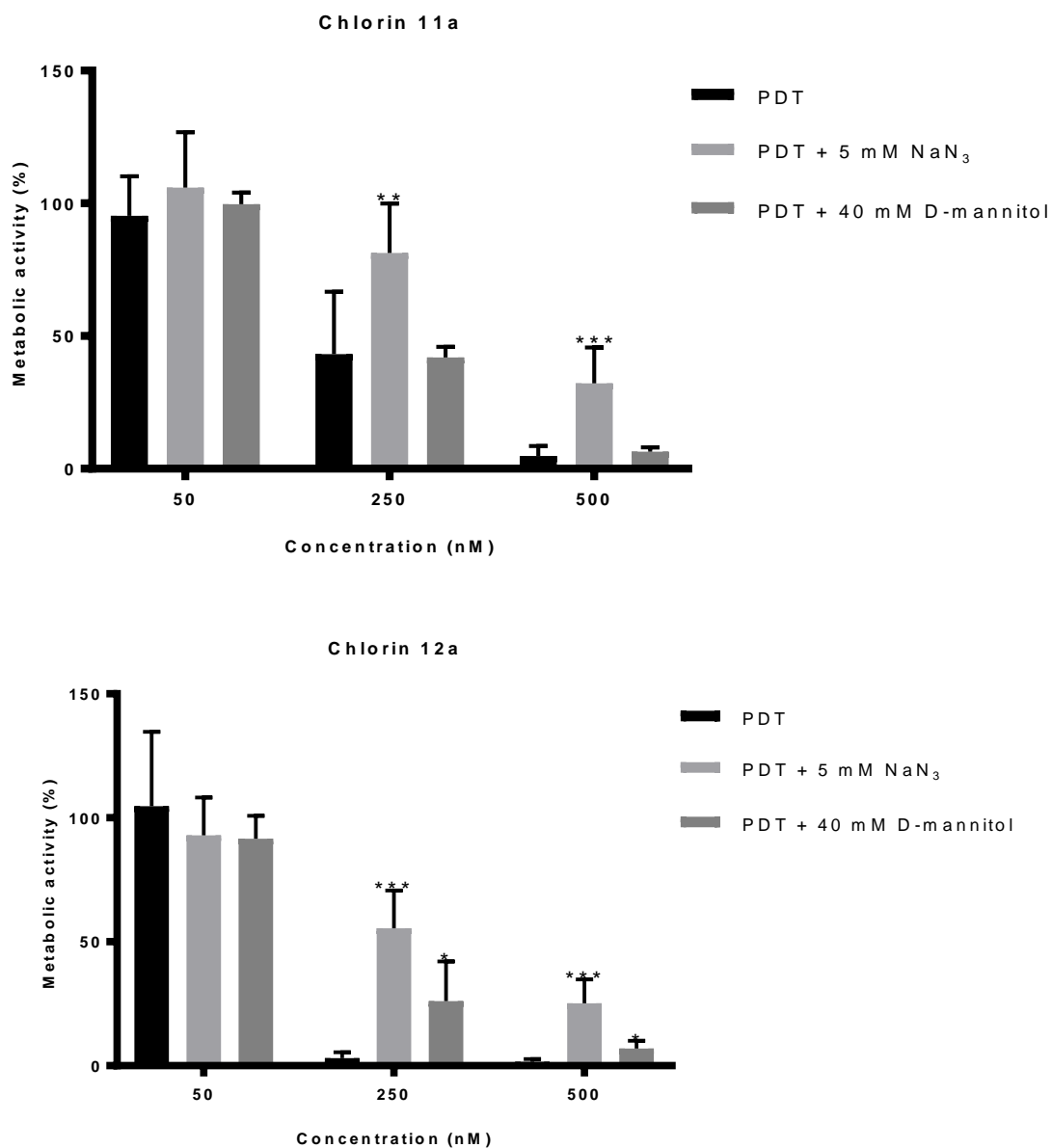
Figura 2.16. Photocytotoxicity of chlorins **11a** and **12a** in the human melanoma cells in the presence of a singlet oxygen quencher (5 mM NaN_3) and of a hydroxyl radical scavenger (40 mM D-mannitol) (light dose of 10 J). The analysis was carried out 24 h after PDT. Results are presented as mean $\pm$ SD (at least n = 6). Significant differences relative to cell cultures treated in the absence of the inhibitors are presented with an *. Statistical significance: * $p<0.05$; ** $p<0.01$, *** $p<0.001$.

Sodium azide and D-mannitol had previously been used in biological assays (Ding et al. 2004; Obata et al. 2009). Ding and collaborators tested the methyl ester of hematoporphyrin in the presence of these ROS inhibitors and found inhibition of the photodynamic reaction by both species.

Thus, these authors concluded that the photodynamic reaction, promoted by this photosensitizer, led to the formation of both singlet oxygen and hydroxyl radical, concluding that these species were involved in the type II and type I reactions, respectively (Ding et al. 2004). Similarly to these studies

it was found that photocytotoxicity in the presence of sodium azide or D-mannitol is significantly reduced, increasing cell viability. Thus, the importance of the singlet oxygen and the type II photodynamic reaction in the treatment with the photosensitizers **11a** and **12a** were confirmed, and that the ROS formed by the type I photodynamic reaction are also involved in this process. For chlorin **11a**, the use of D-mannitol showed no significant differences with respect to the controls also subjected to the treatment. This is indicative that, probably, the concentration of inhibitor used is not sufficient to suppress ROS that are produced.

Type II reaction determines the formation of mainly singlet oxygen that occurs by transferring energy from the photosensitizer to the oxygen. In parallel, in some cases the transfer of an electron from the photosensitizer to the oxygen may also occur, which determines the formation of superoxide anion. Since the formation of this species, typically associated with type I reaction (Agostinis et al. 2011; Juarranz et al. 2008; Plaetzer et al. 2009), also occurs through direct interaction between the photosensitizer and oxygen, some authors to classify it as type II (Foote 1991).

2.2.5.2. Intracellular production of superoxide anion

Dihydroethidium is a permeabilizing compound of the cell membrane, which can undergo two electron oxidation and form a fluorophore, which intercalates into the DNA. The reaction of the dihydroethidium with the superoxide anion is relatively specific, with a minimum of oxidation induced by hydrogen peroxide or hypochlorous acid (Tarpey 2004).

The intracellular production of superoxide anion, shown in **Figure 2.17**, was evaluated 24 hours after the photodynamic treatment with the photosensitizers **11a** and **12a**. For chlorin **12a**, at the lower concentrations of 50 nM and 250 nM, there were no changes in relation to the control cell cultures, whereas a significant reduction of this ROS is observed with the treatment with the concentration of 500 nM to 0.85 ± 0.15 (p = 0.003). For chlorin **11a**, there was a significant reduction of superoxide anion at concentrations of 50 nM (0.71 ± 0.14, p<0.001), 250 nM (0.84 ± 0.12, p<0.015) and 500 nM (0.75 ± 0.12, p<0.001).

2.2.5.3. Intracellular production of peroxides

Dismutation or reduction of the superoxide anion leads to the formation of hydrogen peroxide. Hydrogen peroxide, in turn, may undergo reduction of an electron and form the hydroxyl radical, a highly oxidizing species (Agostinis et al. 2011). 2',7'-dichlorodihydrofluorescein diacetate is one of the most frequently used probes to evaluate the redox state of the cells. It is a membrane permeabilizing compound which is cleaved by intracellular esterases, forming a less permeating intermediate, which upon oxidation produces a fluorescent compound. The fluorescence obtained is proportional to the concentration of intracellular peroxides (Wang and Joseph 1999; Zhang et al. 2008).

As can be seen in **Figure 2.18**, with respect to the intracellular production of peroxides, for chlorin **11a** at the highest concentrations, 250 nM and 500 nM, there was a decrease to 0.59 ± 0.19 (p=0.003) and to 0.52 ± 0.14 (p<0.001), respectively. For chlorin **12a**, there was a significant reduction of peroxides at concentrations of 50 nM (0.70 ± 0.09, p<0.001), 250 nM (0.71 ± 0.06, p<0.001) and 500 nM (0.52 ± 0.16, p<0.001).
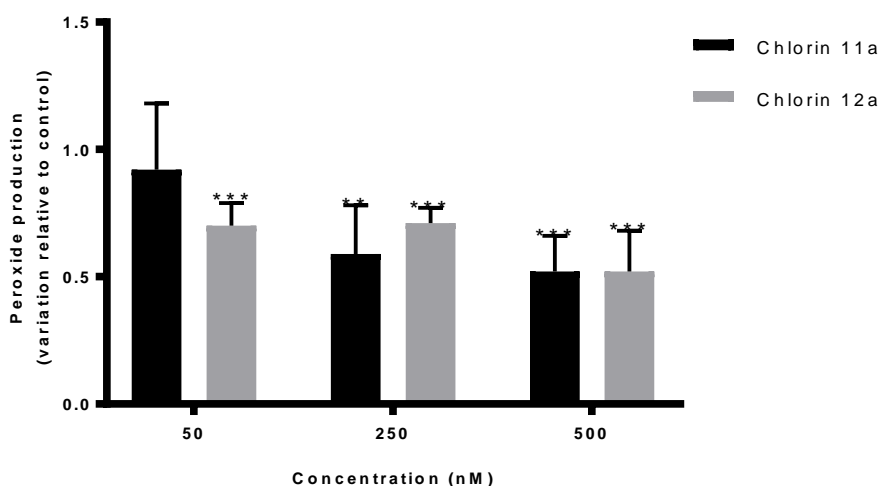
Figure 2.18. Intracellular production of peroxides after chlorins **11a** and **12a** based PDT in the human melanoma A375 cells (light dose of 10 J). The analysis was carried out 24 h after PDT. Results are presented as mean ± SD (at least n = 8). Statistical significance: * p<0.05; ** p<0.01, *** p<0.001.

Ali-Seyed et *al.* evaluated the production of peroxides after PDT with Photolon™ over time. These researchers observed a gradual increase in the production of these ROS from the 30 minutes, with maximum after one hour, followed by a decline until three hours after treatment (Ali-Seyed et

al. 2011). Another study that corroborated the results obtained was the Zhao et *al.* study, who verified that in photosensitized lung adenocarcinoma cells with Photofrin® the intrecellular concentration of ROS was inversely proportional to the concentration of photosensitizer. The concentration of ROS was maximal at the concentration of 2.5 µg/mL and minimal when the photosensitizer concentration was increased to 10 µg/mL (Hongyou Zhao, Xing, and Chen 2011).

Several authors have referred to the cytoprotective mechanisms of tumour cells to avoid the cytotoxic effects of PDT. One of the mechanisms associated with this response depends on the antioxidant molecules present in cells, whose concentration varies greatly between the various types of tumour cells, as is the case with some amino acids, glutathione (GSH), or vitamin E. Another mechanism is associated with the expression of enzymes capable of eliminating ROS, such as superoxide dismutase (Agostinis et al. 2011).

2.2.5.4. Reduced glutathione

Reduced glutathione is an antioxidant enzyme capable of eliminating free radicals and reducing peroxides (Chiou et al. 2010). In response to the photodynamic treatment based on the photosensitizer **11a** and **12a** a reduction of this antioxidant defence is verified 24 hours after the treatment. In human melanoma cells, where the results are represented in **Figure 2.19** for chlorin **11a**, the reduction is significant in the photodynamic treatment with the concentrations of 50 nM to 0.84 ± 0.09 ($p<0.001$), 250 nM to 0.80 ± 0.10 ($p<0.001$), and 500 nM to 0.84 ± 0.08 ($p<0.001$). The same behavior is verified with chlorin **12a**, where the reduction of this enzyme is significant at concentrations of 50 nM to 0.85 ± 0.09 ($p<0.001$), 250 nM to 0.87 ± 0.08 ($p<0.001$), and 500 nM, to 0.90 ± 0.10 ($p=0.024$).
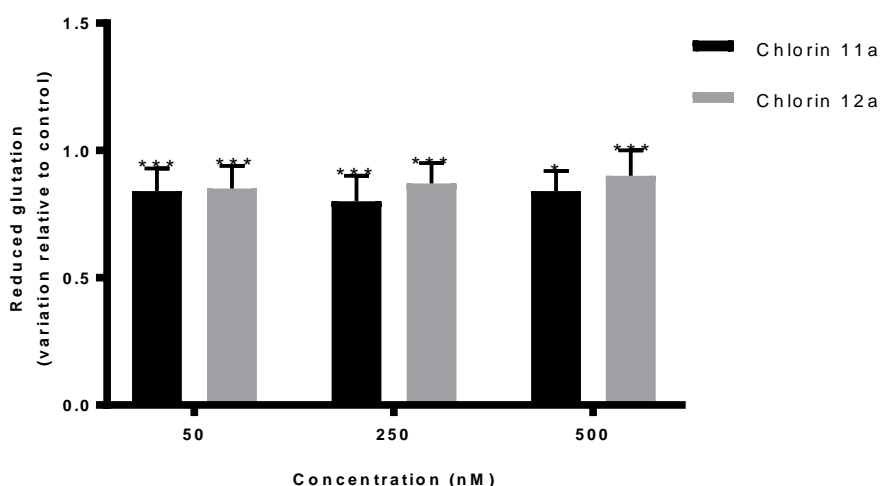
Figure 2.19. Reduced glutathione variation after PDT based in the chlorins **11a** and **12a** in the human melanoma A375 cells (light dose of 10 J). The analysis was carried out 24 h after PDT. Results are presented as mean $\pm$ SD (n = 12). Statistical significance: * $p<0.05$; ** $p<0.01$, *** $p<0.001$.

Changes in reduced glutathione activity were reported after PDT with several photosensitizers and in various cell types (Hadjur et al. 1996; Mikešová et al. 2013; Zhang et al. 2008).

There are several cellular mechanisms capable of interacting with the oxidants to form less reactive products. However, under conditions of high oxidative stress, such as those occurring during PDT, these cytoprotective mechanisms are insufficient and significant damage occurs in the cellular constituents (Szokalska et al. 2009). Taking into account the results obtained and despite changes in the antioxidant defences of the cells, their cytoprotective effect does not appear to be sufficient to significantly limit the effect of photodynamic therapy based on the photosensitizers **11a** and **12a**.

Chapter 3: Conclusions and Future Perspectives

Throughout this dissertation the results obtained in the experimental work were presented and discussed. However, there are important conclusions that need to be emphasized, as well as the prospect of future work.

In this study, we proceeded with the synthesis of a set of platinum chlorins with different substituent groups in their tetrapyrrolic macrocycle (Ar = Ph, $4-ClC_6H_4$ and $4-MeOC_6H_4$) corresponding to different polarities (esters, acids and alcohols). These chlorins were characterized by ^{1}H NMR, ^{13}C NMR, mass spectrometry and UV-visible absorption spectroscopy.

Spectroscopically, it was concluded that the platinum complexes studied aggregated in aqueous medium. Whereby a disaggregation study using different neutral surfactants (Glycerol, Pluronic F127, Pluronic P123 and Tween 20) was performed. By studying the dark cytotoxicity of the two surfactants that were found to disaggregate the metallochlorins, they proved to be cytotoxic *per se*, reason why the other biological studies proceeded with the aggregated platinum complexes. In the future it is intended to study the cytotoxicity of other surfactants, namely, non-ionic surfactants, Triton X-100 and Brij-35.

From the cytotoxicity studies with the metallochlorins (in the aggregated form), in the human cells of bladder carcinoma, esophageal carcinoma and melanocytic melanoma, it was concluded that chlorins **11** (acid) and **12** (alcohol) have a photodynamic effect *in vitro*, unlike chlorins **10** (ester), which were the most hydrophobic tested compounds. In conclusion, the polarity of these derivatives affects their toxicity.

For chlorins **11** and **12**, it was found that the inhibition of metabolic activity is proportional to the increase of the concentration. Chlorins **11a** and **12a** were the photosensitizers that revealed a more promising photodynamic effect against the three human tumour cell lines tested. The aromatic group of these tetrapyrrolic macrocycle is a phenyl group (Ar = Ph). Thus, it can be concluded that the nature of the aryl group of the macrocycle affects the photocytotoxicity of the derivatives studied.

In this work, the dark cytotoxicity of photosensitizers **11a** and **12a** in normal human fibroblasts was also considered. With this study it was determined that light activation is a fundamental requirement for the cytotoxic activity of these photosensitizers and that their toxicity in normal cells, if light activation does not occur, only occurs at concentrations well above the concentrations tested ($> 10 \mu M$).

For chlorins **11a** and **12a**, it was also proved that both apoptosis and necrosis are responses to photodynamic treatment, however, apoptosis is associated with lower concentrations of photosensitizers, whereas necrosis is associated with higher concentrations. Not only singlet oxygen, formed from the type II photodynamic reaction, but also the ROS, formed through the type I reaction, are involved in the lesion following PDT based on the photosensitizers **11a** and **12a**. The activated cytoprotective mechanisms are not sufficient to inhibit the cellular damages consequent to the photodynamic effect.

Photodynamic therapy, due to its dependence on the formation of transient ROS, is usually characterized as a phenomenon with appreciable short-term consequences. For this reason, in the future, we also intend to evaluate the metabolic activity 2 hours after the photodynamic treatment.

The development of this experimental work allowed to gain further knowledge and promote the general optimization of procedures. The aim was to develop photosensitizers with therapeutic ability that, at the same time, can be used in molecular imaging. In the future, it is planned to continue the development of new chlorin derivatives in order to achieve an efficient photodynamic action, namely by conjugation of chlorins **11a** and **12a** with sugars. With this structural change, both an increase in the solubility in aqueous medium and an optimization of the selectivity of these photosensitizers regarding the tumour cells are anticipated.

Chapter 4: Experimental

This chapter is divided into two parts. **Part I** of this chapter refers to **Part I** of **Chapter 2**. In **Chapter 4 - Part I** it is intended to refer the solvents, reagents, instrumentation and methodologies used in **Part I** of **Chapter 2**; to present the synthesis and characterization of compounds synthesized in **Part I** of **Chapter 2**; to present aggregation and disaggregation studies with Pt(II) chlorins.

Part II of this chapter refers to **Part II** of **Chapter 2**. **Chapter 4 - Part II** is intended to present the cell lines and methodologies used in **Chapter 2** - **Part II**. The different *in vitro* studies that will be presented are cell cytotoxicity (metabolic activity and cell viability), cell capture, cell death (types of cell death and mitochondrial membrane potential), cell nucleus alterations (cell cycle) and oxidative stress (singlet oxygen and superoxide radical, intracellular production of superoxide anion, intracellular production of peroxides and reduced glutathione)

4.1. Experimental - Part I

4.1.1. Solvents and reagents

All reagents were provided by Sigma-Aldrich, Merck or Fluka and used without further purification. Solvents were dried, when necessary, according to the methods described in the literature (Armarego and Chai 2003) and distilled before use.

4.1.2. Instrumentation and methodology

Thin layer chromatography

Analytical TLCs were performed using precoated silica gel plates Macherey-Nagel Xtra SIL G/UV254 and visualized by UV irradiation (254 and 350 nm).

Column chromatography

Some of the synthesized compounds were purified by flash column chromatography using silica gel 60 (0.035–0.070 mm), provided by Acros Organics, as the stationary phase.

Microwave

Microwave-assisted reactions were performed in a CEM Discover S-Class single-mode microwave reactor, featuring continuous temperature, pressure and microwave power monitoring.

Nuclear Magnetic Resonance (NMR) spectroscopy

Proton (^{1}H) and carbon (^{13}C) nuclear magnetic resonance spectra were recorded with a Bruker Avance III instrument operating at 400 and 100 MHz, respectively. Chemical shifts are reported in parts per million (ppm) relative to tetramethylsilane (TMS, $\delta = 0.00$ ppm), and coupling constants (J) are expressed in Hz. The deuterated solvent is indicated in each experiment.

Mass spectrometry

High-resolution mass spectra (HMRS) were obtained with a TOF VG Autospect M spectrometer with electrospray ionization (ESI).

Melting Points

Melting points were determined using a Melting Point Device Falc R132467 (open capillary method).

Ultraviolet-visible absorption spectroscopy

UV-Visible absorption spectra were obtained on a Shimadzu UV-2100 spectrophotometer using 1 cm optical glass cells. The molar absorption coefficients were determined after preparation of

solutions between 10^{-5} and 10^{-6} M in toluene. The maximum absorption of each band was plotted as a function of the concentration of different solutions, with the slope value corresponding to the molar absorptivity coefficient. This analogy is transmitted by the Beer-Lambert law, $A = \varepsilon bc$, where A is the absorbance, ε is the molar absorptivity coefficient, b is the optical path travelled by light and c is the concentration of the solution.

4.1.3. Synthesis of diazafulvenium methide precursors

Thiazolidine-4-carboxylic acid (1)
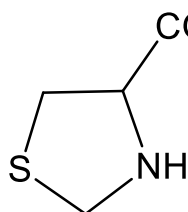
The compound was prepared according to a literature procedure (Sutcliffe et al. 2001). A solution of L-cysteine (14.40 g, 12 mmol) in water (120 mL) was added to a solution of formaldehyde (12 mL, 160 mmol, 37 % aqueous solution) in ethanol (90 mL). The mixture was allowed to stir at room temperature for 24 hours. A white solid formed which was filtered and washed with diethyl ether. The product was obtained in 91 % yield.

¹H NMR (400 MHz, DMSO-d$_6$): δ = 4.21 (d, J = 8.9 Hz, 1H, CH$_2$), 4.02 (d, J = 8.9, 1H, CH$_2$), 3.83 (t, J = 6.7 Hz, 1H, CH), 2.81 (dd, J = 10.0, 6.7 Hz, 1H, CH$_2$) ppm.

N-nitrosothiazolidine-4-carboxylic acid (2)
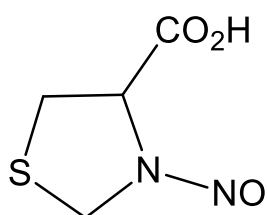
Compound was prepared according to a procedure described in the literature (Sutcliffe et al. 2000). To a suspension of thiazolidine-4-carboxylic acid (**1**, 13.32 g, 100 mmol) in water (50 mL) was slowly added concentrated HCl until the suspension completely dissolved. A solution of sodium nitrite (10.35 g, 150 mmol) in water (50 mL) was added dropwise through an addition funnel to the reaction mixture. Stirring was allowed for 12 hours at room temperature. The mixture was extracted with ethyl acetate (3 x 100 mL), the organic extracts were combined and washed with water and a saturated sodium chloride solution. The organic layer was dried with sodium sulfate and the solvent was evaporated. The residue was precipitated with diethyl ether and a yellow solid formed in 72 % yield, comprising two rotational isomers in the ratio (60/40).

¹H NMR (400 MHz, DMSO-d$_6$): δ = 5.95 (d, J = 6.0 Hz, 1H), 4.73 (d, J = 12.2 Hz, 1H), 4.48 (d, J = 12.2 Hz, 1H), 3.56-3.47 (m, 1H), 3.41-3.38 (m, 1H) ppm (major isomer). δ = 5.70 (d, J = 10.5 Hz, 1H), 5.27 (d, J = 10.5 Hz, 1H), 4.82 (t, J = 7.0 Hz, 1H), 3.56-3.47 (m, 1H), 3.25-3.20 (m, 1H) ppm (minor isomer).

4*H*,6*H*-thiazolo[3,4-*c*][1,2,3]oxadiazolium-3-oxide (3)
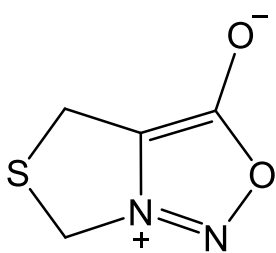
Compound was prepared according to a procedure described in the literature (Sutcliffe et al. 2000). To a suspension of N-nitrosothiazolidine-4-carboxylic acid (**2**, 5.50 g, 33.91 mmol) in diethyl ether (350 mL) was added trifluoroacetic anhydride (4.71 mL, 33.91 mmol) and stirred for 6 hours at 0 °C. Thereafter, the mixture was allowed to stir at room temperature for 24 hours. A precipitate formed which was filtered and washed with cold ether. The product was obtained as a yellow solid in 64 % yield.

¹H NMR (400 MHz, CDCl₃): δ = 5.41 (s, 2H, CH₂), 4.03 (s, 2H, CH₂) ppm.

Dimethyl 1*H*,3*H*-pyrazolo[1,5-*c*]thiazole-6,7-dicarboxylate (5)
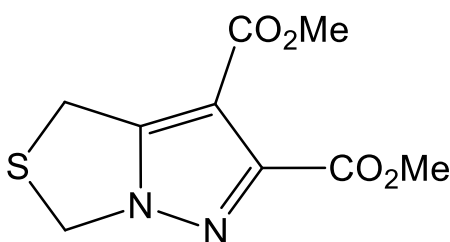
Compound **5** was prepared according to a procedure described in the literature (Sutcliffe et al. 2000). A solution of 4*H*,6*H*-thiazolo[3,4-*c*][1,2,3]oxadiazolium-3-oxide (**3**, 21.57 mmol) and dimethyl acetylenedicarboxylate (34.52 mmol) in xylene (15 mL) was refluxed under an inert atmosphere of N₂ for 3 h. The solvent was evaporated and the product of the reaction medium was precipitated with methanol. The product was obtained as a yellow solid in 62 % yield.

¹H NMR (400 MHz, CDCl₃): δ = 5.24 (s, 2H, CH₂), 4.30 (s, 2H, CH₂), 3.95 (s, 3H, Me), 3.85 (s, 3H, Me) ppm.


Dimethyl 2,2-dioxo-1*H*,3*H*-pyrazolo[1,5-*c*][1,3]thiazole-6,7-dicarboxylate (6)
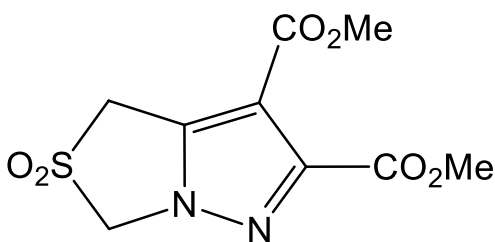
Compound **6** was prepared according to literature procedure (Sutcliffe et al. 2000). To a solution of dimethyl 1*H*,3*H*-pyrrolo[1,2-*c*]thiazole-6,7-dicarboxylate (**5**, 12 mmol) in dichloromethane (90 mL) at 0 ° C, 3-chloroperoxybenzoic acid (77 %) (4 equiv, 48 mmol) was added slowly and allowed to stir for 1 h. Temperature was raised to 25 °C and allowed to stir for 3 h. The mixture was then washed with a 10 % (w/v) aqueous sodium bisulfite solution (2 x 100 mL) and a 10 % (w/v) aqueous sodium hydrogen carbonate solution (2 x 100 mL). The organic layer was dried over sodium sulfate and the solvent was evaporated. Product was purified by column chromatography (hexane/ ethyl acetate, 50:50, v/v). The product was obtained as a white solid in 58% yield.

¹H NMR (400 MHz, CDCl₃): δ = 5.24 (s, 2H, CH₂), 4.70 (s, 2H, CH₂), 3.99 (s, 3H, Me), 3.89 (s, 3H, Me) ppm.

4.1.4. General synthesis of porphyrins 8

Porphyrins **8** were synthetized as described in the literature (Gonsalves, Varejão, and Pereira 1991; Pineiro et al. 1998). To a solution of the desired aldehyde (40 mmol) in glacial acetic acid (140 mL) and nitrobenzene (70 mL), at 120 °C and under stirring, was slowly added pyrrole (40 mmol, 3 mL). After stirring for 1 h, the reaction mixture was cooled to room temperature and methanol (50 mL) was added. The resulting residue was filtered and washed several times with methanol. Porphyrins **8** were obtained as purple solids.

5,10,15,20-tetraphenylporphyrin (8a) (Naik et al. 2003)
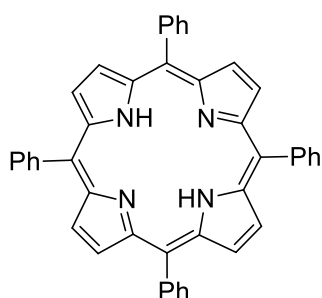
Porphyrin **8a** was obtained in 20 % yield (4.92 g, 8 mmol) from benzaldeyde.

¹H NMR (400 MHz, CDCl$_3$): δ = 8.84 (s, 8H, β-H pyrrolic), 8.22-8.20 (m, 8H, Ar), 7.79-7.66 (m, 12H, Ar), -2.77 (s, 2H, NH) ppm.

UV/Vis (CH$_2$Cl$_2$): λ_{max} (Abs) = 412 (1.95), 478 (0.91), 514 (1.63), 588 (1.11), 645 (1.03) nm.

5,10,15,20-tetrakis(4-chlorophenyl)porphyrin (**8b)** (Naik et al. 2003)
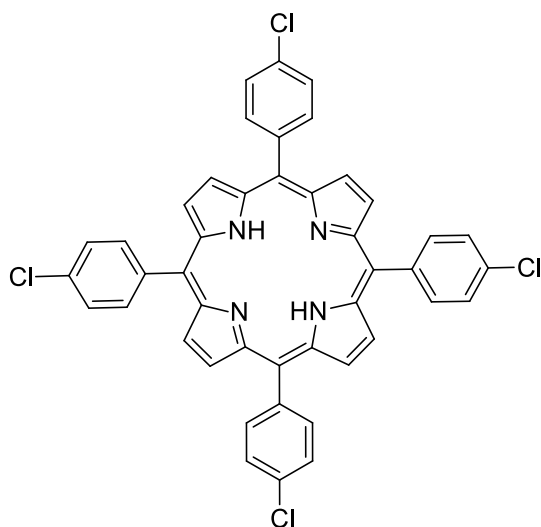
Porphyrin **8b** was obtained in 33 % yield (9.93 g, 13.2 mmol) from 4-chlorobenzaldehyde.

¹H NMR (400 MHz, CDCl$_3$): δ = 8.84 (s, 8H, β-H pyrrolic), 8.13 (d, J = 8.1 Hz, 8H, Ar), 7.75 (d, J = 8.1 Hz, 8H, Ar), -2.86 (s, 2H, NH) ppm.

UV/Vis (CH$_2$Cl$_2$): λ_{max} (Abs) = 485 (1.30), 515 (2.03), 550 (1.65) nm.

5,10,15,20-tetrakis(4-methoxyphenyl)porphyrin (8c) (Naik et al. 2003)

OMe
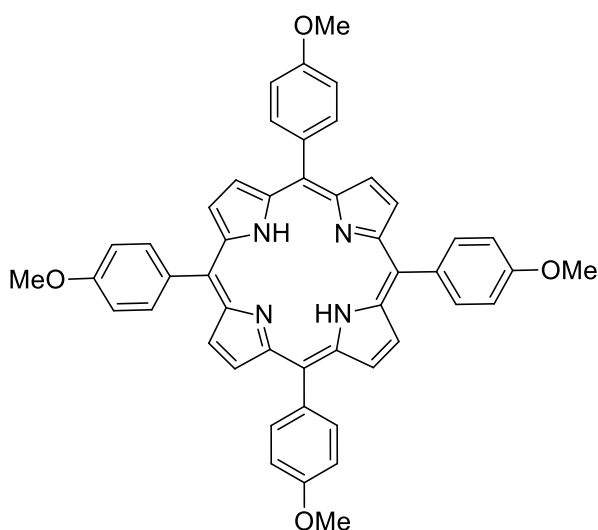
Porphyrin **8c** was obtained in 31 % yield (9.11 g, 12.4 mmol) from 4-methoxybenzaldehyde.

¹H NMR (400 MHz, CDCl₃): δ = 8.86 (s, 8H, β-H pyrrolic), 8.12 (d, J = 8.4 Hz, 8H, Ar), 7.29 (d, J = 8.4 Hz, 8H, Ar), 4.10 (s, 12H, CH₃), -2.75 (s, 2H, NH) ppm.

UV/Vis (CH₂Cl₂): λ_{max} (Abs) = 410 (1.90), 454 (0.88), 518 (0.78), 554 (0.67), 592 (0.36), 648 (0.42) nm.

4.1.5. General synthesis of platinum(II) porphyrins 9

Pt(II) porphyrins **9** were synthesized following an adapted procedure described in the literature (Dean et al. 2008). A solution of porphyrin **8** (0.50 mmol), platinum (II) chloride (1.50 mmol, 3 equiv.) and anhydrous sodium acetate (3 mmol, 5 equiv.) in benzonitrile (3 mL) was irradiated in a microwave reactor with the temperature set to 250 °C for 20 min. After cooling to room temperature, the product was precipitated by adding methanol, filtered, and then purified by flash column chromatography (dichloromethane). Pt(II) porphyrins **9** were obtained as purple solids.

Pt(II) 5,10,15,20-tetraphenylporphyrin (9a) (Chizhova, Kulikova, and Mamardashvili 2013)
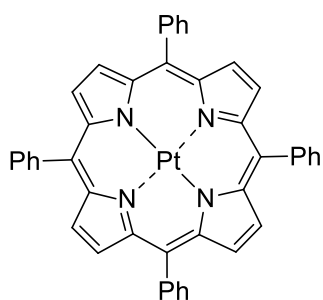
Pt(II) porphyrin **9a** was obtained in 90 % yield (0.36 g, 0.45 mmol) from porphyrin **8a**.

¹H NMR (400 MHz, CDCl₃): δ = 8.77 (s, 8H, β-H pyrrolic), 8.18 (d, J = 7.9 Hz, 8H, Ar), 7.77 (d, J = 7.9 Hz, 8H, Ar), 7.75 (d, J = 7.8 Hz, 4H, Ar) ppm.

UV/Vis (CH₂Cl₂): λ_{max} (logε) = 402 (5.48), 510 (4.40), 540 (4.10) nm.

UV/Vis (acetone): λ_{max} = 403, 508, 537 nm.

Pt(II) 5,10,15,20-tetrakis(4-chlorophenyl)porphyrin (9b) (Chizhova, Kulikova, and Mamardashvili 2013)
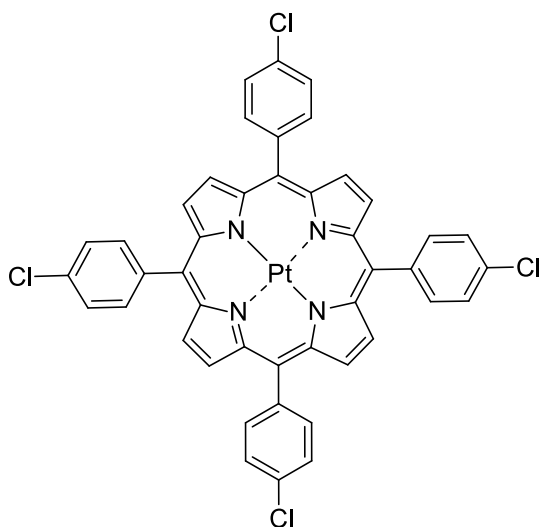
Pt(II) porphyrin **9b** was obtained in 58 % yield (0.27 g, 0.29 mmol) from porphyrin **8b**.

¹H NMR (400 MHz, CDCl₃): δ = 8.77 (s, 8H, β-H pyrrolic), 8.90 (d, J = 8.0 Hz, 8H, Ar), 7.74 (d, J = 8.0 Hz, 8H, Ar) ppm.

UV/Vis (CH₂Cl₂): λ_{max} (logε) = 401 (5.52), 509 (4.46), 539 (4.13) nm.

UV/Vis (acetone): λ_{max} = 399, 508, 538 nm.

Pt(II) 5,10,15,20-tetrakis(4-methoxyphenyl)porphyrin (9c)
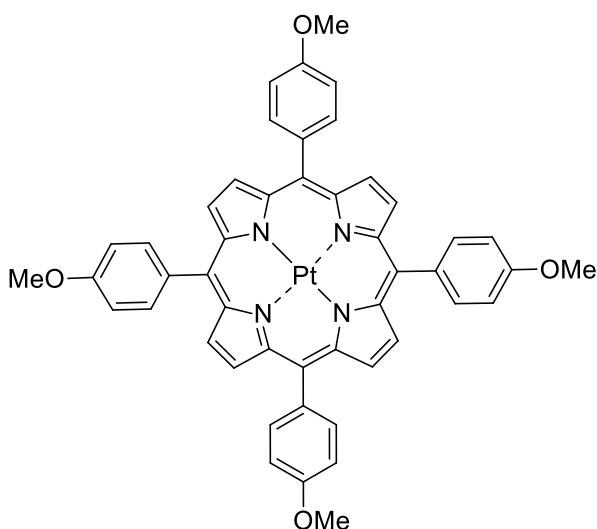
Pt(II) porphyrin **9c** was obtained in 77 % yield (0.36 g, 0.39 mmol) from porphyrin **8c**.

¹H NMR (400 MHz, CDCl₃): δ = 8.77 (s, 8H, β-H pyrrolic), 8.07 (d, J = 8 Hz, 8H, Ar), 7.24 (d, J = 8 Hz, 8H, Ar), 4.06 (s, 12H, CH₃) ppm

¹³C NMR (100 MHz, CDCl₃): δ = 199.4, 143.1, 134.9, 133.8, 130.6, 112.3, 77.3, 77.0, 76.7, 55.6 ppm

ESI-HRMS (m/z): found 927.2371, calcd. 927.2383 (C₄₈H₃₆N₄O₄Pt, M⁺)

UV/Vis (acetone): λ_{max} = 398, 510, 537 nm.

4.1.6. General synthesis of diester platinum(II) chlorins 10

Pt(II) chlorins **10** were prepared using two heating approaches, microwave irradiation (Method A) and conventional heating (Method B), following procedures described in the literature (Pereira et al. 2011; Pereira, Serra, and Pinho E Melo 2010).

Method A

A solution of dimethyl 2,2-dioxo-1*H*,3*H*-pyrazolo[1,5-*d*][1,3]thiazole-6,7-dicarboxylate **6** (0.18 mmol) and Pt(II) porphyrin **9** (0.36 mmol, 2 equiv.) in 1,2,4-trichlorobenzene (4 mL) was flushed with N₂ and irradiated in a microwave reactor with the temperature set to 250 °C for 20 min. After

cooling to room temperature, some drops of triethylamine were added, and the mixture was purified by flash column chromatography (CH₂Cl₂/ethyl acetate) to afford Pt(II) chlorins **10** as purple solids.

Method B

A solution of dimethyl 2,2-dioxo-1*H*,3*H*-pyrazolo[1,5-*d*][1,3]thiazole-6,7-dicarboxylate **6** (0.18 mmol) and Pt(II) porphyrin **9** (0.36 mmol, 2 equiv.) in 1,2,4-trichlorobenzene (4 mL) was stirred at 250 °C for 3.5 h, under N₂. After cooling to room temperature, some drops of triethylamine were added, and the mixture was purified by flash column chromatography (CH₂Cl₂/ethyl acetate) to afford Pt(II) chlorins **10** as purple solids.

Platinum(II) $2^2,2^3$-**bis(methoxycarbonyl)-5,10,15,20-tetraphenyl-2,2^1,2^6,3-tetrahydropyrazolo[1',5':1,6]pyrido[3,4-*b*]chlorin (10a)** (Pereira et al. 2017)
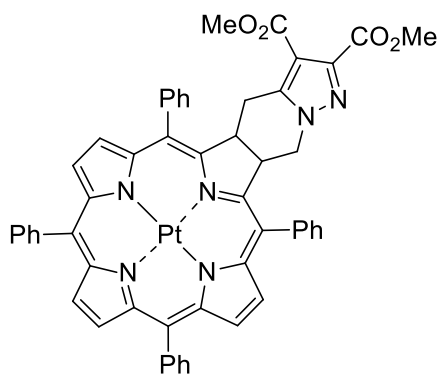
Obtained from porphyrin **9a**. Purification by flash column chromatography [CH₂Cl₂/ethyl acetate (95:5) v/v] gave compound **10a** (Method A: 0.04 g, 20 %; Method B: 0.02 g, 8 %).

¹H NMR (400 MHz, CDCl₃): δ = 8.41 (s, 2H, β-H pyrrolic), 8.38-8.36 (m, 2H, β-H pyrrolic), 8.16-8.13 (m, 2H, β-H pyrrolic), 8.11-7.94 (m, 7H, Ar), 7.82-7.76 (m, 3H, Ar), 7.71-7.60 (m, 10H, Ar), 5.78-5.71 (m, 1H, reduced β-H pyrrolic), 5.39-5.32 (m, 1H, reduced β-H pyrrolic), 4.33 (dd, J = 13.5, 7.7 Hz, 1H, CH₂ fused ring), 3.93 (dd, J = 13.5, 9.8 Hz, 1H, CH₂ fused ring), 3.88 (s, 3H, CO₂Me), 3.74 (s, 3H, CO₂Me), 3.58 (dd, J = 15.8, 6.4 Hz, 1H, CH₂ fused ring), 2.64 (dd, J = 15.8, 10.4 Hz, 1H, CH₂ fused ring) ppm.

¹³C NMR (100 MHz, CDCl₃): δ = 162.6, 162.2, 150.7, 148.4, 146.4, 146.2, 143.3, 143.0, 140.8, 140.6, 140.3, 138.4, 138.2, 135.9, 135.7, 134.5, 134.1, 133.3, 133.2, 132.3, 132.3, 131.6, 131.5, 128.9, 128.7, 128.6, 128.3, 128.1, 128.0, 127.7, 127.6, 127.5, 127.0, 126.9, 126.6, 126.1, 126.0, 113.5, 113.3, 110.7, 52.5, 51.6, 49.2, 45.6, 43.4, 26.2 ppm.

ESI-HRMS (m/z): found 1017.2585, calcd. 1017.2601 (C₅₃H₃₈N₆O₄Pt, M⁺).

UV/Vis (acetone): λ_{max} = 398, 482, 509, 550, 588 nm.

Melting point: > 300 ºC.

Platinum(II) $2^2,2^3$-bis(methoxycarbonyl)-5,10,15,20-tetrakis(4''-chlorophenyl)-2,2^1,2^6,3-tetrahydropyrazolo[1',5':1,6]pyrido[3,4-b]chlorin (10b)
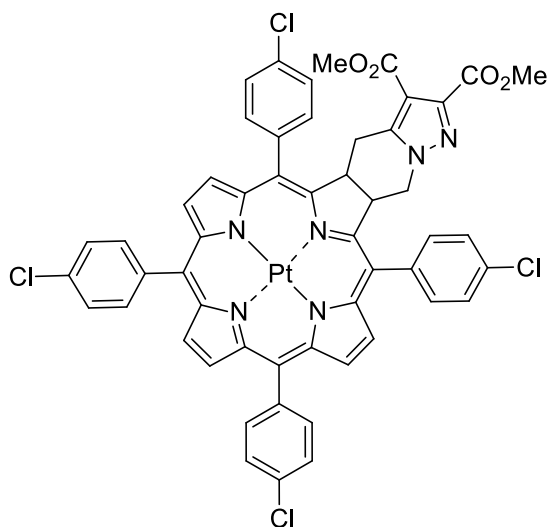
Obtained from porphyrin **9b**. Purification by flash column chromatography [CH$_2$Cl$_2$/ethyl acetate (95:5) v/v] gave compound **10b** (Method A: 0.03 g, 12 %; Method B: 0.02 g, 10 %).

^{1}H NMR (400 MHz, CDCl$_3$): δ = 8.38 (s, 2H, β-H pyrrolic), 8.35 (2d, superimposed doublets, J = 5.0 Hz, 2H, β-H pyrrolic), 8.13 (d, J = 5.1 Hz, 1H, β-H pyrrolic), 8.10 (d, J = 5.1 Hz, 1H, β-H pyrrolic), 8.01-7.95 (m, 3H, Ar), 7.92-7.85 (m, 4H, Ar), 7.78-7.72 (m, 4H, Ar), 7.69-7.60 (m, 6H, Ar), 5.70-5.63 (m, 1H, reduced β-H pyrrolic), 5.38-5.31 (m, 1H, reduced β-H pyrrolic), 4.38 (dd, J = 13.6, 7.4 Hz, 1H, CH$_2$ fused ring), 3.89 (s, 3H, CO$_2$Me), 3.88 (dd, J = 13.6, 9.8 Hz, 1H, CH$_2$ fused ring), 3.79 (s, 3H, CO$_2$Me), 3.54 (dd, J = 15.9, 6.7 Hz, 1H, CH$_2$ fused ring), 2.56 (dd, J = 15.9, 10.1?? Hz, 1H, CH$_2$ fused ring) ppm.

^{13}C NMR (100 MHz, CDCl$_3$): δ = 162.4, 162.0, 150.9, 148.4, 146.3, 146.1, 143.3, 143.0, 142.9, 138.9, 138.8, 138.4, 137.0, 136.1, 134.5, 134.3, 134.2, 132.6, 129.2, 129.0, 128.8, 128.1, 127.6, 127.4, 126.2, 126.1, 125.7, 125.4, 112.4, 112.1, 110.8, 77.3, 77.0, 70.1, 2.6, 51.6, 49.3, 46.9, 43.2, 26.1 ppm.

ESI-HRMS (m/z): found 1153.1021, calcd. 1153.1038 (C$_{53}$H$_{34}$Cl$_4$N$_6$O$_4$Pt, M$^+$).

UV/Vis (acetone): λ_{max} = 339, 482, 510, 550, 590 nm.

Melting point: > 300 ºC.

Platinum(II) $2^2,2^3$-bis(methoxycarbonyl)-5,10,15,20-tetrakis(4''-methoxyphenyl)-2,2^1,2^6,3-tetrahydropyrazolo[1',5':1,6]pyrido[3,4-b]chlorin (10c)
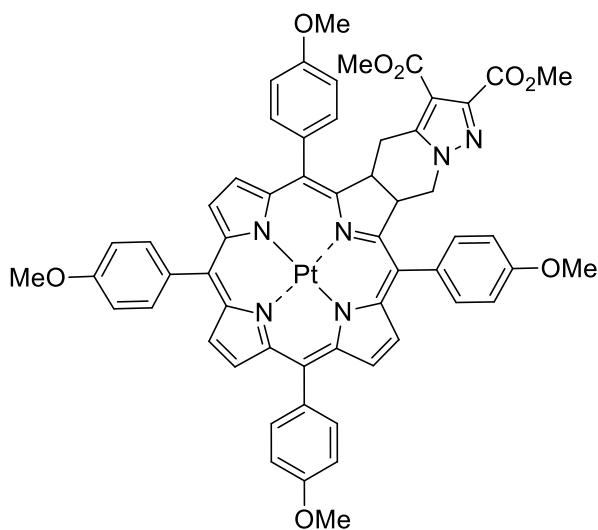
Obtained from porphyrin **9c**. Purification by flash column chromatography [CH$_2$Cl$_2$/ethyl acetate (97:3) v/v] gave compound **10c** (Method A: 0.05 g, 22 %; Method B: 0.004 g, 2 %).

^{1}H NMR (400 MHz, CDCl$_3$): δ = 8.44 (s, 2H, β-H pyrrolic), 8.40 (d, J = 4,8 Hz, 2H, β-H pyrrolic), 8.15 (d, 4,8 Hz, 2H, β-H pyrrolic), 8.03-7.83 (m, 8H, Ar), 7.30-7.26 (m, 2H, Ar), 7.23-7.09 (m, 6H, Ar), 5.73 (dd, J = 8, 12 Hz, 1H, reduced β-H pyrrolic), 5.35 (dd, J = 4, 12 Hz, 1H, reduced β-H pyrrolic), 4.44 (dd, J = 4, 8 Hz, 1H, CH$_2$ fused ring), 4.10 (d, 1H, CH$_2$ fused

ring), 4.06-4.00 (m, 12H, OMe), 3.90 (s, 3H, CO_2Me), 3.75 (s, 3H, CO_2CH_3), 3.59 (dd, J = 4, 4 Hz, 1H, CH_2 fused ring), 2.53 (dd, J = 12, 12 Hz, 1H, CH_2 fused ring) ppm.

ESI-HRMS (m/z): found 1137.3007, calcd. 1137.3023 ($C_{57}H_{46}N_6O_8Pt$, M^+).

UV/Vis (acetone): λ_{max} = 403, 482, 510, 550, 589 nm.

Melting point: > 300 ºC.

4.1.7. General synthesis of platinum(II) diacid chlorins 11

   A solution of Pt(II) chlorin **10** (0.025 mmol) in THF (5 mL) was treated with saturated aqueous KOH (0.5 mL) and the reaction mixture was stirred at room temperature for 24 hours. The solvent was evaporated under reduced pressure. Water (5 mL) was added to the residue, the solution cooled to 0 ºC and then neutralized by the dropwise addition of HCl (1M). Product was filtered and washed with water. Chlorins **11** were purified by flash column chromatography [CH_2Cl_2/methanol (90:10) v/v] and obtained as purple solids.

Platinum(II) **$2^2,2^3$-bis(hydroxycarbonyl)-5,10,15,20-tetraphenyl-2,2^1,2^6,3-tetrahydropyrazolo[1',5':1,6]pyrido[3,4-*b*]chlorin (11a)**
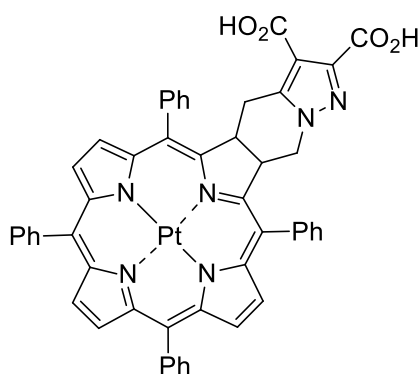
Pt(II) chlorin **11a** was obtained in 61 % yield (0.015 g, 0.015 mmol) from chlorin **10a**.

^{1}H NMR (400 MHz, DMSO-d_6): δ = 8.39 (s, 2H, β-H pyrrolic), 8.30 (dd, J = 5.0, 1.0 Hz 2H, β-H pyrrolic), 8.17 (dd, J = 21.0, 6.6 Hz, 2H, β-H pyrrolic), 8.11-7.90 (m, 8H, Ar), 7.84-7.68 (m, 12H, Ar), 5.97-5.57 (m, 1H, reduced β-H pyrrolic), 5.61-5.56 (m, 1H, reduced β-H pyrrolic), 4.29 (dd, J = 13.4, 6.3 Hz, 1H, CH_2 fused ring), 4.04 (dd, J = 13.4, 6.3 Hz, 1H, CH_2 fused ring), 3.46 (dd, J = 17.2, 10.3 Hz, 1H, CH_2 fused ring), 3.40 (dd, J = 17.2, 10.3 Hz, 1H, CH_2 fused ring) ppm.

ESI-HRMS (m/z): found 990.2370, calcd. 990.2366 [$C_{51}H_{35}N_6O_4Pt$, $(M+H)^+$].

UV/Vis (acetone): λ_{max} = 398, 482, 509, 551, 590 nm.

UV/Vis (toluene): λ_{max} (logε) = 402 (5.15), 511 (4.15), 540 (3.80), 590 (4.15) nm.

Melting point: > 300 ºC.
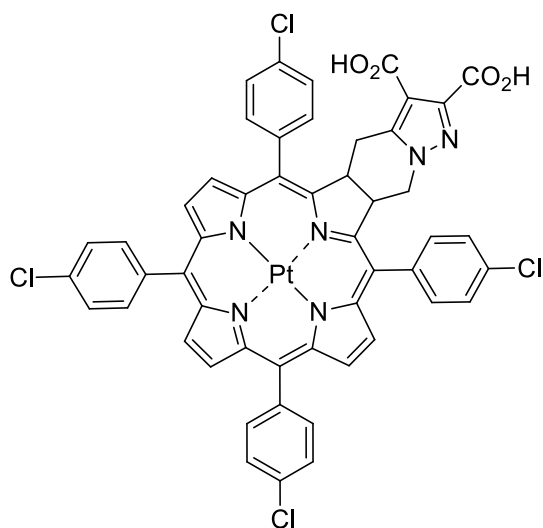
Platinum(II)   2²,2³-bis(hydroxycarbonyl)-5,10,15,20-tetrakis(4''-chlorophenyl)-2,2¹,2⁶,3-tetrahydropyrazolo[1',5':1,6]pyrido[3,4-*b*]chlorin (11b)

Pt(II) chlorin **11b** was obtained in 88 % yield (0.025 g, 0.022 mmol) from chlorin **10b**.

¹H NMR (400 MHz, DMSO-d₆): δ = 8.66 (s, 2H, β-H pyrrolic), 8.20-8.15 (m, 8H, Ar), 8.07 (s, 2H, β-H pyrrolic), 8.05 (s, 2H, β-H pyrrolic), 7.94-7.85 (m, 8H, Ar), 5.40 (m, 1H, reduced β-H pyrrolic), 5.31 (m, 1H, reduced β-H pyrrolic), 4.88 (m, 1H, CH₂ fused ring), 4.33 (m, 1H, CH₂ fused ring), 2.68 (m, 1H, CH₂ fused ring), 2.33 (m, 1H, CH₂ fused ring) ppm.

ESI-HRMS (m/z): found 1122.0475, calcd. 1122.0491 [$C_{55}H_{42}Cl_4N_6O_8Pt$, (M-3⁺)].

UV/Vis (CH₂Cl₂): λ_{max} = 409, 517, 546, 561, 582 nm.

Melting point: > 300 ºC.

Platinum(II)   2²,2³-bis(hydroxycarbonyl)-tetrakis(4''-methoxyphenyl)-2,2¹,2⁶,3-tetrahydropyrazolo[1',5':1,6]pyrido[3,4-*b*]chlorin (11c)
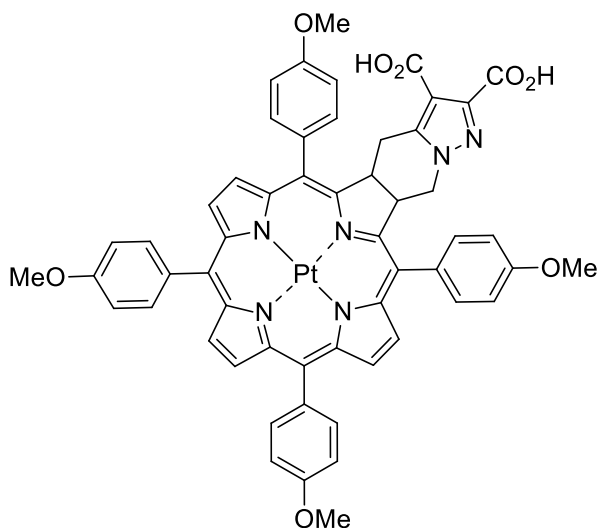
Pt(II) chlorin **11c** was obtained in 76 % yield (0.021 g, 0.019 mmol) from chlorin **10c**.

¹H NMR (400 MHz, DMSO-d₆): δ = 8.37 (s, 2H, β-H pyrrolic), 8.33 (d, J = 5.0, 2H, β-H pyrrolic), 8.17 (d, J = 5.0 Hz, 2H, β-H pyrrolic), 8.11-8.06 (m, 3H, Ar), 8.02-7.87 (m, 7H, Ar), 7.31-7.26 (m, 6H, Ar), 5.92 (m, 1H, reduced β-H pyrrolic), 5.56 (m, 1H, reduced β-H pyrrolic), 4.26 (m, 1H, CH₂ fused ring), 4.10 (m, 1H, CH₂ fused ring), 4.00 (s, 12H, 1H, OMe), 2.68 (m, 1H, CH₂ fused ring), 2.16 (m, 1H, CH₂ fused ring) ppm.

ESI-HRMS (m/z): found 1109.2720, calcd. 1109.2751 ($C_{55}H_{42}N_6O_8Pt$, M⁺).

UV/Vis (acetone): λ_{max} = 404, 482, 516, 551, 591 nm.

Melting point: > 300 ºC.

4.1.8. General synthesis of platinum(II) dialcohol chlorins 12

Pt(II) chlorins **12** were prepared as described in the literature with some changes. A solution of Pt(II) chlorin **10** (0.060 mmol) in dry dichloromethane (3 mL) was added dropwise to a stirred suspension of LiAlH$_4$ (0.72 mmol, 12 equiv.) in dry diethyl ether (3 mL), at 0 °C. After the addition was complete, the mixture was heated to 50 °C and was left stirring during the necessary time for each compound. The reaction mixture was cooled to 0 °C (ice bath) and quenched over a 15 minute period with ethyl acetate (0.5 mL) followed by HCl 1 M (0.5 mL). Solvents were evaporated under reduced pressure and the residue redissolved in dichlomethane and purified by flash column chromatography [ethyl acetate/methanol (95:5) v/v]. Chlorins **12** were obtained as purple solids.

Platinum(II) 2²,2³-bis(hydroxymethyl)-5,10,15,20-tetraphenyl-2,2¹,2⁶,3-tetrahydropyrazolo[1',5':1,6]pyrido[3,4-*b*]chlorin (12a) (Pereira et al. 2017)
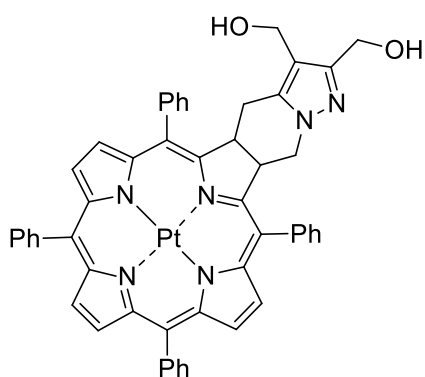
Pt(II) chlorin **12a** was obtained in 81 % yield (0.047 g, 0.049 mmol) from chlorin **10a**. Reaction time: 5 hours.

¹H NMR (400 MHz, CDCl$_3$): δ = 8.40 (s, 2H, β-H pyrrolic), 8.38-8.35 (m, 2H, β-H pyrrolic), 8.17-8.16 (m, 2H, β-H pyrrolic), 8.10-8.08 (m, 1H, Ar), 8.06-7.93 (m, 6H, Ar), 7.82-7.80 (m, 1H, Ar), 7.76-7.58 (m, 12H, Ar), 5.72-5.65 (m, 1H, reduced β-H pyrrolic), 5.35-5.29 (m, 1H, reduced β-H pyrrolic), 4.52 (s, 2H, CH$_2$OH), 4.22 (d, J = 12.6 Hz, 1H, CH$_2$OH), 4.15 (d, J = 12.6 Hz, 1H, CH$_2$OH), 4.10 (dd, J = 13.3, 7.8 Hz, 1H, CH$_2$ fused ring), 3.89 (dd, J = 13.3, 9.5 Hz, 1H, CH$_2$ fused ring), 2.91 (dd, J = 15.2, 6.3 Hz, 1H, CH$_2$ fused ring), 2.47 (dd, J = 15.2, 10.2 Hz, 1H, CH$_2$ fused ring) ppm.

¹³C NMR (100 MHz, CDCl$_3$): δ = 151.4, 149.5, 149.3, 146.2, 146.1, 140.8, 140.5, 138.2, 138.1, 137.8, 135.8, 135.6, 134.7, 134.3, 133.2, 132.2, 132.1, 131.6, 131.5, 128.7, 128.6, 128.5, 128.1, 127.9, 127.6, 127.4, 127.3, 127.0, 126.6, 126.4, 126.0, 115.8, 113.5, 57.9, 54.2, 53.4, 48.5, 46.1, 44.3, 25.0 ppm.

ESI-HRMS (m/z): found 961.2691, calcd. 961.2702 (C$_{51}$H$_{38}$N$_6$O$_2$Pt, M$^+$).

UV/Vis (acetone): λ_{max} = 398, 484, 513, 551, 590 nm.

Melting point: > 300 ºC.

Platinum(II) 2²,2³-bis(hydroxymethyl)-tetrakis(4''-chlorophenyl)-2,2¹,2⁶,3-tetrahydropyrazolo[1',5':1,6]pyrido[3,4-*b*]chlorin (12b)
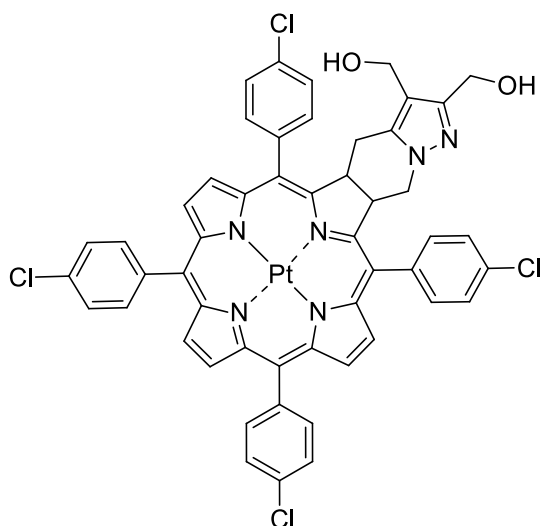
Pt(II) chlorin **12b** was obtained in 73 % yield (0.048 g, 0.049 mmol) from chlorin **10b**. Reaction time: 5 hours.

¹H NMR (400 MHz, CDCl₃): δ = 8.33-8.29 (m, 4H, β-H pyrrolic), 8.12 (d, J = 4 Hz, 1H, β-H pyrrolic), 8.07 (d, j = 4 Hz, 1H, β-H pyrrolic), 7.72-7.66 (m, 4H, Ar), 7.99-7.52 (m, 8H, Ar), 5.61-5.54 (m, 1H, reduced β-H pyrrolic), 5.26-5.24 (m, 1H, reduced β-H pyrrolic), 4.43-4.34 (m, 3H, CH₂OH), 4.17 (m, 2H, CH₂OH), 4.09-4.05 (m, 2H, CH₂OH), 3.80 (dd, J = 8 Hz, 1H, CH₂ fused ring), 2.41 (dd, J = 8, 12 Hz, 1H, CH₂ fused ring), 2.84 (dd, J = 4 Hz, 1H, CH₂ fused ring) ppm.

¹³C NMR (100 MHz, CDCl₃): δ = 151.7, 150.0, 149.5, 145.1, 139.0, 138.9, 137.4, 136.7, 135.7, 136.4, 136.2, 134.8, 134.5, 134.2, 132.7, 132.6, 132.3, 132.2, 129.0, 128.9, 128.5, 127.9, 127.3, 126.1, 125.4, 125.2, 77.4, 77.1, 76.7, 54.4, 54.0, 48.4, 45.9, 44.0, 29.7, 25.0 ppm.

ESI-HRMS (m/z): found 1097.1165, calcd. 1097.1140 (C₅₁H₃₄Cl₄N₆O₂Pt, M⁺).

UV/Vis (acetone): λ_{max} = 398, 484, 513, 551, 590 nm.

Melting point: > 300 ºC.

Platinum(II) 2²,2³-bis(hydroxymethyl)-tetrakis(4''-methoxyphenyl)-2,2¹,2⁶,3-tetrahydropyrazolo[1',5':1,6]pyrido[3,4-b]chlorin (12c)
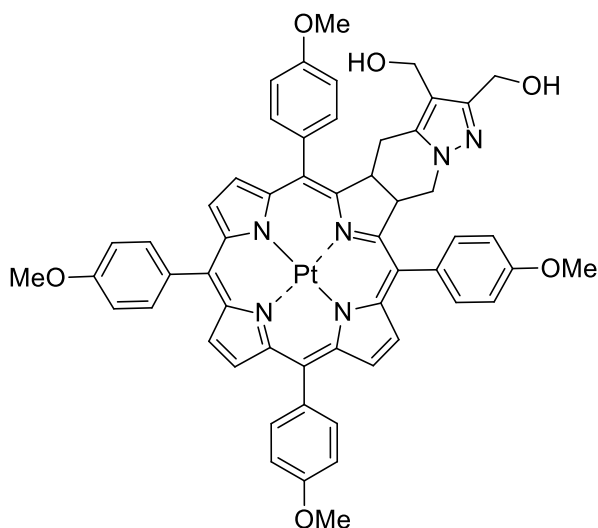
Pt(II) chlorin **12c** was obtained in 20 % yield (0.013 g, 0.049 mmol) from chlorin **10c**. Reaction time: 32 hours.

¹H NMR (400 MHz, CDCl₃): δ = 8.40 (s, 2H, β-H pyrrolic), 8.37 (d, J = 4.6 Hz, 2H, β-H pyrrolic), 8.34 (d, J = 4.6 Hz, 2H, β-H pyrrolic), 8.14-8.07 (m, 3H, Ar), 7.20-6.96 (m, 15H, Ar), 5.65 (m, 1H, reduced β-H pyrrolic), 5.21 (m, 1H, reduced β-H pyrrolic), 4.49 (s, 2H, CH₂OH), 4.15 (m, 1H, reduced β-H pyrrolic), 4.06 (s, 2H, CH₂OH), 4.02 (s, 2H, CH₂OH), 3.98 (s, 3H, OMe), 3.94 (s, 3H, OMe), 3.93 (s, 2H, CH₂OH), 3.90 (s, 3H, OMe), 3.87 (s, 3H, OMe), 2.85 (m, 1H, CH₂ fused ring), 2.34 (m, 1H, CH₂ fused ring) ppm.

ESI-HRMS (m/z): found 1082.3204, calcd. 1082.3204 (C₅₅H₄₆Cl₄N₆O₆Pt, M⁺).

UV/Vis (acetone): λ_{max} = 403, 484, 513, 551, 590 nm.

Melting point: > 300 ºC.

4.2. Experimental - Part II

4.2.1. Cell Culture

Three human cell lines of different tumour tissues were used, one of bladder cancer, one of esophageal cancer and one of melanocytic melanoma. The bladder carcinoma cell line is designated HT1376 and the melanoma cell line is designated A375. Both were obtained from the American Type Culture Collection (ATCC, CRL-1472 and CRL-1619, respectively). The esophageal carcinoma cell line is designated OE19 and was obtained from the European Collection of Cell Cultures (ECACC, JROECL19).

For the HT1376 and A375 cell lines was used Dulbecco's Modified Eagle's Medium (DMEM, Sigma D-5648) supplemented with 10% fetal bovine serum (FBS, Sigma F7524), 100 µM sodium pyruvate (Gibco 11360), and 1% antibiotic (100 U/mL penicillin and 10 µg/mL streptomycin; Gibco 1360). For the OE19 cell line Roswell Park Memorial Institute 1640 Medium (RPMI, Sigma R4130) culture medium supplemented with 10% fetal bovine serum, 1 mM sodium pyruvate and 1% antibiotic was used.

Cell lines used were thawed and propagated in adherent culture according to providers' recommendations and maintained at 37 °C in a humidified atmosphere with 95 % air and 5 % CO_2 in *Binder* incubator.

Cells form a monolayer, growing adherent to the solid support (flasks or cell culture plates). In order to carry out the *in vitro* studies these cells need to be transferred to suitable carriers, multiwell plates, and enzymatic methods were used to prepare the cell suspensions. Thus, cell cultures were initially washed with a phosphate buffered saline (PBS), consisting of 137 mM NaCl (Sigma S7653), 2.7 mM KCl (Sigma P9333), 10 mM NaH_2PO_4 (Sigma S5011) and 1.8 mM KH_2PO_4 (Sigma P0662), pH was set at 7.4 and incubated at 37 °C with 3 mL of a trypsin-EDTA solution at 0.25 % (Sigma T4049) for the time required for the cells to release from the flask. Thereafter, 6 mL of culture medium was added to inactivate the enzymatic solution, the cell suspension was homogenized and the cell concentration was determined. To do this, a known volume of cell suspension was diluted in equal volume of trypan blue and counted in an inverted microscope (Motic AE31), with a 10x magnification, using the hemocytometer (*Neubauer* chamber). The trypan blue method allows cells to be counted in a cell suspension. This technique is simple and inexpensive, providing reliable information on the total number of cells in the suspension (Sarma, Ray, and Antony 2000). After counting, the volume of the cell suspensions was adjusted with culture medium in order to obtain the desired cell concentration for each study.

4.2.2. Photodynamic treatment

The photosensitizers were solubilized in dimethylsulfoxide (DMSO, Fisher Chemical, 200-664-3) at a concentration of 1 mg/mL, being that the desired concentrations were achieved by successive dilutions in the same solvent. The concentration of all solutions of photosensitizers was adjusted, so that their addition only altered at most the volume of culture medium from the cell compartments by 1 %. Tested concentrations ranged from 5 nM to 10 μM.

The cell cultures submitted to the photodynamic treatment were incubated for 24 hours with the desired photosensitizer concentrations. After this time, a wash was carried out with PBS, pH 7.4, which ensured that all the photosensitizer not internalized by the cells was removed, and culture medium was added to the cell cultures. In all studies the cultures were irradiated with a photon flux of 7.5 mW/cm² to a total of 10 J. Irradiation for photodynamic treatment was performed using a fluorescent light source equipped with a red filter ($\lambda_{\text{cut off}} < 560$ nm). The evaluation by the methodologies described below was performed 24 hours after the photodynamic treatment.

4.2.3. Photocytotoxicity and dark cytotoxicity

To evaluate the effect of the photosensitizers on the metabolic activity of the cells, the MTT (3-(4,5-dimethylthiazol-2-yl)-2,5-diphenyltetrazolium bromide assay) was performed. This compound is reduced by metabolically active cells due to the action of dehydrogenase enzymes, mainly through the action of complex II of the mitochondrial respiratory chain, succinate dehydrogenase or succinate-coenzyme Q reductase. The dehydrogenases have the ability to cleave the MTT tetrazolium rings and form dark blue formazan crystals which can be subsequently solubilized and quantified by spectrophotometric means. Thus, this method is an indirect way of evaluating mitochondrial cell function and the amount of formazan crystals obtained is directly proportional to the metabolic activity of the cell (Mosmann 1983).

The cell suspensions of HT1376, OE19 and A375 were distributed into 48-well plates. These plates were incubated overnight to allow cell adhesion. Sensitizers were administered at varying concentrations between 5 nM and 10 μM. In all assays two controls were performed: untreated cell cultures and cell cultures subjected to the sensitizer delivery vehicle (DMSO). Metabolic activity analysis was performed 24 hours after the photodynamic treatment. For the evaluation of metabolic activity, the cell cultures medium was aspirated and washed with PBS from each well. Subsequently, 150 μL of a solution of MTT (0.5 mg/mL; Sigma M5655) in PBS, pH 7.4, was placed in each well and incubated in the dark at 37 °C for 3 hours. To solubilize the obtained formazan crystals, 150 μL of a 0.04 M solution of hydrochloric acid (Merck Millipore 100317) in isopropanol (Sigma 278475) was added to each well and the plates allowed to stir until complete dissolution. The contents of each well were subsequently homogenized and transferred to a 96-well plate (Costar 3596), and the absorbance was quantified at 570 nm with a reference filter of 620 nm using the Biotek® Synergy HT spectrophotometer.

Dark cytotoxicity studies were performed against the three human tumour cell lines, as described previously, but without the step of irradiation.

In addition, dark cytotoxicity was also performed in a human non-tumour cell line to evaluate the selectivity of the synthesized sensitizers for tumour cells. The cell line chosen was a fibroblasts cell line designated HFF1, purchased from ATCC. This cell line was received, thawed and cultured in adherent culture according to the supplier's recommendations. The cell line was maintained at 37 °C in a humidified atmosphere with 95 % air and 5 % CO_2 in *Binder* incubator. DMEM culture medium supplemented with 20 % fetal bovine serum, 100 μM sodium pyruvate and 1 % antibiotic was used. For cytotoxicity studies, the cells were incubated in 48-well plates with the photosensitizers according to the same procedure already described and the MTT assay was performed according to the methodology referred to above.

The metabolic activity was expressed as a percentage of the metabolic activity of the cultures submitted to the photodynamic treatment in relation to the metabolic activity of the cultures treated with the sensitizer administration vehicle alone. This procedure allowed to establish dose-response curves and to determine the concentration of the sensitizers that inhibits the metabolic activity of the cultures in 50 % (IC_{50}). The obtained results were analysed, processed in the program OriginPro 9.0 and adjusted to a sigmoid curve according to the equation:

$$MA = \frac{100}{1 + e^{(\log x_0 - \log C) \times s}}$$

where MA represents the metabolic activity, C is the concentration, s is the slope of the central region of the sigmoid and x_0 is the IC_{50}. The 95 % confidence intervals for the IC50 were obtained from the parameters obtained by curve fitting ($\log x_0$ and respective standard error).

4.2.4. Cell viability

The sulforhodamine B (SRB) assay allows assessment of cell viability by correlation with total protein content. Sulforrodamine B is a purplish, anionic and pH dependent dye, with affinity for amino acids, to which it binds electrostatically. Under acidic conditions it binds to the amino acids of cellular proteins and, under alkaline conditions, can be extracted. After fixation, solubilization and measurement by spectrophotometric methods, the results obtained correlate with the number of cells through total protein content (Papazisis et al. 1997; Vichai and Kirtikara 2006).

In order to carry out cell viability and subsequent studies it has been chosen to use only the A375 melanoma cell line.

Sensitizers **11a** and **12a** were administered at concentrations of 50 nM, 250 nM and 500 nM. In each study two controls were performed, one with untreated cells and the other with the sensitizer delivery

vehicle. Photodynamic treatment was performed as described above, and the SRB assay was performed 24 hours after irradiation.

For the SRB assay, 200 µL of trichloroacetic acid 96% (Panreac 151067) were added and incubated for 1 hour at 4 °C. After this time, the supernatant was discarded and 200 µL of SRB at 0.4% (Sigma S9012) dissolved in 1% acetic acid (Sigma 109088) in methanol (Sigma 322415) were added to each well and plates were stored for 1 hour in the dark. After this time, the plates were washed to remove excess SRB and, after drying the plate, 200 µL of TRIS-NaOH (pH 10) (Sigma T1503) were added. Absorbance reading was done at wavelength 540 nm, with a reference filter of 690 nm, in a Biotek® Synergy HT spectrophotometer. The results were expressed as percentage of the protein content of the cultures submitted to the photodynamic treatment in relation to the protein content of the cultures treated only with the sensitizer delivery vehicle.

4.2.5. Cell death

4.2.5.1. Types of cell death

Types of cell death were evaluated by flow cytometry. Flow cytometry allows to count, examine and classify cells or other microscopic particles suspended in liquid medium. This technique allows rapid analysis of various physical and chemical characteristics of cells in a suspension by means of an optoelectronic device. In order to evaluate the cell death resulting from the photodynamic therapy, the double labelling with annexin V (AnV) linked to fluorescein isothiocyanate (FITC) and propidium iodide (PI) was used to distinguish different types of cell death, necrosis and apoptosis. Annexin V allows the identification of apoptotic cells, since the FITC binds specifically to phosphatidylserine, a phospholipid of the lipid bilayer that, in apoptotic cells, moves from the inner leaflet to the outer leaflet of the cell membrane. Complementarily, propidium iodide is a dye that intercalates in the DNA of cells, marking the nuclei of those that are in late apoptosis or necrosis. In this way, it is possible to distinguish four groups of cells: the living cells, which are negative for both labellings, the annexin V and the propidium iodide, the apoptotic cells, which are positive for annexin V and negative for propidium iodide, the cells that are in late apoptosis/necrosis, which are positive for both labellings, and the necrotic cells, which are negative for annexin V and positive for propidium iodide.

For these studies, cell cultures were subjected to photodynamic treatment with the photosensitizer in concentrations of 50 nM, 250 nM and 500 nM.

About 1.5×10^6 cells of each condition were obtained after centrifugation of a cell suspension at 1300 xG for 5 minutes. The pellet was incubated with 100 µL of binding buffer (consisting of 0.01 M Hepes [Sigma H7523], 0.14 M NaCl [Sigma S7653] and 0.25 mM $CaCl_2$ [Sigma C4901]), 2.5 µL AnV-FITC (Immunostep ANXVFKIT Immunotech) and 1 µL of IP (KIT Immunotech) for 15 minutes at room temperature in the dark. After incubation, 400 µL of PBS was added and analysed on the cytometer FACSCalibur cytometer (BD Biosciences) with the excitation wavelength of 494 nm and the emission wavelength of 519 nm. For the analysis and quantification of the information,

a specific software (Paint-a-Gate 3.02, Machintosh Software) was run in a dedicated computer. The results are presented as percent live cells, apoptotic, late apoptosis/necrosis and necrotic.

4.2.5.2. Mitochondrial membrane potential

The mitochondrial membrane potential was determined using a fluorescent probe, JC-1 (5,5', 6,6'-tetrachloro-1,1',3,3'-tetraethylbenzimidazolcarbocyanine iodide). JC-1 is a lipophilic cation that exists in two forms, in monomers (M) and aggregates (A), depending on the polarization/depolarization state of the mitochondrial membrane, emitting fluorescence at different wavelengths. When the membrane potential is high, it forms clusters that emit red fluorescence (590 nm). In turn, as the mitochondrial membrane potential decreases, or in cases where the membrane is depolarized, JC-1 is excluded from mitochondria and remains in the cytoplasm as monomers, which emit green fluorescence (529 nm). Thus, the ratio between green and red fluorescence (M/A, ratio monomers/aggregates), determined by flow cytometry, provides an estimate of mitochondrial membrane potential (St John et al. 2006).

For the accomplishment of these studies, the cellular cultures were submitted to the photodynamic treatment with the photosensitizers in the concentrations of 50 nM, of 250 nM and of 500 nM.

Approximately 1.5×10^6 cells were centrifuged with PBS for 5 minutes at 1300 xG and then suspended in 1 mL of the same buffer. The cell suspensions were incubated for 15 minutes at 37 °C and protected from light with 1 µL of JC-1 (Sigma T4069), prepared in 5 mg/mL of DMSO and subsequently diluted to give a final concentration of 5 µg/mL. The suspension was then washed again with PBS and resuspended in 400 µL of the same buffer. Detection was performed on the cytometer with an excitation wavelength of 488 nm. The results obtained correspond to the mean fluorescence intensity (MFI) for the aggregates and for the monomers, and the M/A ratio for each experimental condition was calculated.

4.2.6. Cell cycle

In order to characterize the effect of the photodynamic treatment, not only in the DNA, but also in the cellular nucleus, flow cytometry studies were performed to characterize the phases of the cell cycle.

To determine possible changes in the cell cycle, propidium iodide (IP) was used, a dye commonly used for DNA and cell cycle analysis by flow cytometry. Since this dye has the ability to bind to DNA by intercalating into the double strand of the macromolecule, the amount of dye attached is proportional to the amount of DNA. Thus, it is possible to quantify the DNA content, which allows us to know the distribution of a population of cells throughout the different phases of the cell cycle. Cells can be classified as G2 and M, G0, G1 and S cells (Douglas et al. 1995; Kalejta, Shenk, and Beavis 1997).

For the accomplishment of these studies, the cell cultures were submitted to the photodynamic treatment with the photosensitizers **11a** and **12a** in the concentrations of 50 nM, of 250 nM and of 500 nM.

The evaluation was done through PI/RNase solution (PI/RNase, Immunostep). For this assay the cells were centrifuged at 1300 xG for 5 minutes, and the supernatant was discarded. 200 µL of 70% ethanol (Sigma 24102) was added to the stirred tube in the vortex. The tubes were incubated for 30 minutes at 4 °C. Thereafter, the cells were washed with 2 mL of PBS and centrifuged at 1300 xG for 5 minutes. The supernatant was discarded and 500 µL PI/RNase solution was added and incubated for 15 minutes in the dark at 37 °C. Detection was performed on the FACSCalibur cytometer (BD Biosciences), where an excitation wavelength of 488 nm was used. The results are presented as percentage of cells in the G1 or G0 phase, the S phase or the G2 and M phases.

4.2.7. Oxidative Stress

The oxidative stress is fundamental in the photodynamic reaction. Therefore, the implication of several ROS in the PDT, based on the photosensitizers **11a** and **12a**, was also studied, as well as some antioxidant defences that may have a cytoprotective role, possibly limiting the therapeutic result.

4.2.7.1. Singlet oxygen and hydroxyl radical

Singlet oxygen is often considered the most important ROS in PDT. In the impossibility of directly evaluating its intracellular concentration after PDT based on **11a** and **12a** photosensitizers, studies were conducted in the presence of an inhibitor of this species. Sodium azide, which is a quencher of this oxygen reactive species, was used. In the same way studies were performed in the presence of D-mannitol constituting a scavenger of the hydroxyl radical.

For this study, we adapted a protocol developed by Obata *et al.* (Obata et al. 2009), whereby cell suspensions of the melanoma lines were prepared and distributed in 48-well plates. Cell cultures were incubated for 24 hours with the photosensitizer at concentrations of 50 nM, of 200 nM and of 500 nM. Before irradiation, the medium was replaced by culture medium without photosensitizer, supplemented with 5 mM sodium azide (Sigma 71290) or with 40 mM D-mannitol (Sigma M4125). Plates were irradiated with 10 J as described previously and after 30 minutes the medium was replaced by culture medium without inhibitors and without photosensitizer. The evaluation of metabolic activity was performed 24 hours after the photodynamic treatment, through the MTT assay as previously described.

4.2.7.2. Intracellular production of superoxide anion

The evaluation of superoxide radical production was performed using the DHE probe. This compound easily crosses the cell membranes and is converted by the superoxide radical into ethidium, a red fluorescent compound that intersperses in the DNA remaining within the cell. This reaction is relatively specific to the superoxide radical, since it only occurs with minimal oxidation by hydrogen peroxide, nitrite peroxide or hypochlorous acid (Hongtao Zhao et al. 2005).

For the accomplishment of these studies, the cellular cultures were submitted to the photodynamic treatment with the photosensitizers **11a** and **12a** in the concentrations of 50 nM, of 250 nM and of 500 nM.

Approximately 1.5×10^6 cells obtained after centrifugation of a cell suspension at 1300 xG for 5 minutes were used. The supernatant was removed and the pellet washed once with PBS. Then, the pellet was suspended in 1 mL of PBS and 5 µL of DHE (Sigma Aldrich D7008) were added to give a final concentration of 5 µM. Incubated for 15 minutes at 37 °C and the suspension was washed with PBS, centrifuged at 1300 xG for 5 minutes and suspended in 400 µL of the same buffer. An excitation wavelength of 465/40 nm and an emission wavelength of 530/25 nm were selected on Biotek® Synergy HT fluorimeter for detection purposes. Each of these results was shown to be the fluorescence intensity and correlated with cell cultures having a value of 1 (Dias Ferreira 2017).

4.2.7.3. Intracellular production of peroxides

Intracellular expression of peroxides was also determined by the intracellular oxidation of the non-fluorescent probe 2',7'-dichlorodihydrofluorescein diacetate (DCFH2-DA). This liposoluble compound enters cells and accumulates mainly in the cytosol, where it is deacetylated by intracellular esterases in 2',7'-dichlorodihydrofluorescein (DCFH). This non-fluorescent product is oxidized in the presence of peroxides with the formation of 2',7'-dichlorofluorescein (DCF), a compound which is easily visualized by the fluorescence emission, which is proportional to the concentration of intracellular peroxides, namely hydrogen peroxide (Dikalov, Griendling, and Harrison 2007; Tarpey 2004).

For these studies, the cellular cultures were submitted to the photodynamic treatment with the photosensitizers **11a** and **12a** in the concentrations of 50 nM, of 200 nM and of 500 nM.

Thus, a cell suspension was centrifuged with approximately 1.5×10^6 cells at 1300 xG for 5 minutes and PBS was added to wash. The pellet was suspended in 1 mL PBS and incubated for 45 minutes, without light, at 37 °C with 5 µM of DCFH2-DA (Invitrogen Life technologies D399). The suspension was washed with PBS, centrifuged at 1300 xG for 5 minutes and suspended in buffer. An excitation wavelength of 485/20 nm and an emission wavelength of 528/20 nm were selected on Biotek® Synergy HT fluorimeter for detection purposes. The results are obtained on the average fluorescence intensity form and were presented in relation to the control cell cultures, which were assigned the value 1.

4.2.7.4. Reduced glutathione

In order to evaluate the intracellular expression of reduced glutathione (GSH), a non-enzymatic antioxidant defence, a fluorescent compound, the orange of mercury, was used. This compound reacts rapidly with GSH, giving rise to a reaction product that emits intense red fluorescence (Hedley and Chow 1994).

For these studies, the cellular cultures were submitted to the photodynamic treatment with the photosensitizers **11a** and **12a** in the concentrations of 50 nM, of 250 nM and of 500 nM.

For this procedure, the cells were centrifuged at 1300 xG for 5 minutes and the supernatant was discarded. The pellet was suspended in 1 mL of PBS and 4 µL of 10 mM mercury orange (Sigma M7750) were added. The suspension was homogenized and incubated for 15 minutes in the dark at 37 °C. Thereafter, the suspension was washed with PBS and centrifuged at 1300 xG for 5 minutes, and suspended in buffer. An excitation wavelength of 485/20 nm and an emission wavelength of 590/35 nm were selected on Biotek® Synergy HT fluorimeter for detection purposes. The results were obtained on the average fluorescence intensity form and were presented as a ratio to control cell cultures to which the value 1 was assigned.

4.2.8. Statistical Analysis

Statistical analysis was performed via IBM® SPSS® software, version 22.0 (IBM Corporation, ARMONK, New York, USA). The results of the *in vitro* studies are presented as mean ± standard deviation (SD) or mean ± standard error (SE). The normality of the distribution of each quantitative variable was evaluated according to the Shapiro-Wilk test, with the aim of determining the use of parametric or non-parametric tests in the intended comparisons.

The comparison of the metabolic activity and cell viability of the cell cultures submitted to treatment was performed with the one sample t-test, comparing the sample value of each group with the 100 % normalization value.

The comparison of the values of the experimental conditions obtained in the studies of intracellular production of superoxide anion, peroxides and reduced glutathione were carried out with the one sample t-test with a comparing value of 1.

As regards the evaluation of the influence of singlet oxygen and hydroxyl radical, the metabolic activity and respective standard deviation for the concentrations of photosensitizers in question were determined initially from the dose-response curves previously obtained. The comparison of the experimental values obtained in combination with the values calculated from the curves was performed by the t-student test.

In the cases of types of cell death, mitochondrial membrane potential and cell cycle, the comparison between conditions was performed with ANOVA (*Analysis of variance)* test in cases where normal distribution and homogeneity of variances were verified or with the Kruskal-Wallis test in the

otherwise. Between some pairs of experimental groups multiple comparisons were made which were corrected using Bonferroni method with a significance level of 5 % for all comparisons.

Bibliography

Academy, Romanian, and Complexo Interdisciplinar. 2008. "Microwave-Assisted Synthesis of Unsymmetrical Tetrapyrrolic Compounds." (9): 969–72.

Acedo, P., J. C. Stockert, M. Cañete, and A. Villanueva. 2014. "Two Combined Photosensitizers: A Goal for More Effective Photodynamic Therapy of Cancer." *Cell Death and Disease.*

Agostinis, Patrizia et al. 2011. "Photodynamic Therapy of Cancer: An Update." *CA: A Cancer Journal for Clinicians* 61(4): 250–81. http://doi.wiley.com/10.3322/caac.20114.

Alexandridis, Paschalis, Josef F. Holzwarth, and T. Alan Hatton. 1994. "Micellization of Poly(Ethylene Oxide)-Poly(Propylene Oxide)-Poly(Ethylene Oxide) Triblock Copolymers in Aqueous Solutions: Thermodynamics of Copolymer Association." *Macromolecules* 27(9): 2414–25.

Ali-Seyed, Mohamed, Ramaswamy Bhuvaneswari, Khee Chee Soo, and Malini Olivo. 2011. "Photolon??? - Photosensitization Induces Apoptosis via ROS-Mediated Cross-Talk between Mitochondria and Lysosomes." *International Journal of Oncology.*

Allison, Ron R., and Claudio H. Sibata. 2010. "Oncologic Photodynamic Therapy Photosensitizers: A Clinical Review." *Photodiagnosis and Photodynamic Therapy* 7(2): 61–75.

Allison, Ron R. 2014. "Photodynamic Therapy: Oncologic Horizons." *Future Oncology* 10(1): 123–24. http://www.futuremedicine.com/doi/10.2217/fon.13.176.

Almeida, Ramiro D, Bruno J Manadas, Arsélio P Carvalho, and Carlos B Duarte. 2004. "Intracellular Signaling Mechanisms in Photodynamic Therapy." *Biochimica et biophysica acta.*

Armarego, Wilfred L.F., and Christina Li Lin Chai. 2003. Purification of Laboratory Chemicals: Fifth Edition *Purification of Laboratory Chemicals: Fifth Edition.*

Benov, Ludmil. 2015. "Photodynamic Therapy: Current Status and Future Directions." In *Medical Principles and Practice*, , 14–28.

Boyle, Ross W., and David Dolphin. 1996. "Structure and Biodistribution Relationships of Photodynamic Sensitizers." *Photochemistry and Photobiology* 64(3): 469–85.

Brown, Stanley B, Elizabeth A Brown, and Ian Walker. 2004. "The Present and Future Role of Photodynamic Therapy in Cancer Treatment Photodynamic Therapy." *Lancet Oncolog* 5(8): 497–508. http://www.ncbi.nlm.nih.gov/pubmed/15288239.

Buytaert, Esther, Michael Dewaele, and Patrizia Agostinis. 2007. "Molecular Effectors of Multiple Cell Death Pathways Initiated by Photodynamic Therapy." *Biochimica et Biophysica Acta - Reviews on Cancer* 1776(1): 86–107.

Castano, A.P., T.N. Demidova, and M.R. Hamblin. 2005. "Mechanisms in Photodynamic Therapy: Part Two - Cellular Signaling, Cell Metabolism and Modes of Cell Death." *Photodiagnosis and Photodynamic Therapy* 2(1 SPEC. IS): 1–23.

Castano, Ana P., Tatiana N. Demidova, and Michael R. Hamblin. 2005. "Mechanisms in Photodynamic Therapy: Part Three - Photosensitizer Pharmacokinetics, Biodistribution, Tumor Localization and Modes of Tumor Destruction." *Photodiagnosis and Photodynamic Therapy* 2(2): 91–106.

Castano, Ana P., Pawel Mroz, and Michael R. Hamblin. 2006. "Photodynamic Therapy and Anti-Tumour Immunity." *Nature Reviews Cancer* 6(7): 535–45.

Castano, Ana P, Tatiana N Demidova, and Michael R Hamblin. 2004. "Mechanisms in Photodynamic Therapy: Part One-Photosensitizers, Photochemistry and Cellular Localization." *Photodiagnosis and photodynamic therapy* 1(4): 279–93. http://www.pubmedcentral.nih.gov/articlerender.fcgi?artid=4108220&tool=pmcentrez&rendertype=abstract.

Celli, Jonathan P. et al. 2010. "Imaging and Photodynamic Therapy: Mechanisms, Monitoring, and Optimization." *Chemical Reviews* 110(5): 2795–2838.

Che, Chi Ming, Vanessa Kar Yan Lo, Cong Ying Zhou, and Jie Sheng Huang. 2011. "Selective Functionalisation of Saturated C-H Bonds with Metalloporphyrin Catalysts." *Chemical Society Reviews* 40(4): 1950–75.

Chiou, Jeng-Fong et al. 2010. "Verteporfin-Photoinduced Apoptosis in HepG2 Cells Mediated by Reactive Oxygen and Nitrogen Species Intermediates." *Free Radical Research*.

Chizhova, N. V., O. M. Kulikova, and N. Zh. Mamardashvili. 2013. "Synthesis and Properties of Ms- and β-Substituted Pt(II) and Pt(IV) Tetraphenylporphyrinates." *Russian Journal of General Chemistry* 83(11): 2108–11. http://link.springer.com/10.1134/S107036321311025X.

Crouch, Andrew M., and Cooper H. Langford. 1990. "Photophysical Behaviour of Zinc Tetraphenylporphyrins in Solutions and Polymer Films." *Journal of Photochemistry and Photobiology, A: Chemistry* 52(1): 55–64.

Daziano, Jean Pierre et al. 1996. "Photophysical and Redox Properties of a Series of Phthalocyanines: Relation with Their Photodynamic Activities on TF-1 and Daudi Leukemic Cells." *Photochemistry and Photobiology* 64(4): 712–19.

Dean, Michelle L., Jason R. Schmink, Nicholas E. Leadbeater, and Christian Brückner. 2008. "Microwave-Promoted Insertion of Group 10 Metals into Free Base Porphyrins and Chlorins: Scope and Limitations." *Journal of the Chemical Society. Dalton Transactions* (10): 1341–45.

St. Denis, Tyler G. et al. 2011. "Combination Approaches to Potentiate Immune Response after Photodynamic Therapy for Cancer." *Photochemical and Photobiological Sciences* 10(5): 792–801.

Dias Ferreira, João. 2017. "Advances on Photodynamic Therapy: New Pyridine-Fused Diphenylchlorins as Photosensitizers for Melanoma Treatment." : 104.

Dikalov, Sergey, Kathy K. Griendling, and David G. Harrison. 2007. "Measurement of Reactive Oxygen Species in Cardiovascular Studies." *Hypertension* 49(4): 717–27.

Ding, X et al. 2004. "Hematoporphyrin Monomethyl Ether Photodynamic Damage on HeLa Cells by Means of Reactive Oxygen Species Production and Cytosolic Free Calcium Concentration Elevation." *Cancer Lett*.

Dougherty, T. J. et al. 1975. "Photoradiation Therapy. II. Cure of Animal Tumors with Hematoporphyrin and Light." *Journal of the National Cancer Institute* 55(1): 115–21.

Douglas, Raymond S. et al. 1995. "A Simplified Method for the Coordinate Examination of

Apoptosis and Surface Phenotype of Murine Lymphocytes." *Journal of Immunological Methods* 188(2): 219–28.

Eastwood, D, L Edwards, M Gouterman, and J Steinfeld. 1966. "Spectra of Porphyrins Part VII. Vapor Absorption and Emission of Phthalocyanines." *Journal of Molecular Spectroscopy* 20(4): 381–90.

Ethirajan, Manivannan, Yihui Chen, Penny Joshi, and Ravindra K. Pandey. 2011. "The Role of Porphyrin Chemistry in Tumor Imaging and Photodynamic Therapy." *Chem. Soc. Rev.* 40(1): 340–62. http://xlink.rsc.org/?DOI=B915149B.

Foote, Christopher S. 1991. "DEFINITION OF TYPE I and TYPE II PHOTOSENSITIZED OXIDATION." *Photochemistry and Photobiology*.

Frangioni, John V. 2003. "In Vivo Near-Infrared Fluorescence Imaging." *Current Opinion in Chemical Biology* 7(5): 626–34.

Garg, Abhishek D., Dominika Nowis, Jakub Golab, and Patrizia Agostinis. 2010. "Photodynamic Therapy: Illuminating the Road from Cell Death towards Anti-Tumour Immunity." *Apoptosis* 15(9): 1050–71.

Gariboldi, Marzia B et al. 2009. "Photodynamic Effects of Novel 5,15-Diaryl-Tetrapyrrole Derivatives on Human Colon Carcinoma Cells." *Bioorganic & medicinal chemistry*.

Ghosh, A. 2000. "Electronic Structure of Porphyrins and Metalloporphyrins: Past, Present and Future." In *Journal of Porphyrins and Phthalocyanines*, , 380–81.

Giovannetti, Rita. 2012. "The Use of Spectrophotometry UV-Vis for the Study of Porphyrins." In *Macro To Nano Spectroscopy*, http://www.intechopen.com/books/macro-to-nano-spectroscopy/the-use-of-spectrophotometry-uv-vis-for-the-study-of-porphyrins.

Gonsalves, A. M.d.A.Rocha, Jorge M.T.B. Varejão, and Mariette M. Pereira. 1991. "Some New Aspects Related to the Synthesis of Meso-substituted Porphyrins." *Journal of Heterocyclic Chemistry* 28(3): 635–40.

Gouterman, Martin. 1959. "Study of the Effects of Substitution on the Absorption Spectra of Porphin." *The Journal of Chemical Physics* 30(5): 1139–61.

———. 1961. "Spectra of Porphyrins." *Journal of Molecular Spectroscopy* 6(C): 138–63.

Granville, David J. et al. 1998. "Rapid Cytochrome c Release, Activation of Caspases 3, 6, 7 and 8 Followed by Bap31 Cleavage in HeLa Cells Treated with Photodynamic Therapy." *FEBS Letters*.

Grossweiner, Leonard I., James B. Grossweiner, B. H. Gerald Rogers, and Linda R. Jones. 2005. The Science of Phototherapy: An Introduction *The Science of Phototherapy: An Introduction*.

Hadjur, Christophe et al. 1996. "Photodynamic Effects of Hypericin on Lipid Peroxidation and Antioxidant Status in Melanoma Cells." *Photochemistry and Photobiology*.

Hamblin, M R, and P Mroz. 2008. Advances in Photodynamic Therapy Basic Translational and Clinical *Advances in Photodynamic Therapy: Basic, Translational, and Clinical*. http://books.google.com/books?id=obgcmRyD7NYC&pgis=1.

Hamzeloo-Moghadam, M, and N Taiebi. 2014. "The Effect of Some Cosolvents and Surfactants on Viability of Cancerous Cell Lines." *Research Journal of ….*

Hedley, D W, and S Chow. 1994. "Evaluation of Methods for Measuring Cellular Gluthione Content Using Flow Cytometry." *Cytometry* 15: 349–58.

Hötzer, Benjamin, Igor L. Medintz, and Niko Hildebrandt. 2012. "Fluorescence in Nanobiotechnology: Sophisticated Fluorophores for Novel Applications." *Small* 8(15): 2297–2326.

Huang, Zheng et al. 2008. "Photodynamic Therapy for Treatment of Solid Tumors--Potential and Technical Challenges." *Technology in cancer research & treatment* 7(4): 309–20. http://www.ncbi.nlm.nih.gov/pubmed/18642969%5Cnhttp://www.pubmedcentral.nih.gov/articlerender.fcgi?artid=PMC2593637.

Ivanov, AV. 2000. "One More PDT Application of Chlorin E6." *BiOS 2000 The …*: 1–7. http://proceedings.spiedigitallibrary.org/proceeding.aspx?articleid=916366.

Josefsen, Leanne B., and Ross W. Boyle. 2008. "Photodynamic Therapy and the Development of Metal-Based Photosensitisers." *Metal-Based Drugs* 2008.

Juarranz, Ángeles et al. 2008. "Photodynamic Therapy of Cancer. Basic Principles and Applications." *Clinical and Translational Oncology*.

Kalejta, R F, T Shenk, and a J Beavis. 1997. "Use of a Membrane-Localized Green Fluorescent Protein Allows Simultaneous Identification of Transfected Cells and Cell Cycle Analysis by Flow Cytometry." *Cytometry* 29(4): 286–91.

Kamuhabwa, A R et al. 2001. "Cellular Photodestruction Induced by Hypericin in AY-27 Rat Bladder Carcinoma Cells." *Photochemistry and photobiology*.

Kelkar, Sneha S., and Theresa M. Reineke. 2011. "Theranostics: Combining Imaging and Therapy." *Bioconjugate Chemistry* 22(10): 1879–1903.

Kessel, David, and Yu Luo. 1999. "Photodynamic Therapy: A Mitochondrial Inducer of Apoptosis." *Cell Death and Differentiation*.

Kessel, David, M. Graça H. Vicente, and John J. Reiners. 2006. "Initiation of Apoptosis and Autophagy by Photodynamic Therapy." *Autophagy*.

Kleban, Ján et al. 2008. "Mechanisms Involved in the Cell Cycle and Apoptosis of HT-29 Cells Pre-Treated with MK-886 Prior to Photodynamic Therapy with Hypericin." *Journal of Photochemistry and Photobiology B: Biology*.

Klionsky, Daniel J. 2005. "The Molecular Machinery of Autophagy: Unanswered Questions." *Journal of Cell Science* 118(1): 7–18. http://jcs.biologists.org/lookup/doi/10.1242/jcs.01620.

Kübler, Alexander C. 2005. "Photodynamic Therapy." *Medical Laser Application* 20(1): 37–45.

Laranjo, M. 2014. "Fotossensibilizadores Para Terapia e Imagem Em Oncologia." : 266.

Laranjo, Mafalda et al. 2013. "2-Bromo-5-Hydroxyphenylporphyrins for Photodynamic Therapy: Photosensitization Efficiency, Subcellular Localization and in Vivo Studies." *Photodiagnosis and Photodynamic Therapy* 10(1): 51–61.

Lemos, Américo, and João P. Lourenço. 2010. "Cycloaddition Reactions of Nitrosoalkenes, Azoalkenes and Nitrile Oxides Mediated by Hydrotalcite." *Arkivoc* 2010(5): 170–82.

Lindoy, Leonard F., Ki Min Park, and Shim Sung Lee. 2013. "Metals, Macrocycles and Molecular Assemblies-Macrocyclic Complexes in Metallo-Supramolecular Chemistry." *Chemical Society Reviews* 42(4): 1713–27.

Littler, B. J. et al. 1999. "Refined Synthesis of 5-Substituted Dipyrromethanes." *Journal of Organic Chemistry* 64(4): 1391–96.

Longuet-Higgins, H. C., C. W. Rector, and J. R. Platt. 1950. "Molecular Orbital Calculations on Porphine and Tetrahydroporphine." *The Journal of Chemical Physics* 18(9): 1174–81.

Luo, Shenglin et al. 2011. "A Review of NIR Dyes in Cancer Targeting and Imaging." *Biomaterials* 32(29): 7127–38.

MacDonald, I. J., and T. J. Dougherty. 2001. "Basic Principles of Photodynamic Therapy." In *Journal of Porphyrins and Phthalocyanines*, , 105–29.

Maisch, T. et al. 2007. "The Role of Singlet Oxygen and Oxygen Concentration in Photodynamic Inactivation of Bacteria." *Proceedings of the National Academy of Sciences*.

Marchal, Sophie et al. 2005. "Necrotic and Apoptotic Features of Cell Death in Response to Foscan® Photosensitization of HT29 Monolayer and Multicell Spheroids." *Biochemical Pharmacology*.

Martinez De Pinillos Bayona, Alejandra, Pawel Mroz, Connor Thunshelle, and Michael R. Hamblin. 2017. "Design Features for Optimization of Tetrapyrrole Macrocycles as Antimicrobial and Anticancer Photosensitizers." *Chemical Biology and Drug Design* 89(2): 192–206.

Massoud, Tarik F, and Sanjiv S Gambhir. 2003. "Molecular Imaging in Living Subjects: Seeing Fundamental Biological Processes in a New Light." *Genes & development* 17(5): 545–80. http://genesdev.cshlp.org/content/17/5/545.short%5Cnpapers3://publication/doi/10.1101/gad.1047403.

Mazor, O. et al. 2005. "Novel Water-Solu Ble Bacterioc h Lorop h y I I Derivatives for Vascular-Targeted Photodynamic Therapy: Synthesis, Solubility, Phototoxicity and the Effect of Serum Proteins?" *Photochemistry and Photobiology* 81: 983–93. https://www.weizmann.ac.il/Biological_Regulation/YoramSalomon/YS-1971-2008pdfs/2005-Brandis.pdf.

Menezes, P F C et al. 2004. "Spectroscopic Studies of Photobleaching and Photoproduct of the Photosensitizer Photogem during Intense Illumination." *Laser Physics* 14(9): 1214–18.

Mesquita, Mariana Q. et al. 2014. "Photodynamic Inactivation of Bioluminescent Escherichia Coli by Neutral and Cationic Pyrrolidine-Fused Chlorins and Isobacteriochlorins." *Bioorganic and Medicinal Chemistry Letters* 24(3): 808–12.

Mikeš, Jaromír et al. 2007. "Necrosis Predominates in the Cell Death of Human Colon Adenocarcinoma HT-29 Cells Treated under Variable Conditions of Photodynamic Therapy with Hypericin." *Photochemical and Photobiological Sciences*.

Mikešová, Lucia et al. 2013. "Conjunction of Glutathione Level, NAD(P)H/FAD Redox Status and Hypericin Content as a Potential Factor Affecting Colon Cancer Cell Resistance to Photodynamic Therapy with Hypericin." *Photodiagnosis and Photodynamic Therapy.*

Minaev, Boris et al. 2006. "Density Functional Theory Study of Vibronic Structure of the First Absorption Qx Band in Free-Base Porphin." *Spectrochimica Acta - Part A: Molecular and Biomolecular Spectroscopy* 65(2): 308–23.

Moan, Johan, and David Kessel. 1988. "Photoproducts Formed from Photofrin II in Cells." *Journal of Photochemistry and Photobiology, B: Biology* 1(4): 429–36.

Moghissi, K. 2004. "Photodiagnosis and Photodynamic Therapy: The Birth of a Journal." *Photodiagnosis and Photodynamic Therapy* 1(1): 1.

Mosmann, T. 1983. "Rapid Colorimetric Assay for Cellular Growth and Survival: Application to Proliferation and Cytotoxicity Assays." *Journal of immunological methods* 65(1–2): 55–63. http://www.ncbi.nlm.nih.gov/pubmed/6606682.

Mroz, Pawel, Anastasia Yaroslavsky, Gitika B. Kharkwal, and Michael R. Hamblin. 2011. "Cell Death Pathways in Photodynamic Therapy of Cancer." *Cancers* 3(2): 2516–39.

Naik, Rajan, Padmakar Joshi, Sharada P. Kaiwar, and Rajesh K. Deshpande. 2003. "Facile Synthesis of Meso-Substituted Dipyrromethanes and Porphyrins Using Cation Exchange Resins." *Tetrahedron* 59(13): 2207–13.

Nemykin, Victor N., and Ryan G. Hadt. 2010. "Interpretation of the UV - Vis Spectra of the Meso (Ferrocenyl)-Containing Porphyrins Using a TDDFT Approach: Is Gouterman's Classic Four-Orbital Model Still in Play?" *Journal of Physical Chemistry A* 114(45): 12062–66.

Nishie, Hirotada et al. 2018. "Excellent Antitumor Effects for Gastrointestinal Cancers Using Photodynamic Therapy with a Novel Glucose Conjugated Chlorin E6." *Biochemical and Biophysical Research Communications.*

Nyman, Emma S., and Paavo H. Hynninen. 2004. "Research Advances in the Use of Tetrapyrrolic Photosensitizers for Photodynamic Therapy." *Journal of Photochemistry and Photobiology B: Biology* 73(1–2): 1–28.

Obata, Makoto et al. 2009. "In Vitro Heavy-Atom Effect of Palladium(II) and Platinum(II) Complexes of Pyrrolidine-Fused Chlorin in Photodynamic Therapy." *Journal of Medicinal Chemistry* 52(9): 2747–53.

Ormond, Alexandra B., and Harold S. Freeman. 2013. "Dye Sensitizers for Photodynamic Therapy." *Materials* 6(3): 817–40.

Pansare, Vikram J., Shahram Hejazi, William J. Faenza, and Robert K. Prud'Homme. 2012. "Review of Long-Wavelength Optical and NIR Imaging Materials: Contrast Agents, Fluorophores, and Multifunctional Nano Carriers." *Chemistry of Materials* 24(5): 812–27.

Papazisis, K. T., G. D. Geromichalos, K. A. Dimitriadis, and A. H. Kortsaris. 1997. "Optimization of the Sulforhodamine B Colorimetric Assay." *Journal of Immunological Methods* 208(2): 151–58.

Patel, Sunita, and Anindya Datta. 2009. "Fluorescence Investigation of the Binding of Model PDT

Drugs to Nonionic and Zwitterionic Surfactants." *Photochemistry and Photobiology.*

Pereira, Nelson A.M. et al. 2011. "[8π+2π] Cycloaddition of Meso-Tetra- and 5,15-Diarylporphyrins: Synthesis and Photophysical Characterization of Stable Chlorins and Bacteriochlorins." *European Journal of Organic Chemistry* (20–21): 3970–79.

———. 2015. "Novel 4,5,6,7-Tetrahydropyrazolo[1,5-a]Pyridine Fused Chlorins as Very Active Photodynamic Agents for Melanoma Cells." *European Journal of Medicinal Chemistry* 103: 374–80.

———. 2017. "Platinum(II) Ring-Fused Chlorins as Near-Infrared Emitting Oxygen Sensors and Photodynamic Agents." *ACS Medicinal Chemistry Letters* 8(3): 310–15.

———. 2018. "Advances on Photodynamic Therapy of Melanoma through Novel Ring-Fused 5,15-Diphenylchlorins." *European Journal of Medicinal Chemistry.*

Pereira, Nelson A.M., Arménio C. Serra, and Teresa M.V.D. Pinho E Melo. 2010. "Novel Approach to Chlorins and Bacteriochlorins: [8π+2π] Cycloaddition of Diazafulvenium Methides with Porphyrins." *European Journal of Organic Chemistry* (34): 6539–43.

Piette, Jacques et al. 2003. "Cell Death and Growth Arrest in Response to Photodynamic Therapy with Membrane-Bound Photosensitizers." In *Biochemical Pharmacology,*.

Pineiro, Marta et al. 1998. "Photoacoustic Measurements of Porphyrin Triplet-State Quantum Yields and Singlet-Oxygen Efficiencies." *Chemistry - A European Journal* 4(11): 2299–2307.

Plaetzer, K. et al. 2009. "Photophysics and Photochemistry of Photodynamic Therapy: Fundamental Aspects." *Lasers in Medical Science* 24(2): 259–68.

Platt, John R. 1950. "Molecular Orbital Predictions of Organic Spectra." *The Journal of Chemical Physics* 18(9): 1168–73.

Rocha, Luis B., Lígia C. Gomes-Da-Silva, Janusz M. Dąbrowski, and Luis G. Arnaut. 2015. "Elimination of Primary Tumours and Control of Metastasis with Rationally Designed Bacteriochlorin Photodynamic Therapy Regimens." *European Journal of Cancer* 51(13): 1822–30.

Rotomskis, R., S. Bagdonas, and G. Streckyte. 1996. "Spectroscopic Studies of Photobleaching and Photoproduct Formation of Porphyrins Used in Tumour Therapy." *Journal of Photochemistry and Photobiology B: Biology* 33(1): 61–67.

Saito, Shohei, and Atsuhiro Osuka. 2011. "Expanded Porphyrins: Intriguing Structures, Electronic Properties, and Reactivities." *Angewandte Chemie - International Edition* 50(19): 4342–73.

Sarma, K. D., D. Ray, and A. Antony. 2000. "Improved Sensitivity of Trypan Blue Dye Exclusion Assay with Ni2+ or Co2+ Salts." *Cytotechnology* 32(2): 93–95.

Sasnauskiene, Ausra et al. 2009. "Apoptosis, Autophagy and Cell Cycle Arrest Following Photodamage to Mitochondrial Interior." *Apoptosis.*

Scaffidi, Carsten, Jan Paul Medema, Peter H. Krammer, and Marcus E. Peter. 1997. "FLICE Is Predominantly Expressed as Two Functionally Active Isoforms, Caspase-8/a and Caspase-8/B." *Journal of Biological Chemistry.*

Sevick-Muraca, Eva M., Jessica P. Houston, and Michael Gurfinkel. 2002. "Fluorescence-

Enhanced, near Infrared Diagnostic Imaging with Contrast Agents." *Current Opinion in Chemical Biology* 6(5): 642–50.

Shao, Jingwei et al. 2012. "Inhibition of Human Hepatocellular Carcinoma HepG2 by Phthalocyanine Photosensitiser PHOTOCYANINE: ROS Production, Apoptosis, Cell Cycle Arrest." *European Journal of Cancer.*

Shen, B., R. G. Jensen, and H. J. Bohnert. 1997. "Mannitol Protects against Oxidation by Hydroxyl Radicals." *Plant physiology.*

Sobral, Abílio J.F.N. et al. 2003. "One-Step Synthesis of Dipyrromethanes in Water." *Tetrahedron Letters* 44(20): 3971–73.

Sousa Brites, Gonçalo. 2016. "TERAPIA FOTODINÂMICA EM COMBINAÇÃO COM A QUIMIOTERAPIA: Uma Opção No Osteossarcoma." https://estudogeral.sib.uc.pt/bitstream/10316/36527/1/Tese GB docx.pdf.

St John, J et al. 2006. "The Analysis of Mitochondria and Mitochondrial DNA in Human Embryonic Stem Cells." *Methods in molecular biology (Clifton, N.J.)* 331: 347–74. papers3://publication/uuid/7984D35E-4214-4C2A-B450-F378FD9C1DED.

Sternberg, Ethan D., David Dolphin, and Christian Brückner. 1998. "Porphyrin-Based Photosensitizers for Use in Photodynamic Therapy." *Tetrahedron* 54(17): 4151–4202.

Stillman, Martin, John Mack, and Nagao Kobayashi. 2002. "Theoretical Aspects of the Spectroscopy of Porphyrins and Phthalocyanines." *Journal of Porphyrins and Phthalocyanines* 06(04): 296–300.

Streckyt, G., and R. Rotomskis. 1993. "Phototransformations of Porphyrins in Aqueous and Micellar Media." *Journal of Photochemistry and Photobiology, B: Biology* 18(2–3): 259–63.

Sutcliffe, Oliver B., Richard C. Storr, Thomas L. Gilchrist, and Paul Rafferty. 2000. "Cycloadditions to Pyrrolo[1,2-c]Thiazoles and Pyrazolo[1,5-c]Thiazoles." *Tetrahedron* 56(51): 10011–21.

———. 2001. "Azafulvenium Methides: New Extended Dipolar Systems." *Journal of the Chemical Society. Perkin Transactions 1* 15: 1795–1806.

Szokalska, Angelika et al. 2009. "Proteasome Inhibition Potentiates Antitumor Effects of Photodynamic Therapy in Mice through Induction of Endoplasmic Reticulum Stress and Unfolded Protein Response." *Cancer research.*

Tarpey, M. M. 2004. "Methods for Detection of Reactive Metabolites of Oxygen and Nitrogen: In Vitro and in Vivo Considerations." *AJP: Regulatory, Integrative and Comparative Physiology* 286(3): 431R–444. http://ajpregu.physiology.org/cgi/doi/10.1152/ajpregu.00361.2003.

Triesscheijn, M., P. Baas, J. H. M. Schellens, and F. A. Stewart. 2006. "Photodynamic Therapy in Oncology." *The Oncologist* 11(9): 1034–44. http://theoncologist.alphamedpress.org/cgi/doi/10.1634/theoncologist.11-9-1034.

Verna, L. K., D. Chen, G. Schluter, and G. M. Williams. 1998. "Inhibition by Singlet Oxygen Quenchers of Oxidative Damage to DNA Produced in Cultured Cells by Exposure to a Quinolone Antibiotic and Ultraviolet a Irradiation." *Cell Biology and Toxicology.*

Vichai, Vanicha, and Kanyawim Kirtikara. 2006. "Sulforhodamine B Colorimetric Assay for Cytotoxicity Screening." *Nature Protocols* 1(3): 1112–16.

Vistica, David T., Anne Monks, Angela Pittman, and Michael R. Boyd. 1991. "Tetrazolium-Based Assays for Cellular Viability: A Critical Examination of Selected Parameters Affecting Formazan Production." *Cancer Research.*

Wang, Hong, and James A. Joseph. 1999. "Quantifying Cellular Oxidative Stress by Dichlorofluorescein Assay Using Microplate Reader." *Free Radical Biology and Medicine.*

Wiehe, Arno, Ekaterina J. Simonenko, Mathias O. Senge, and Beate RÖder. 2001. "Hydrophilicity vs Hydrophobicity - Varying the Amphiphilic Structure of Porphyrins Related to the Photosensitizer m-THPC." *Journal of Porphyrins and Phthalocyanines* 5(10): 758–61.

Woodburn, Kathryn et al. 1994. "BIODISTRIBUTION AND PDT EFFICACY OF A KETOCHLORIN PHOTOSENSITIZER AS A FUNCTION OF THE DELIVERY VEHICLE." *Photochemistry and Photobiology.*

Yano, Shigenobu et al. 2011. "Current States and Future Views in Photodynamic Therapy." *Journal of Photochemistry and Photobiology C: Photochemistry Reviews* 12(1): 46–67.

Yoo, Je-Ok, and Kwon-Soo Ha. 2012. International review of cell and molecular biology *New Insights into the Mechanisms for Photodynamic Therapy-Induced Cancer Cell Death.*

Zhang, Ruifen et al. 2008. "In Vitro and in Vivo Induction of Apoptosis by Capsaicin in Pancreatic Cancer Cells Is Mediated through ROS Generation and Mitochondrial Death Pathway." *Apoptosis.*

Zhao, Hongtao et al. 2005. "Detection and Characterization of the Product of Hydroethidine and Intracellular Superoxide by HPLC and Limitations of Fluorescence." *Proceedings of the National Academy of Sciences of the United States of America* 102(16): 5727–32. http://www.pubmedcentral.nih.gov/articlerender.fcgi?artid=556312&tool=pmcentrez&rendertype=abstract.

Zhao, Hongyou, Da Xing, and Qun Chen. 2011. "New Insights of Mitochondria Reactive Oxygen Species Generation and Cell Apoptosis Induced by Low Dose Photodynamic Therapy." *European journal of cancer (Oxford, England : 1990).*